TÉCNICO LISBOA

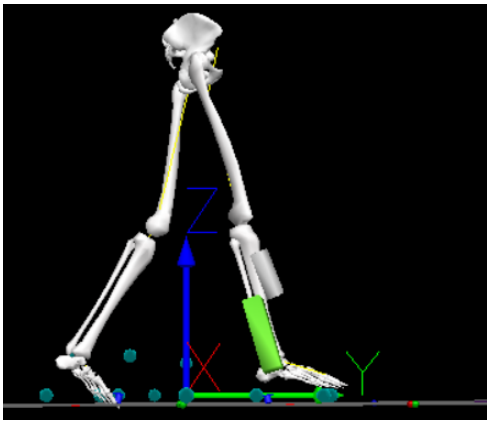

Development of a Wearable Active Exoskeleton with Self-aligning Mechanism

Ricardo Luís Nunes Andrade

Thesis to obtain the Master of Science Degree in

Biomedical Engineering

Supervisors: Prof. Miguel Pedro Tavares da Silva
Prof. Cristina Peixoto Santos

Examination Committee

Chairperson: Prof. João Orlando Marques Gameiro Folgado
Supervisor: Prof. Miguel Pedro Tavares da Silva
Member of the Committee: Prof. Jorge Manuel Mateus Martins

November 2022

I declare that this document is an original work of my own authorship and that it fulfills all the requirements of the Code of Conduct and Good Practices of the Universidade de Lisboa.
The work presented in this thesis was performed at the Biomedical Robotic Devices Laboratory, Center for Microelectromechanical Systems, University of Minho (Guimarães, Portugal), during the period February-August 2022, under the supervision of Prof. Cristina Peixoto Santos. The thesis was co-supervised at Instituto Superior Técnico by Prof. Miguel Tavares da Silva.

Acknowledgments

I would like to thank all the people from BIRDLab at the University of Minho, for welcoming me into their group and ensuring an easy integration. I can safely say that friendships were developed in these few months, which I hope to keep. Within this group of people, some people deserve special mention.
First, Nuno Ribeiro, who first brought me into the laboratory to work on an unrelated project in the summer of 2021, and that first opened the possibility for me to do my master thesis with them. His amazing leadership skills, eagerness for knowledge, and frank and honest friendship are deeply appreciated.
To Joana Figueiredo, who, between teaching, FCT applications, and leading the SmartOs team, tirelessly worked with me on this thesis, choosing to devote part of the little time she had left. From the guidance provided at the beginning of the project, to the extensive meetings and the seemingly endless hours spent at LABIOMEP in Porto, this work is an expression of her unfathomable work ethic, attention to detail, and incredible energy.
Finally, Prof. Cristina Santos, who, as the leader of BIRDLab, welcomed me into the laboratory, ensuring that I was well received and that the work I was doing also met my expectations. Her contributions, guidance, wisdom, willingness to devote the necessary time to my work (despite having a laboratory to run, classes to teach and I don't know how many research projects and master's thesis to coordinate), and openness to explore new avenues were invaluable for this work.
At Laboratório de Biomecânica da Universidade do Porto (LABIOMEP), I thank Pedro Fonseca, who was the main force behind the implementation of the experimental protocol here described. Pedro was the main operator at Porto, setting up the hardware and software and processing most of the kinematic data, and taught me most of what I know regarding Visual 3D, providing an invaluable contribution to furthering my skills.
I would further like to thank my supervisor at Instituto Superior Técnico, Prof. Miguel Tavares, for accepting the challenge made by Prof. Cristina back in February to work together on this thesis, and providing invaluable input in every part of this work.
To everyone back home in Bombarral and Lisbon, for their support and patience. To my friends, for providing necessary relief from the anxieties of everyday life. To my brother, for the timeless partnership and camaraderie and for sharing everything that is important to me, from work to politics and movies,

and everything in between. Finally, to my mother, for the daily words of encouragement, for the bottomless well of patience, knowledge, and reassuring words of wisdom, and for everything she has done and will continue to do, ensuring that the only barriers to my success are the ones from my own making.

”Never doubt that a small group of thoughtful and committed citizens can change the world.
It’s the only thing that ever has.”
- Jed Bartlet.

Abstract

Diseases like cerebral palsy, stroke, or ataxia result in a vast array of symptoms and complications for the individual, such as asymmetrical/abnormal gait patterns, loss of balance, and muscle spasticity, which will require gait rehabilitation. Robotic devices like exoskeletons and orthosis aim to assist the user during gait rehabilitation, through both torque transmission and support. Despite the increase in research on these devices, the physical human-robot interface (pHRI) has not been properly developed, leading to high abandonment. An important factor behind this statistic is the onset of soft and musculoskeletal tissue injuries due to forces and torques at the interface. Within this work, the human-robot joint misalignment problem was addressed, which is, partly, the cause of spurious forces and torques at the pHRI. An experimental protocol was developed to assess misalignment, fixation displacement, pressure interactions, and user-perceived comfort in three different ankle foot orthoses, corresponding to three different pHRI designs. These were ankle-foot orthosis with a frontal shin guard (SOF), lateral shin guard (SOL), and the commercially available ankle modulus of the H2 exoskeleton. The SOF device showed reduced misalignment and related interactions and higher user-perceived comfort in comparison with H2 while improving the SOL device in pressure and comfort. Finally, five alignment solutions were designed and implemented in the SOF device. Within these, three were manual alignment solutions for vertical, horizontal and shin guard alignment, and two were kinematic redundancy solutions based on the release of the inversion/eversion of the ankle and the introduction of a prismatic joint.

Keywords

Alignment Mechanisms; Exoskeletons and Ankle-Foot-Orthosis; Human-Exoskeleton Misalignment; Physical Human-Robot Interaction; Rehabilitation Robotics.

Resumo

Doenças como paralisia cerebral, AVC, ou ataxia resultam em sintomas e complicações para o indivíduo, tais como padrões de marcha assimétricos/anormais, perda de equilíbrio, e espasticidade muscular, o que exigirá uma reabilitação da marcha. Dispositivos robóticos como exoesqueletos e ortóteses visam ajudar o utilizador durante a reabilitação da marcha, tanto através da transmissão de torque como do apoio. Apesar do aumento da investigação sobre estes dispositivos, a interface homem-robot (pHRI) não foi ainda devidamente desenvolvida, levando a um elevado abandono. Um fator importante por detrás desta estatística são lesões nos tecidos moles e músculo-esqueléticos devido a forças e torques na interface. Neste documento, foi abordado o problema do desalinhamento da articulação homem-robot, que é, em parte, a causa de forças e torques na pHRI. Foi desenvolvido um protocolo experimental para avaliar desalinhamento, deslocamento de fixação, interações de pressão e conforto do utilizador em três ortóteses do tornozelo, correspondentes a três designs diferentes de pHRI. Estas eram ortóteses do tornozelo com caneleira frontal (SOF), caneleira lateral (SOL), e o módulo de tornozelo do exosqueleto H2. O dispositivo SOF mostrou desalinhamento e interações reduzidos e um maior conforto do utilizador em comparação com a H2, enquanto melhorava o dispositivo SOL em termos de pressão e conforto. Finalmente, cinco soluções de alinhamento foram concebidas e implementadas no SOF. Dentro destas, três eram soluções de alinhamento manual para alinhamento vertical, horizontal e caneleira, e duas eram soluções de redundância cinemática baseadas na libertação da inversão/eversão do tornozelo e na introdução de uma junta prismática.

Palavras Chave

Mecanismos de Alinhamento; Exoesqueletos e Ortoteses; Desalinhamento Humano-Exoesqueleto; Interação Física entre Humano e Robot; Robótica para Reabilitação.

Contents

List of Figures

List of Tables

Acronyms

AFO Ankle Foot Orthosis

BIRDLab Biomedical Robotic Devices Laboratory

CAD Computer Aided Design

CPA Cuff Pressure Algometry

CSD-OPUS Client Satisfaction with Device - Orthotics and Prosthetic Users Survey

CoP Center of Pressure

DOF Degree of Freedom

FPMs Force Platform Moments

FSR Force Sensitive Resistor

FoS Factor of Safety

GRF Ground Reaction Forces

HUMA Human Universal Mobility Assistance

ICR Instantaneous Center of Rotation

IR Infra-Red

LABIOMEP Laboratório de Biomecânica do Porto

MACCEPA Mechanically Adjustable Compliance and Controllable Equilibrium Position Actuator

MIT Massachusetts Institute of Technology

PDT Pain Detection Threshold

HRI Human-Robot Interface

PPT Pressure Pain Threshold

PTT Pain Tolerance Threshold

QUEST 2.0 Quebec User Evaluation of Satisfaction with Assistive Technology 2.0

ROM Range of Motion

SOF SMARTOs Frontal

SOL SMARTOs Lateral

SmartOs Smart, Active Lower Limb Orthotic System

1

Introduction

Exoskeletons and orthosis are at the vanguard of clinical rehabilitation research and for the treatment of diseases as diverse as stroke, ataxia, or cerebral palsy [1]. Wherein this category of devices, lower limb exoskeletons have become a focus of research for gait rehabilitation and training, with a subsection of these devices focusing on the ankle joint as a target for rehabilitation. These devices can be used in a clinical setting to provide repetitive, targeted rehabilitation to the patient while releasing the therapist from some of the load associated with conventional physical therapy [2, 3].

This dissertation is integrated into the Smart, Active Lower Limb Orthotic System (SmartOs) project, currently ongoing at the Biomedical Robotic Devices Laboratory (BIRDLab) at Universidade do Minho, whose main objective is to develop a wearable lower limb orthosis for gait rehabilitation. The project currently houses three different Ankle Foot Orthosiss (AFOs) for gait training and rehabilitation, each with its own approach to the Human-Robot Interface (HRI) and consequent misalignment problems. As such, this dissertation intends to address the misalignment problem in the context of these three devices, through a two-step methodology.

First, the interface of the three AFOs was assessed in a laboratory setting in order to conclude which interface leads to the least misalignment and interactions at the HRI, as well as higher user-perceived comfort. For this, the capabilities of the LABIOMEP, the biomechanics laboratory at the Universidade do Porto [4] were used, in particular, their Infra-Red (IR) marker-based motion-captured and pressure-measuring systems were used to assess misalignment and its effects. A questionnaire regarding the user's perception of each device was also filled out by each participant for each device.

After capturing and discussing the results, the prototype which resulted in the least misalignment and related interactions and the highest user-perceived comfort was subject to a thorough evaluation of its structure, aided by both the results from the previous step and systematic research of literature on AFOs with solutions for solving misalignment and/or reducing its effects. This resulted in the idealization and Computer Aided Design (CAD) of 5 different alignment solutions for the chosen prototype. These

solutions, when applicable, were properly validated through mechanical and motion simulations. Finally, a new prototype was developed in the same CAD environment, joining the previous iteration with the current solutions.

1.1 BIRDLab and SmartOs

The BIRDLab is a research group from Universidade do Minho focused on robotic and computational technology development to better understand biological systems. With over 20 members between researchers, Ph.D. and MSc students, a large amount of this group's work is focused on developing rehabilitation technologies for a variety of common diseases like Parkinson's, strokes, and ataxia. These efforts gain expression in developing devices like orthoses, prostheses, walkers, robotic canes, and new rehabilitation environments through augmented and virtual reality. Among BIRDLab's projects is the SmartOs [5]. Focused on gait rehabilitation for stroke patients, this project aims to develop a smart, wearable active lower limb orthotic system. This project intends to integrate a wearable motion lab and AI-based gait analysis tools, a bioinspired control architecture, a biofeedback system, and a wearable active orthosis, to which the work developed for this dissertation contributed.

1.2 Motivation and Problem Statement

Clinical physiotherapy remains the gold standard of rehabilitation after a disease that severely impairs the patient's musculoskeletal system [6–8]. Diseases like cerebral palsy, stroke, or ataxia result in a vast array of symptoms and complications for the individual, such as asymmetrical/abnormal gait patterns, loss of balance, and muscle spasticity. These subjects will require gait rehabilitation, where robotic devices of the lower limbs like exoskeletons and orthosis have gained increased importance in the last decade [2, 3]. These devices act in parallel with the human body, not only guaranteeing a controlled environment for rehabilitation through the precision provided by robotics but a necessary relief for therapists by relieving them of repetitive, straining tasks, necessary for long-term recovery [2, 3]. Depending on the disease and the tasks at hand, these devices can be classified according to which joints and how many joints they support (via passive or active means) [9]. One of the main avenues by which robotic devices can be used in gait rehabilitation is by strengthening muscle action through torque transmission, thereby reproducing functional gait patterns and improving the symptoms through neuroplasticity. For instance, study [10] demonstrated that for both healthy and neurologically impaired participants there was an increase in metabolic cost (measured by VO2) from the baseline, indicating active therapy and muscle activation and, as such, clinical effectiveness of these devices for rehabilitation

Another avenue for applying exoskeletons in rehabilitation is to provide passive support for limbs and

joints in different conditions, as follows. At the initial stage of rehabilitation, the exoskeleton can provide support to patients with trouble standing in an upright position [1, 10], allowing them to engage in these rehabilitation exercises. Furthermore, this support also improves repetition accuracy and training duration [11, 12]. Moreover, AFOs have been used to assist patients with drop foot syndrome, where dorsiflexion of the ankle joint is highly affected [13–15]. An individual with this syndrome would have toe drag, slow walking speed, short step length, high metabolic cost, and high risk of tripping [16, 17]. For this syndrome, AFOs are used to improve gait stability by reducing movements of the tibiotalar and subtalar joints, restraining the natural ROM of the two (subtalar and tibiotalar) joints of the ankle, improving ankle joint alignment and walking speed, and reducing energy consumption [18]. Furthermore, the active AFOs (i.e. AFOs with a joint powered by an actuation system) can actively assist with ankle dorsiflexion [19] and increase foot clearance from the ground [15, 20]. A review of some active AFOs and their results can be found in [21].

Despite the increasing number of exoskeletons and AFOs being developed and the ones already available on the market, the interface between humans and robots has not yet been properly designed [22]. In fact, these devices have a high abandonment rate, with as much as a third of all devices being dropped by their user, with limitations in usability being the main hurdle for exoskeleton devices [23,24]. Problems related to poor assistance given by the exoskeleton leading to the onset of fatigue, disturbance of normal movement patterns, and soft and musculoskeletal tissue injuries are recognized to be the main reasons for this statistic [24–27]. For anthropomorphic devices, defined in [27] as the devices "where any hinge corresponds to a Degree of Freedom (DOF) of the human limb", like AFOs, a proper alignment of these hinges (or robotic joints) with the biological joints is paramount to reduce these effects [28]. In fact, it is widely agreed that this misalignment between the robotic and biological joints results in spurious forces and torques at the interface between human and robot, leading to discomfort, pain, or long-term injury [24, 25, 27–33]. It is, paramount that, in the development of these rehabilitation devices, the issue of misalignment is accounted for, measured, and corrected.

Within this paradigm, these issues should be addressed in the ongoing development of the AFO within the SmartOs. This project iterates on a device that currently exists in the market for research, the ankle module of the H2 exoskeleton [34]. Within this project, research has found human-robot misalignment to be an important design flaw of this device [35, 36]. Two AFOs have been developed within this project that iterates on the H2 device and, through novel interface designs, intended to resolve the issue of misalignment [35]. It is important to assess which of three different design philosophies for the Human-Robot Interface (HRI) (the H2 and the two in-house devices) lead to less misalignment and interactions. Finally, the knowledge from this assessment should be used to develop a new prototype that solves the underlying misalignment issues through dedicated alignment solutions. Within the scope of the research done, no previous study has assessed all three of misalignment, interactions, and user-perceived

comfort of an AFO in the same study, as well as using this assessment to compare different HRI designs.

1.3 Goals and research questions

The main goal of this dissertation is to propose, design, and develop alignment solutions for an active AFO towards minimum-to-null human-AFO misalignment and related interactions at the HRI. and maximum user's perceived comfort and satisfaction during gait rehabilitation. With a focus on proper HRI, this dissertation aims to design alignment solutions based on a quantitative analysis of the human-AFO misalignment and the interactions at the Human-Robot Interface (HRI) through direct measures of interface normal forces and displacement. The found misalignments and vertical displacements are used as requirements for the mechanical design of the alignment solutions. This analysis aims also to identify, from three AFO's fixation mechanisms (which differ in the way that the AFO is attached to the user's shank and foot), the prototype rated with higher user acceptability and more compliant HRI. The selected AFO fixation mechanism will be improved with the design of alignment solutions. This work also addressed the validation of the final design of each solution through motion and mechanical stress simulations, that verify both the expected ROM of the solutions and the mechanical stability of the final structure. To achieve these goals, it is necessary to pursue the following objectives:

- Objective 1: To acquire knowledge from related literature studies on misalignment effects, assessment methods, and alignment solutions for lower limb exoskeletons and orthoses, as follows. First, to review how the human-robot joint misalignment is defined in the literature and its relation to increased interactions at the HRI. Second, to identify the causes and biomechanical effects of human-robot joint misalignment, and the methods used to quantify both human-AFO/exoskeleton misalignment and related interactions. Third, to review the alignment solutions and mechanisms designed for lower limb exoskeletons and orthoses to reduce misalignment itself, to assess their strengths and weakness regarding key device characteristics and their effects on the user. This review will serve as a base for the design of the protocol to evaluate the human-AFO misalignment for the three available prototypes of AFOs (Chapter 3) and for designing the alignment solutions (Chapter 4). Chapter 2 presents these surveys.

- Objective 2: To assess the human-robot joint misalignment, interface displacement, and related interactions for the three AFO prototypes during gait. This involved, first, defining an experimental protocol based on the research in Chapter 2. This protocol will provide a thorough overview of the characteristics of the HRI of each AFO in three domains: direct misalignment, interactions at the interface, and user-perceived comfort. Second, implement this protocol in a motion analysis laboratory, by involving healthy subjects in two common conditions for AFO's use, treadmill

and level-ground walking, using both motion capture and force-sensing hardware. This work is described in Chapter 3.

- Objective 3: To identify the AFO, within the three available, that corresponds to reduced misalignment and interactions and higher user-perceived comfort. This involves comparing the data captured from the protocol with safety values from the literature. This comparison concerns using the following sources captured in the protocol: the direct misalignment in two dimensions, the relative displacement between the AFO's interface and the user's soft tissues, the pressure values at the interface, and the user's answers on a custom-made questionnaire concerning user-perceived comfort and interactions. From the results that come from these comparisons, to make an informed decision regarding the AFO. The comparison results and the final decision can be found in Chapter 3.

- Objective 4: To set the requirements for the design of the alignment solutions. The intention is to analyze which measures captured in the protocol represent relevant problems related to misalignment and to quantify this measurement in a way that could help both idealize and design the relevant alignment solutions. This is presented in Chapter 4.

- Objective 5: To idealize, design, and validate the necessary alignment solutions related to the requirements defined before. First, to utilize the research on alignment solutions from Chapter 2 to help design appropriate solutions for each of the requirements set, and to use these requirements to properly dimension each solution, keeping them within the identified needs. Secondly, to design each solution iteratively, starting by implementing each solution separately on the initial prototype and performing the necessary validation tests. These pertain to motion and mechanical stress simulations that guarantee the applicability of the solutions, both concerning their intended use and the overall safety and durability of the device. Finally, to make an assessment of the result of each validation and make a decision concerning the state of the given solution, to either continue to iterate or accept the design. This pertains to work in Chapter 4.

- Objective 6: To integrate the proposed alignment solutions into the design of the active AFO and perform the needed final validations. This is the final part of Chapter 4.

In order to reach the goal of developing an AFO with reduced misalignment, the following main research questions (RQs) are addressed.

- RQ1: How is the human-robot joint misalignment assessed? This RQ is related to Objective 1 and is answered in Chapter 2.

- RQ2: Which are the main solutions designed to reduce misalignment in lower limb orthoses? This RQ is related to Objective 1 and is answered in Chapter 2.

- RQ3: Which AFO's fixation mechanism, within the three available, leads to the smallest misalignment and interactions and high user satisfaction? This RQ is related to Objective 3 and is answered in Chapter 3.
- RQ4: Which are the needed alignment solutions in the AFO that answers RQ3? This RQ is related to Objective 5 and is answered in Chapter 4.

1.4 Contributions

The main contributions outlined in this Master's dissertation are:

- A descriptive literature review reporting the causes and effects of human-robot joint misalignment, and the assessment methods used to quantify human-AFO misalignment.
- A narrative review of the alignment solutions and mechanisms designed for lower limb exoskeletons and AFOs.
- A protocol detailing the procedures and the outcomes to assess the human-AFO joint misalignment, interface displacement and pressure, and user-perceived comfort and satisfaction.
- Quantification of the human-AFO joint misalignment, interface displacement and pressure,
- Assessment of the best fixation mechanism among three different designs, concerning its misalignment, interface displacement and pressure, and user-perceived comfort and satisfaction.
- Design a manual alignment solution to address horizontal misalignment and validate it on the initial prototype.
- Design a manual alignment solution to address vertical misalignment and validate it on the initial prototype.
- Design a manual alignment solution to address shin-guard fitness and displacement and validate it on the initial prototype.
- Design a kinematic redundancy alignment solution based on the release of the inversion and eversion DOF of the ankle joint to address initial and trough gait misalignment and validate it on the initial prototype.
- Design a kinematic redundancy alignment solution based on a rail guide to address vertical fixation displacement and validate it on the initial prototype.
- Integration of the solutions on the final prototype and final validation.

Furthermore, the developed work allowed the elaboration of two journal papers to be submitted for review. The first reflects the work done in this dissertation regarding misalignment and interaction assessment in AFOs (Chapter 3 of this document), while the second reflects the work done in the design, development, and validation of alignment solutions in an AFO (Chapter 4 of this document).

1.5 Dissertation Outline

This dissertation is structured as follows:
Chapter 2 gives a thorough overview of the state of the art on misalignment in lower-limb exoskeletons and orthosis, detailing its causes, its effects on the user, and commonly applied methods to assess both human-robot joint misalignments and their biomechanical effects in a laboratory setting. Furthermore, it details a narrative review of the literature on alignment solutions for AFOs and lower limb exoskeletons that include an ankle joint.
Chapter 3 describes the experimental protocol implemented in a motion analysis laboratory (Laboratório de Biomecânica do Porto (LABIOMEP)) to evaluate the misalignment and interactions at the HRI for the three AFOs (which differ in fixation mechanism to the human shank and foot segments). The Chapter goes into detail on the methods chosen to assess these characteristics, their results, and relevant conclusions to the problem at hand. The main takeaway of this Chapter is answering the second research question, providing an AFO design that can be further iterated on in the next Chapter. Finally, this Chapter allows the dimensioning of the solutions in Chapter 4 from the captured data.
Chapter 4 discloses the five alignment solutions designed for the AFO selected in the previous Chapter. The rationale behind each solution is described, supported by the research made in Chapter 2 and the results from Chapter 3. This Chapter also details the relevant mechanical and motion simulations used to validate these solutions.
Finally, Chapter 5 presents the most relevant conclusions of this dissertation and possible future work.

2

State of the Art on the Misalignment of Exoskeletons and Orthosis

The focus of this Chapter is a comprehensive assessment of misalignment's causes and effects regarding lower limb exoskeletons and orthosis, and a narrative review of alignment solutions from the literature.

Regarding the state-of-the-art in misalignment research, this Chapter presents the theoretical basis behind the relation between human-robot joint misalignment and prejudicial interactions at the HRI, and proper transmission of the assistive torque. A focus is also given to the importance of these interactions and their reported incidence for a number of exoskeletons in development. Finally, a comprehensive review of methods to assess misalignment and its effects is presented, which allowed a proper development of the protocol in Chapter 3.

The last focus of this Chapter is a general overview of available alignment solutions and their characterization in the literature. Furthermore, a narrative review of alignment solutions for AFOs is described, including their methodology, results, and conclusions. This work allowed a more effective design of the solutions in Chapter 4.

2.1 Human-robot joint misalignment

2.1.1 Introduction on the Physical Human-Robot Interaction

A crucial feature of the development and design of wearable assistive robotics is the HRI, i.e., the interface between the user and the robot. This is because, in most cases, the purpose of a wearable exoskeleton is to apply loads to the human musculoskeletal tissue, both through passive support and

active torque transmission [9]. The transmission of these loads is mediated at the interface between the user's soft tissues and the device's mechanical supports. Within this interface, pressure and sheer loads are applied to the user. A narrative review on adverse effects in stationary gait robots (devices that support the user through a harness [37]) found that the top two most occurring adverse effects are either soft tissue or musculoskeletal related (figure 2.1). Among these adverse effects, most are soft tissue related, like bruising, irritation and skin abrasion [25].

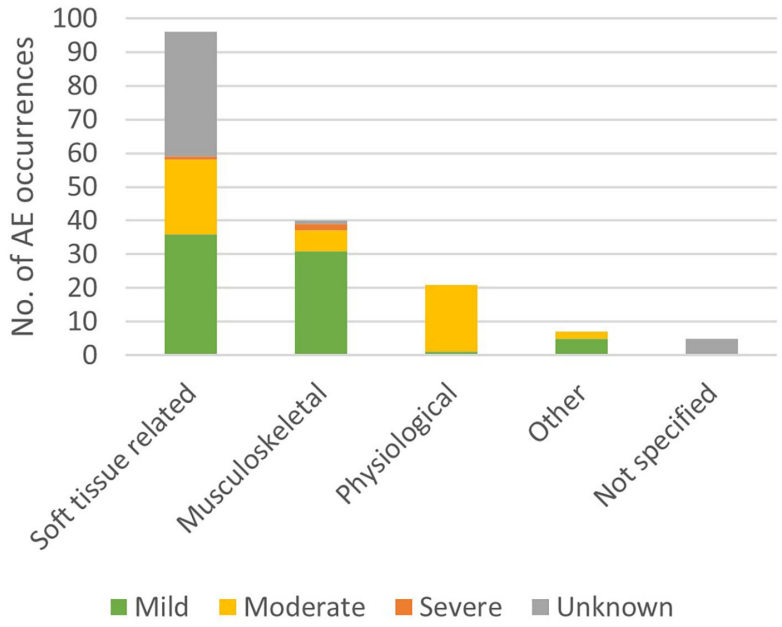

Figure 2.1: Occurrence of adverse effects in overground exoskeletons. Taken from [25]

The same study pointed to cuffs and straps as responsible for some of these injuries. A similar study in overground exoskeletons (ambulatory devices that assist the user during walking over different surfaces and settings [38]) found, similarly, that most of the adverse effects were correlated with soft tissue injuries [39]. Both studies identified both soft and musculoskeletal tissue adverse effects as primary risk factors for exoskeleton use. Literature also differentiates soft tissue interactions. Study [22] ranked four different interactions according to their safety hazard to the user which is presented from least to most avoidable, as follows:

1. Forces perpendicular to the limb's axis (figure 2.2 a). These forces are essential for proper fixation and torque transmission since, without these interactions, there would not be a proper fixation and the coupling of both robotic and human systems would not represent a closed chain. However, it is essential that they stay below safety values and are located in low-compliant areas of soft tissue to reduce misalignment effects, as will be described further.

2. Moments an axis perpendicular to the limb's axis (figure 2.2 b). These moments result in high-

stress concentrations at two opposite points of the limb. These should be carefully applied.

3. Forces along the limb's axis (figure 2.2 c). These forces should be avoided since they represent the transmission of forces through friction, which according to [24], is stated to be the most related to pain and discomfort.

4. Moments around the limb's axis (figure 2.2 d). These moments should be the first taken into consideration since they lead to large muscle deformations and the transmission of forces through friction.

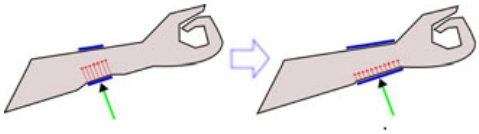

(a) Forces perpendicular to the limb's axis.

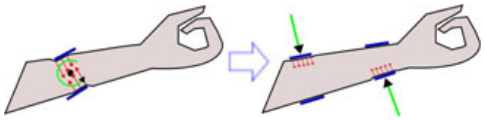

(b) Moments around an axis perpendicular to the limb's axis.

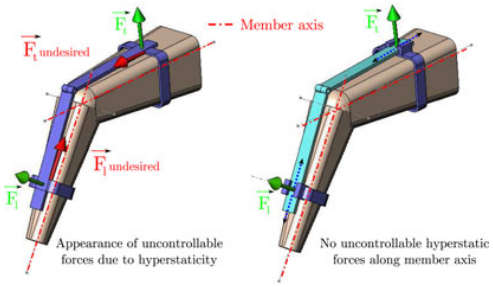

(c) Forces along limb's axis.

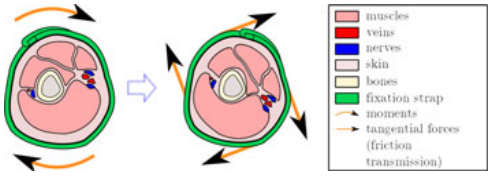

(d) Moments around limb's axis.

Figure 2.2: Possible interactions in the HRI. Taken from [22].

The kinematic compatibility between the user and the robot is the most fundamental part of exoskeleton design to solve these interactions [9]. This represents the notion that the mechanical design of the exoskeleton (even before implementing actuation, and control strategies, among other technologies) should aim to ensure comfort, safety, and adequate wearability. As such, there are three main design avenues (illustrated in figure 2.3) regarding kinematic structures of rigid exoskeletons([9]):

1. End-effector-based devices include structures, where the only attachment to the user is at the distal end of the limb [30].

2. Wearable and kinematically equivalent structures (anthropomorphic), where any DOF of the device directly correlates to a biological DOF.

3. Wearable but kinematically not equivalent structures, where the device has more DOFs than its biological counterpart.

This last structure can be considered a solution for misalignment problems that arise from anthropomorphic exoskeletons and, as such, will be addressed in section 2.2. These structures have different

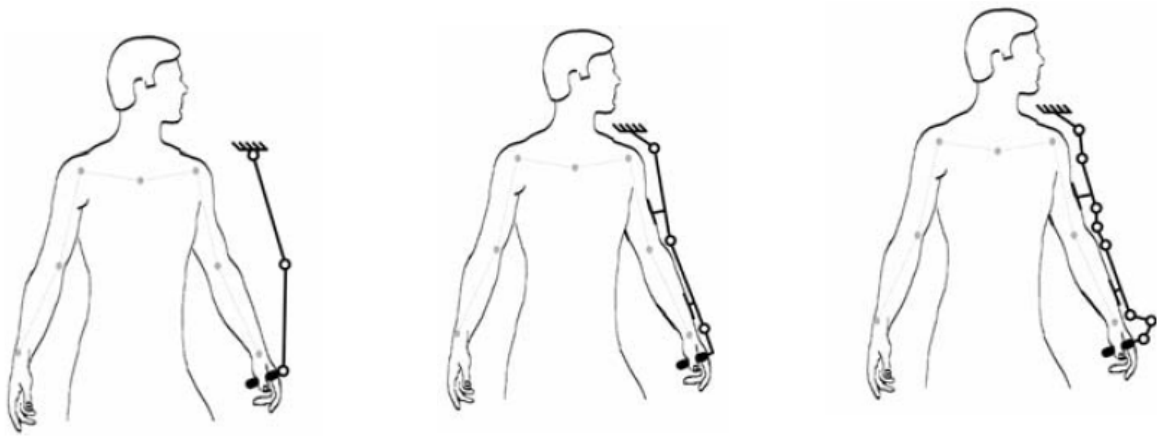

(a) End-effector.

(b) Wearable and kinematically equivalent.

(c) Wearable but not kinematically equivalent.

Figure 2.3: Different kinematic structures for an exoskeleton. Taken from [9].

advantages and in general target different problems of exoskeleton development. Anthropomorphic devices aim to directly mimic the kinematics of biological DOFs. They are the most common for rehabilitation purposes since mechanical design and control strategies allow precise and individual control of the included DOFs, which is crucial in rehabilitation environments [27].

2.1.2 Causes of Misalignment

Anthropomorphic devices, such as the ones explored in this dissertation, have to fully replicate biological DOFs. For this purpose, an exact knowledge of human joint kinematics and the location of the Instantaneous Center of Rotation (ICR) of the joint is necessary to properly transmit the required loads and torques [28] and to guarantee that neither system (the human or robot) restricts each other's movements [40]. This requirement, nevertheless, leads to four main causes of misalignment, as described by [27]:

1. Initial offset between both joints.
2. Migration of the biological ICR during gait.
3. Kinematic mismatch.
4. Movement mismatch.

These causes are the main challenges when developing anthropomorphic structures with reduced misalignment.

Regarding the first cause, there is difficulty in assessing the center of rotation of a given joint, both during the fitting of the device to the user and during use. The first issue is the high variability of morphology

between subjects. Parameters like limb length, axis orientation, and distance are necessary to have a full understanding of the closed chain formed by the human and exoskeleton. However, these parameters vary widely between subjects and are not always well understood, making it a challenge to design a structure for a large array of subjects [22, 27, 41]. Besides this issue, human joints are covered with a multitude of tissue, making it nigh impossible to properly assess ICR without imaging techniques and as such ensure correct initial alignment [9, 27]. These facts will lead to initial offsets between both joints. These are macro misalignments, with a magnitude of a few centimeters [42].

Besides this initial offset, another cause of misalignment is the migration of the ICR due to the complexity of biological joints, leading to inevitable micromisalignments. Human biological joints have, generally, translational DOFs as well as rotational DOFs. Examples of this behavior can be found both in the knee and shoulder joints (figure 2.4).

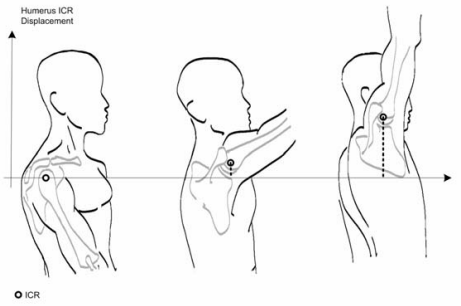

(a) Translational movement of the shoulder's ICR. Taken from [9].

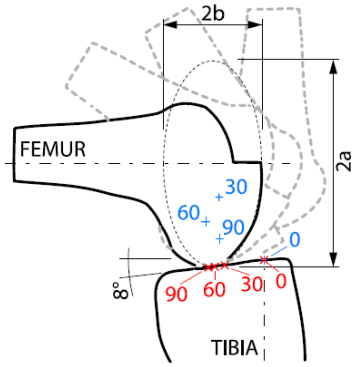

(b) Model of the knee joint. In blue, the ICR of the femur relative to the tibia for some representative knee angles. Taken from [43]

Figure 2.4: ICR migration in the shoulder and knee joints.

In the case of the shoulder joint, an upwards migration of the ICR during shoulder elevation occurs, while in the knee joint there is a rolling mechanism between the femur and the tibia during flexion that leads the ICR to migrate forward during extension. A simple hinge joint is not enough to take into account these translations and, as such, misalignments will change during a gait cycle. It is important to note that, depending on the initial offsets, the translational DOFs can lead to a reduction or increase in misalignment. However, these initial offsets are not known.

The kinematic mismatch is directly related to the complexity of human joint kinematics. Natural biological joints are not ideal hinge joints but rather have complex behaviors and surface geometries, making it complex to replicate their behavior in the robotic system [22, 30]. An example of this fact is the ankle joint, which has two hinge joints with two different non-parallel axes of rotation, both responsible for movements in the sagittal and frontal planes (figure 2.5) [44, 45]. However, most exoskeleton devices tend to simplify it as one hinge rotation (one DOF), due to the high subject variability and the trouble of

identifying the ICR [46]. Developing a single joint structure that would perfectly mimic the kinematics of the human joint would result in high costs both in the mass and complexity of the structure [27]. As such, most devices approximate the user's joint to a single DOF in the user's sagittal plane. This strategy is especially used for knee and ankle devices [27] since the torque generated by these joints in the sagittal plane comprises most of the torque necessary for normal gait, and both joints have reduced ranges of motion in the rotational DOFs of the frontal and axial planes [40]. Nevertheless, this simplification leads to a kinematic mismatch and an inevitable misalignment.

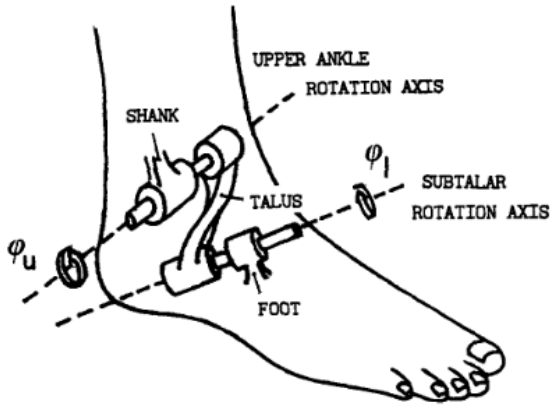

Figure 2.5: Kinematic model of the ankle joint. Taken from [44].

Finally, movement mismatch is due to the non-rigidity of the interfaces (both due to soft tissue compliance and compliance of the exoskeleton fixations), which can lead to interface migration during gait. This will negatively affect any alignment previously accomplished [27].

2.1.3 Effects of Misalignment

There is an intrinsic relation between misalignment, cuff rotation/displacement, and spurious pressure/sheer forces, as described in figure 2.6. Figure 2.6 shows three different cases that describe the relation between joint misalignment and fixation movement. In the first case, there is perfect alignment, with ideal torque transmission from the robotic device to the user, which is impossible to achieve. In figure 2.6 (b) rigid fixations are considered (no relative movement between the two) and an initial misalignment of magnitudes x and y. This misalignment leads to a resulting force F_{res} due to the acting torque T_{act}. Finally, figure 2.6 (c) presents a more realistic situation where due to the compliance of fixation (both the cuff material and soft tissue are compliant) relative movement between the two chains is allowed. Thus the same x and y misalignment cause a movement L of the cuff and a rotation γ relative to the skin. In this model, the study [30] states that misalignments as small as $y = 1cm$ and $x = 2cm$, considering angle $\alpha = 45\,\mathrm{deg}$ and link length $l = 20cm$, will lead to a displacement L of 4 cm, a sizable value that will result in sizable pressure and sheer interactions. Furthermore, a high enough

acting torque will lead to musculoskeletal injuries at the level of the joint since the scenario described in figure 2.6 (b) also partly occurs.

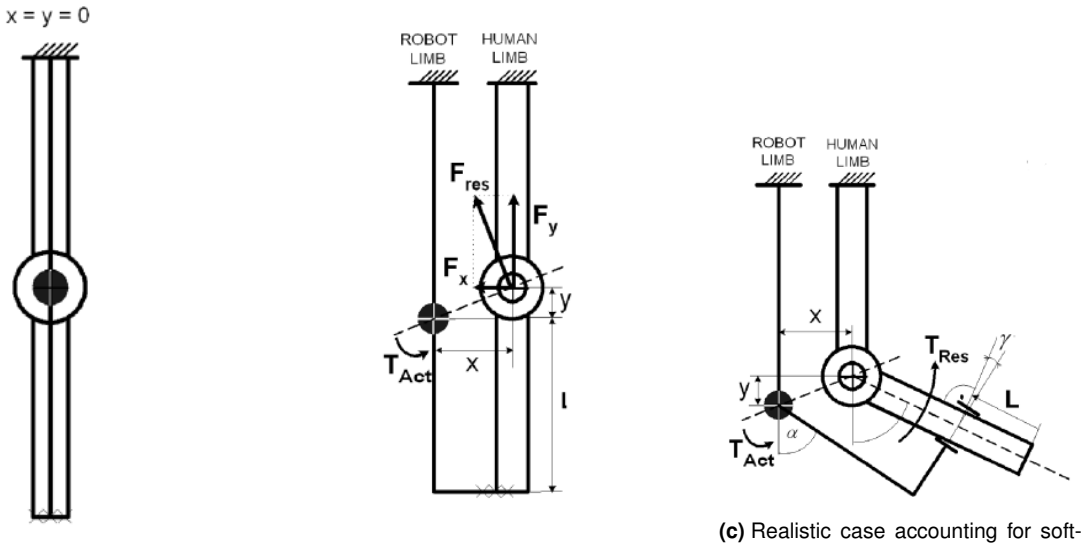

(a) Perfect alignment case.

(b) Full rigid attachment case.

(c) Realistic case accounting for soft-tissue and fixation compliance.

Figure 2.6: Schematic of the misalignment and its effects. Taken from [30].

Similar schematics have been described in [27] and [41]. Finally, study [24] highlights the pressure and sheer force hazards resulting from an unappropriated human-robot joint alignment. This study further identifies misalignment as a safety hazard of rehabilitation robots. Regarding AFOs, misalignment may lead to the movement of the calf band, causing a pistoning effect and, as such, transference of force to the leg [47].

2.1.4 Misalignment Assessment Methods

The importance of considering misalignment during the design process of an anthropomorphic exoskeleton for rehabilitation has already been stated. As such, literature shows significant efforts to assess misalignment and its effects, to guide the design process of an alignment solution. Research efforts in this field can be divided into three types: a) directly assess misalignment, mainly through motion capture; b) directly assess interactions (pressure and sheer forces) through the use of sensors like load cells and Force Sensitive Resistors (FSRs) at the interface; c) indirectly assess interactions by measuring fixation displacement. A summary of the methods described in this section can be found in table 2.1.

Table 2.1: Summary of misalignment assessment methods.

Measure	Misalignment	Fixation Displacement	Pressure	Shear stresses	Muscoskeletal Interactions
Assessment Type	Direct misalignment assessment	Indirect soft tissue interaction assessment	Direct soft tissue interaction assessment at the HRI	Direct soft tissue interaction assessment at the HRI	Direct muscoskeletal tissue interaction assessment on a surrogate
Sensors	Motion capture	Motion capture	FSR-based	3 or 6 Axis Load Cell	Dummy limb
Procedure	Human/Robot joint center assessment trough 3D modelling	Computation of the distance between two markers at the soft tissue and fixation	Capture voltage variation of FSR sensors at relevant points at the interface	Capture voltage variation of a load cell placed in the exoskeleton structure	Instrumentation of a dummy that replicates a biological joint.
Data Outputs	3D distance between joint centers	Relative displacement between exoskeleton fixation and human soft tissue.	Point pressure values and/or pressure distributions at the HRI	Force and/or torque transfer from the exoskeleton to the user	Forces and torques applied to the musculoskeletal tissue

Direct misalignment assessment is not common in the literature. One of the reasons for this paradigm is that the introduction of an exoskeleton in a motion capture environment gives rise to several problems. First, the introduction of devices like treadmills, necessary if fixed exoskeletons are being tested or for assessment of effects for longer use increases the difficulty of motion capture post-processing by obscuring relevant markers. Second, if the robotic device has a large volume it will obscure important markers or, in the worst case, the whole human joint, making it impossible to calculate misalignment. Within the scope of the research done, only two very recent studies quantified misalignment through motion capture [33, 48]. Study [48] quantified the misalignment of a knee brace by involving a dummy limb (figure 2.7 a). In this study, motion capture was used to assess only rotation misalignment. On the other hand, [33] performed sit-to-stand tests on human subjects with an active knee exoskeleton. The design of the exoskeleton, with an anterior frame instead of a lateral one, facilitated the use of motion capture since the frame did not obscure any of the markers used to capture the knee joint position. In this study, three different misalignment conditions were assessed by inducing macromisalignments both above and below the knee joint, while also applying three different actuation profiles (zero, low and high actuation). Both x and y directions were captured, providing a 2D assessment of misalignment. This study provided interesting results for misalignment assessment (both initial and its variation during gait), showing that even in what was considered an ideal case there was still misalignment between the two joints.

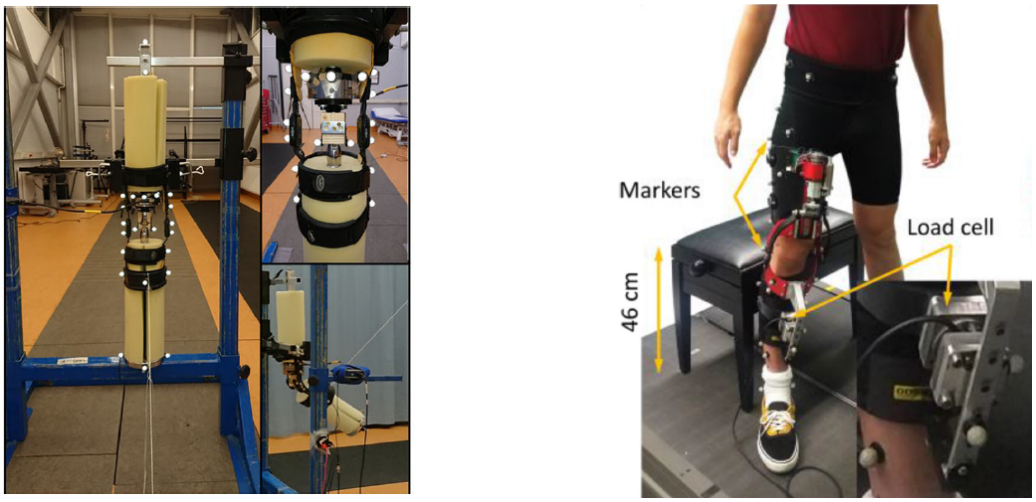

(a) Experimental setup of [48].

(b) Experimental setup of [33].

Figure 2.7: Misalignment assessment through motion capture data.

Direct assessment of interactions is more commonly applied to assess misalignment effects. This can be done at the level of the soft tissue or the musculoskeletal tissue. At the level of soft tissue, both forces (pressure and shear) and moments can be measured. The main purpose of assessing pressure forces is to perform safety validation of a given exoskeleton design [24], being relevant to measure the

pressure values and their distribution. With this in mind, FSR sensors are commonly used. These sensors are made of a material that changes its internal resistance when a force is applied. As such, when pressure is applied a voltage variation is recorded and this voltage variation is correlated with a pressure value. These sensors can be used in either a matrix-based pressure mat to capture pressure distribution or a standalone to make local assessments of pressure. Pressure tends to peak at bony prominences and along the edges of fixations, and, as such, sensors that cover a large contact area are preferred [24]. As an example, three different studies used custom-made pressure mats to assess pressure [49–51], as illustrated in figure 2.8. Study [49] used an array of 24 FSRs on the upper-arm cuff of an exoskeleton, showing that this matrix properly transferred the loads from the interface to the sensors. The study also highlights the value of having an assessment of pressure distribution in comparison with single-point data from separated sensors when assessing the ergonomic properties of the HRI. The work done by [50] used a 70-point force sensor to assess pressure at the knee and tibial interfaces of a knee exoskeleton. The device was useful in confirming an uneven distribution of pressure along the interface, specifically at the edges of the cuffs, confirming the benefit of assessing pressure distribution. Finally, [51] developed a real-time, wireless, pressure-sensing system for a lower limb exoskeleton. Pressure pads at the thighs had 6 FSRs, while pads at the shins included 4 FSRs. The main advantage of this device was its real-time wireless capabilities, with the study proving that the system allowed for real-time monitoring of pressure and the possibility of giving real-time alerts if certain pressure thresholds were surpassed.

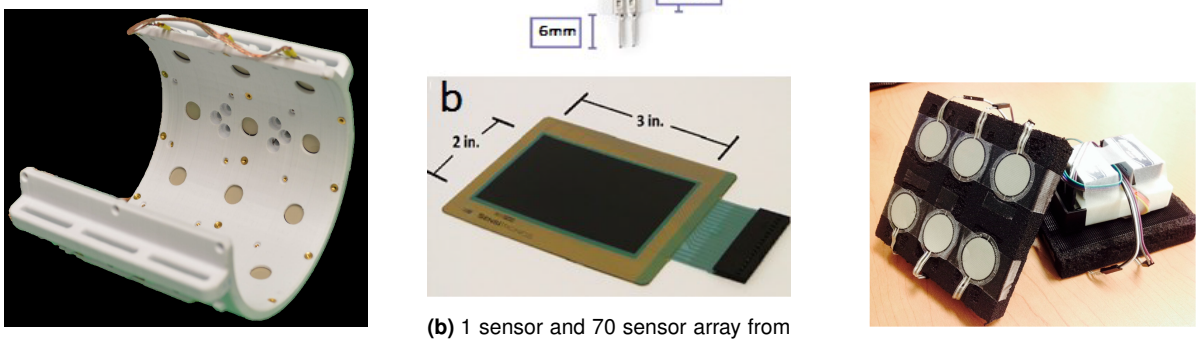

(a) 24 sensor array by [49].

(b) 1 sensor and 70 sensor array from [50].

(c) Six-sensor array from [51].

Figure 2.8: Pressure mat usage in three different studies for pressure assessment.

These measurement devices based on pressure pads have some design flaws. First, the contact surface should have low stiffness and properly conduct load, such that it does not change the interface when compared with normal use without the sensors. Secondly, they can be restrictive in their appli-

cation. By having a fixed shape and form, these sensors are not usually adjustable to different-shaped devices or locations besides their original intended use. The use of sensors in a curved matrix also affects the voltage output and, as such, compromises the results [52]. Single FSRs are, then, a reasonable and cheap alternative. They provide a more versatile use and are also thinner than conventional pressure mats, reducing the risk of interference with the contact area, with the downside of largely not being able to assess pressure distribution. Figure 2.9 shows the FSR usage in three studies [52–54]. Study [52] installed a single FSRs at 16 different HRI of a lower limb exoskeleton to assess regions of significant pressure for three different movements (two steps forward, two steps backward, and two left sidesteps) and the main differences in pressure peaks for these movements. The study was successful in capturing these results in real time. Furthermore, the same study successfully identified peak pressure differences between movements and interfaces. A similar study [54] used the same technology in conjunction with electromyography to determine the relationship between these interaction forces, muscle activation, and relative movement between the exoskeleton and the user. They found that the pressure measured by these sensors is largely due to exoskeleton movement. Finally, the study [53] used FSRs throughout the lower limb exoskeleton (9 FSRs on each shank and thigh, 18 FSRs at the hip strap, and 3 FSRs on each crutch handle to aid with locomotion) to verify if these pressures were lower than the Pressure Pain Thresholds (PPTs). PPTs are defined as the pressure threshold above which the pain caused is unbearable for the user [9]. This study shows that FSRs use is valid to assess the real-time pressure and to compare peak values with those from literature.

(a) FSRs distribution from [52]. **(b)** FSRs distribution from [54]. **(c)** FSRs distribution from [53].

Figure 2.9: FSRs usage in three different studies for pressure assessment.

Further studies have proposed the combined use of several FSRs to account for systematic errors, such as sensor drift, hysteresis, and loss of sensitivity during cyclic loading [55]. Furthermore, the introduction of another layer of material between the user and the device and issues like curvature and compliance changes the measured results, with part of the applied pressure being lost at, for exam-

ple, the edges of the sensor [56]. Interactions at the interface can also be assessed in more than one axis/DOF. There is a high number of research on developing thin sensors to use at the interfaces. However, force-transducer-based technology is still the most robust and reliable way to capture the force exchange between the user and the device [24].

While these are not placed directly at the interface, 3- or 6-axis load cells can be fitted into the exoskeleton structure to capture three types (one normal and two sheer forces) or six types (one normal, two sheer forces, and three moments) of interactions [22,31,33,57,58]. The main challenge of these sensors concerns their cost and volume, which is not small enough for the intended applications. Furthermore, they measure the net forces exchanged between the two systems, and not the sheer forces directly at the interface. These sensors can be enough to validate designs that intend to reduce these types of interactions, however, they do not allow any safety assessment regarding the forces applied to the soft tissue of the user, since they do not measure their magnitude. As such, these sensors can only be used to compare two different conditions or structures, in order to make a conclusion regarding which one transfers less force to the user. To tackle this issue, there is an ongoing effort regarding thin sheer stress sensors [24]. At the forefront in this field are sensors based on detecting capacitance changes in a polymer structure.

Direct assessment of interactions at the musculoskeletal level is still a challenge due to the invasive nature of measuring the stress in bones and joints. The options tend to rely on instrumented dummies [48]. However, replicating the conditions of a normal human-device interface remains a challenge. As described before, much of the misalignment problem is due to a kinematic mismatch between the robotic and biological joints, and the behavior of these biological joints is still not well understood. As such, the development of an instrumented dummy with simplified joints is not an option, since it would solve part of the mismatch that could lead to the interactions being measured. As such, a valid measurement system for musculoskeletal interactions has not yet been developed. A wrap-up of the state-of-the-art of direct interaction assessment at the HRI can be done from [59] which reviewed 33 studies on Human-Device interface measurement, comprising 9 exoskeletons, 7 orthoses, and 17 prostheses. Regarding the type of load measured, all studies measured pressure loads, while a fraction of these (around 15%) also measured sheer loads. No study measured only the latter, which strengthens the previous analysis made on the difficulty of assessing sheer forces interactions. Of the 33 studies, the FSR was the most used sensor (11 studies), forward by fiber optic, and the F-scan/F-socket sensors (a matrix-based sensor from Tekscan, Norwood, MA, United States), with 5 studies each. Of the 5 studies that addressed sheer interactions, 3 of them used strain gauges, 1 a capacitive sensor, and 1 a tri-axial force transducer, all custom-made for the given studies. The fact that 16 out of the 33 studies (the largest group of sensors) used FSRs-based technology shows that, overall, they are a more robust and consolidated technology.

Moreover, sheer forces have a larger effect on soft skin injuries [24]. This fact consolidates the need for

indirectly assessing these sheer forces. Displacement is measured through motion capture analysis in two different studies [60, 61]. Even though the capturing technology is the same as for capturing misalignment, there is no need for model building or kinematic calculations. In fact, the main theory behind the following studies is that a fixation displacement, i.e., relative movement between a strap/cuff and the human soft tissue, will lead to these interaction forces. This displacement is measured by subtracting the positions of a marker in the user's limb and a marker in the fixation system (strap/cuff). As such, measuring these displacements can lead to an indirect assessment of soft tissue sheer interactions, as explored in the following studies. Although there is not, in practice, quantification of these forces (unless an analytical model of the HRI had been developed and validated beforehand), the working hypothesis of these studies is that fixation displacement in a number of different situations can be compared, and a conclusion can be made about which situation has higher/lower interactions. A study [62] measured deformation on a lower limb walking orthosis. In this study, motion capture data was used to assess marker positions and, from these positions, angular variations between structural segments of the orthosis. As such, the method is capable to detect even small deformations in a rather rigid orthosis, with distances between markers as small as 3.2 mm being captured. Another study [60] used the same theoretical basis to capture displacements in an exoskeleton for the hand and wrist. The method was especially useful since normal kinematics could not be captured due to the size of the device. The scale of the experiment was in millimeters, with displacements ranging from 0.2 to 40 mm, with a mean noise level of 0.23 mm and an upper limit (95% confidence interval) of 0.59 mm. This study gives a clear indication that this method can be used not only for small initial distances but also for small displacements. The work in [61] used the same method but to assess the displacement of the cuffs of a physician assistant robot, which was then used to estimate interaction forces through a mathematical model. In this case, markers were used to capture the angle of each link of the robot, since the cuffs were connected to these links. Before each trial, the initial cuff position was captured in relation to each link. Afterward, the cuff position was traced by monitoring each link's position. This is an alternate method to [60] which, in theory, can be more robust. Since it is not based on the position of a single marker, it will suffer less from occasional errors like marker drift or dislodging. The displacement results were then used to fit a spring-damper model that describes the HRI. Overall, these studies show that fixation displacement can be properly assessed from motion capture data and that this method is valid for displacements of a magnitude of a couple of millimeters. Figure 2.10 gives an overview of these studies.

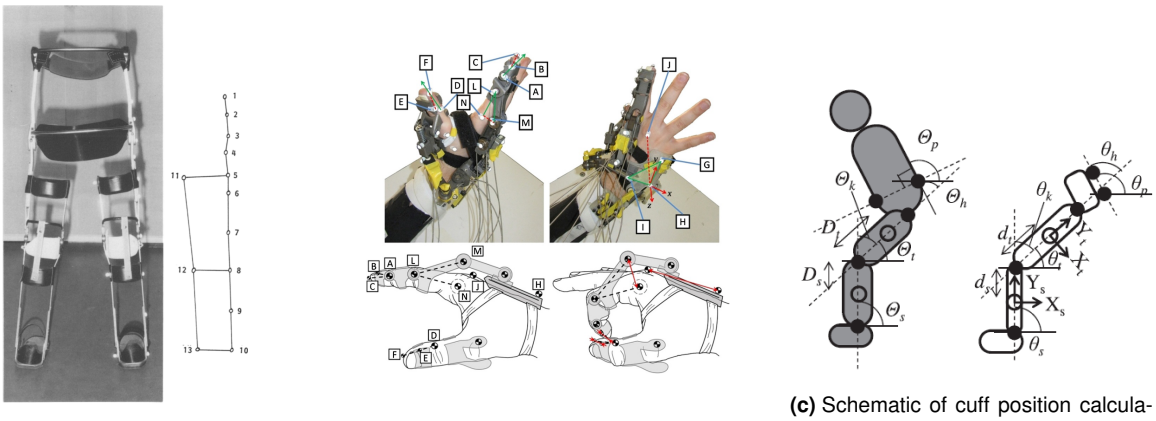

(a) Orthosis (left) and marker distribution from [62].

(b) Marker distribution and distances calculated from [60].

(c) Schematic of cuff position calculation (hollow circles) from link angles, from [61].

Figure 2.10: Examples of fixation displacement assessment.

2.2 Alignment Solutions

2.2.1 Introduction on Alignment Solutions

As stated previously, one of the first steps in designing the structure of an anthropomorphic, rigid, exoskeleton, is to consider its kinematic compatibility with the human system. After evaluating the structure and quantifying misalignment and interactions in an experimental setting, alignment solutions should be idealized and implemented. As such, a review of available solutions and their characteristics is presented.

A review of alignment studies [27] states three requirements these solutions should have. The first is kinematic compatibility, regarding which the same study [27] states that alignment solutions should introduce elements that allow for better initial, and during gait, alignment, and should not restrain the biological Range of Motion (ROM) of the user. The second requirement is a metabolic benefit. Implemented solutions should be designed to be lightweight and compact, such that they do not compromise the intended metabolic benefit the exoskeleton provides to the user. This can happen when the solution either significantly increases the robot's inertia (reducing transmission efficiency) or frees certain DOFs in the kinematic structure, where part of the torque will be transferred to.

The final requirement is that they should not compromise the user's acceptance. One of the reasons for reduced user acceptance of assistive devices is a lack of consideration for the user's opinion and an incorrect assessment of the user's needs and priorities [23]. According to [27], important aspects related to user acceptance are effectiveness, durability, safety, and comfort, which should be taken into consideration when designing assistive devices.

Effectiveness is related to how well the device reaches its main goal (metabolic benefit) and how little it

hinders the user (kinematic compatibility). Durability is that the device should be robust and durable and require low maintenance. Safety is directly related to the health risks the device might pose to the user. As such, alignment solutions should not compromise other aspects of the user's safety. The final aspect is comfort. Even if a device is perfectly safe, durable, and effective, users are more likely to not use a device that is uncomfortable or obtrusive.

A narrative review of available alignment solutions in the literature has divided these solutions according to their working principles and ranks them according to several performance indicators [27]. An overview of these solutions can be found in figure 2.11.

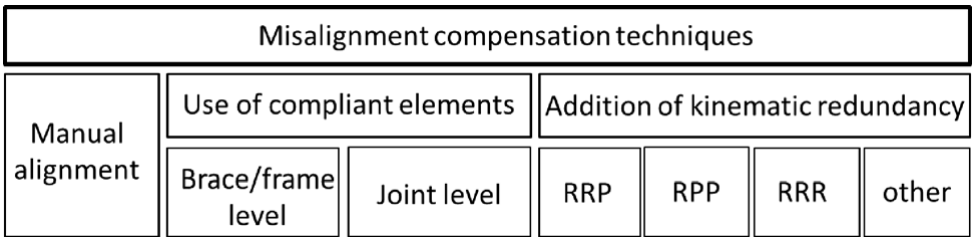

Figure 2.11: Alignment solutions. The kinematic redundancy subdivision states the most common DOFs added, where R - revolute and P - prismatic. Taken from [27].

Manual alignment solutions are the simplest to design [27]. The strategy behind this implementation is that the robotic joint location can be changed according to the user's joint location. This can be done horizontally, vertically, or even by rotating the structure. This design mostly addresses macromisalignments, since it is not feasible for structures to allow for adaptation of a joint's location of more than half a centimeter at a time. Furthermore, the main challenge behind this design is correctly identifying the biological joint's location. This process will always carry a systematic error since it is not possible to determine the exact ICR of a joint due to the tissues that cover it [9, 27, 31]. Furthermore, the slippage of cuffs and braces that connect the user to the robot, coupled with the natural compliance of the skin, will further alter the joint's position and remove part of the alignment this solution initially provided [63, 64]. While a skilled operator, with knowledge of the relevant anatomical landmarks, can provide good results [65], studies have shown that, even with proper alignment, there is always some misalignment. Study [32] reported misalignments of 10 cm, while [33] reported vertical misalignments of around 5 cm and horizontal misalignments of around 3 cm. Nevertheless, this solution can solve a big part of the initial offset, and it is relatively simple to design and implement. However, it does not cover the micromisalignments that come from a kinematic mismatch between the two joints or from the migration of the joint's ICR.

The introduction of compliant elements is another strategy. This can be done either at the structure/fixation level (frame and brace) or at the joint level. At the brace level, the idea is not to solve misalignment but rather to reduce its effects by changing the characteristics of the interface. A more compliant mate-

rial at the interface has been shown to reduce the forces directly transferred to the user [31]. However, part of these forces will arise at the level of the interface due to the relative displacement between the cuffs and the human limb (see figure 2.6 and [65]), reducing the user's comfort. Compliance can also be incorporated at the level of the frame. The principle is to allow some deformation (effectively releasing a DOF with a small ROM) at the structure level. These solutions allow for reducing misalignment during gait (e.g. by allowing the device to follow the normal movement of the user's limb). As such, these solutions can be implemented by releasing biological DOFs that were previously constrained or by allowing small ROMs in the planes other than the actuation through the use of flexible materials.

Compliance can also be implemented at the joint level where the initial single DOF mechanism is replaced by a compliant coupling. This releases DOFs since the connection is now able to deform, which can be accomplished usually by using shape-changing materials. These DOFs have necessarily small ROMs [27].

The most complex strategy in alignment solutions is adding kinematic redundancy in the exoskeleton's kinematic chain [27]. This type of solution has been given increased attention [30, 32, 58, 66]. The working principle is that by adding more DOFs to the structure of the exoskeleton than the ones actuated it can better approximate the kinematics of the user. These mechanisms can allow for movement of the exoskeleton in relation to the user, in order to unload the user of the interactions of joint misalignment or decrease kinematic mismatch by releasing additional DOFs. Contrary to brace and frame compliance, these DOFs are usually implemented in series with the actuated DOF and have larger ROMs. A schematic of the purpose of an RRP (revolute-revolute-prismatic) joint configuration can be found in figure 2.12.

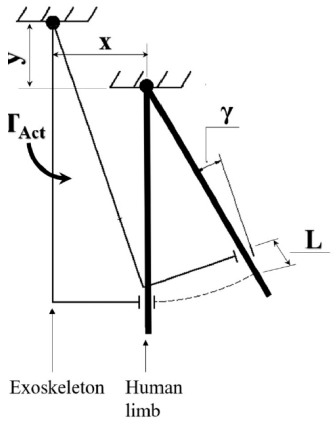

(a) In this case, an x and y misalignment leads, through the action of torque, to a displacement L and a rotation γ of the cuff .

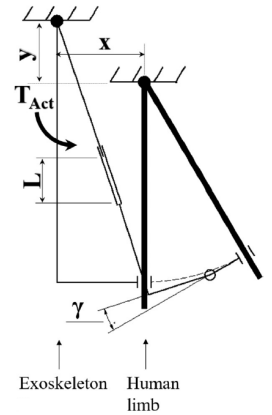

(b) In an RRP joint configuration, the prismatic joint will compensate for the displacement L, while the revolute joint will compensate for rotation γ.

Figure 2.12: Example of frame compliance solutions in a hip (a) and knee (b) exoskeletons. Taken from [27]

These solutions can be implemented with two different rationales. One is when there is a need to

match the kinematics of the human limb, so the fixations follow the user's movements. The intent is to solve the problem of hyperstaticity, where incorrect alignment leads to restrained mobility of the kinematic chains [28]. Another is when, either through analysis of the system kinematics or previous experiments, there is some knowledge of the movement at the fixations and, as such, the added DOFs counteract this movement. Within this last case, several studies have tried to develop theoretical frameworks by which the human-robot system can be analyzed and a conclusion can be made about which DOFs should be released [22, 28, 41]. While these studies are not the focus of this work, all three frameworks allow the user to make an informed choice regarding which DOFs to implement into the structure, based on different assumptions. All three studies used their frameworks in specific devices and validated the resulting mechanisms in real life. All showed a significant reduction in interactions.

The literature review [27] also set a performance scoring, that can serve as a barometer when deciding which solutions to implement. Each type of solution was rated according to compensation ability (how well the solution solves the misalignment problem), volume, mass (both pertain to the device's capability of reducing the user's metabolic cost), simplicity, expandability (how well the solution expands from a 1 active DOF exoskeleton to several DOFs), force transmission, angle relation between the two joints, and donning procedure. Each solution was rated on a 5 point scale (- -, -, ±, + and ++). The results are summarized in figure 2.13.

		Compliance		Kinematic redundancy			
	Manual alignment	*Brace/frame*	*Joint*	*RPP*	*RRR*	*RRP*	*Other*
Literature							
Devices utilizing the strategy	[14,77–82]	[84,85]	[28,86,87]	[11,39,89, 93,95,96,107]	[10,39,58,74,88,97, 101,104]	[35,53,92]	[60,71,105,109, 111,113]
Evaluation							
Compensation ability	±	±	±	++	+	++	++
Volume	++	++	++	− −	+	+	+/−
Mass	++	++	++	− −	+	+	+/−
Simplicity	++	+	+	−	−	−	− −
Expandability	− −	+	+	++	−	− −	++/− −
Force transmission	++	+	+	−	−	−	++/− −
$\delta\alpha_{exo} = \delta\alpha_{bio}$	+	−	−	++	+	− −	++/− −
Donning procedure	− −	− −	− −	++	+	++	+/++

Figure 2.13: Performance rating of each solution type on a 5-point scale, from [27].

Firstly, manual alignment solutions score very well on volume, mass, simplicity, force transmission, and angle relation. It is not surprising, as such, that most of these exoskeletons have some type of manual alignment implemented into their structure. In fact, they are easy to implement and do not compromise the main purpose of the device due to their low mass, volume, and high force transmission. The compensation ability of these solutions is not stellar but is also not poor. This is due to their ability to account for macromisalignments while still not being able to solve micromisalignments. Expandability is very poor. While the sagittal axis of rotation can be found more or less through visual means (mostly in

the ankle and knee joints), other axes are much more hidden (e.g. hip rotation axis, which goes from the center of the thigh through the torso [27]) and as such, manual alignment is very imprecise. Donning procedure is also more complex since the device needs to be fitted to the specific location of the user's joint.

Compliance solutions score well in all departments besides compensation ability, angle relation, and donning procedure, similar to manual alignment. The purpose of these solutions is to take into consideration also micromisalignments. However, they are always dependent on the initial alignment, since a small correction on a joint that wasn't properly aligned will be seldom effective.

Finally, kinematic redundancy solutions are, generally, highly effective in compensating for misalignment. In theory, these solutions employ several components and joints, that take into account most if not all of the misalignment's causes and effects. The studies analyzed show these same results. This, however, leads to bulky, heavy, and complex structures, which are hugely detrimental to the metabolic performance of the device. However, this can be counteracted through the continuous research of more elegant solutions. Furthermore, for rehabilitation purposes, part of the components can be implemented on a fixed frame and, as such, have less effect on the exoskeleton's mass and inertia. Furthermore, due to the number of DOFs, force transmission is also lower, since it is difficult to design kinematic chains where part of the assistive torque is not lost to the additional DOFs.

A parallel avenue for addressing misalignment problems is through the development of soft or compliant exoskeletons, commonly denominated exosuits. Compared to the three kinematic structures before, which pertain to rigid exoskeletons, soft exoskeletons use soft and compliant structures at three different levels: actuation, structure, and interface fixation [67, 68]. These exoskeletons are made up of an integrated garment that attaches to the body, a textile that is responsible for force transmission and actuated segments [67]. The misalignment issue and its effects come into play at the level of the structure and/or of the interface. Flexible materials like neoprene or common textiles in the form of straps, sleeves, socks, boots, etc. are usually used for these applications [68]. The advantage of these devices pertaining to misalignment is that, since they do not contain a rigid structure, human kinematics are seldom restricted, misalignment issues are diminished [69], and their increased flexibility allows for larger tolerances for misalignments [70]. Furthermore, the exosuit can actuate more than one joint simultaneously [69].

One drawback is that the device can not support compressive loads, with the musculoskeletal tissue of the user being responsible for supporting both the normal loads present and the ones generated by the device [67]. This can be problematic if the user has issues like chronic pain or weaker musculoskeletal tissue due to a prolonged hospital stay, for example. Finally, exosuit design's generally lead to lower assistive forces, both due to the actuation and the structure. On one hand, the lack of a rigid structure means that the introduction of generic, powerful actuators (e.g. electric based) is impossible, and other,

less powerful, actuation strategies based on pneumatic or elastic actuators have to be chosen [68]. When electrical motors are used, the transmission is cable-based, where power is also lost due to cable friction [70]. On the other, the lack of a load-bearing, rigid structure lowers load transmission between the actuator and the user [67]. For these reasons, soft exoskeletons have not performed better than conventional rigid exoskeletons in a rehabilitation setting [67].

2.2.2 Search Methodology

A narrative review was made of existing exoskeletons that included at least one ankle joint and a misalignment compensation technique. To do this, a search was made for scientific publications in four online databases (PubMed, WoS, Scopus, IEEE Xplore) using the following search terms: (Exoskeleton OR Orthosis) AND (Alignment OR Misalignment) AND (Lower Limb OR Lower Extremity OR Leg OR Ankle). From this point, records that did not concern the design of a single exoskeleton/orthosis (e.g. review studies, theoretical frameworks, or biomechanical studies) were removed, as well as reports that detailed exoskeleton designs that did not include an ankle joint. Only reports in English were included. Reports were evaluated through the following inclusion criteria: i) the device described included at least one ankle DOF; ii) the device described included at least one alignment solution other than manual alignment; iii) a working prototype of the device was manufactured and validated in a real-life environment. The following details were extracted for each report: i) actuated DOFs; ii) actuation type; iii) alignment solution; iv) weight of the device.

2.2.3 Results

Figure 2.14 summarizes the literature search process. The literature search resulted in 198 publications, where 56 were removed as duplicates. An initial screening of the resulting 142 reports was done by the study's abstract and introduction, and each study was tagged according to its focus/objective and if it included a single exoskeleton design, in which joints were a part of the device. The resulting 57 reports were subject to a full reading. The final count was 25 reports (see figure 2.14), which described the design of 19 different devices. With this process, a database of important knowledge regarding lower limb exoskeletons was constructed, each tagged according to their objective and subject. Results of this review can be found in table 2.2.

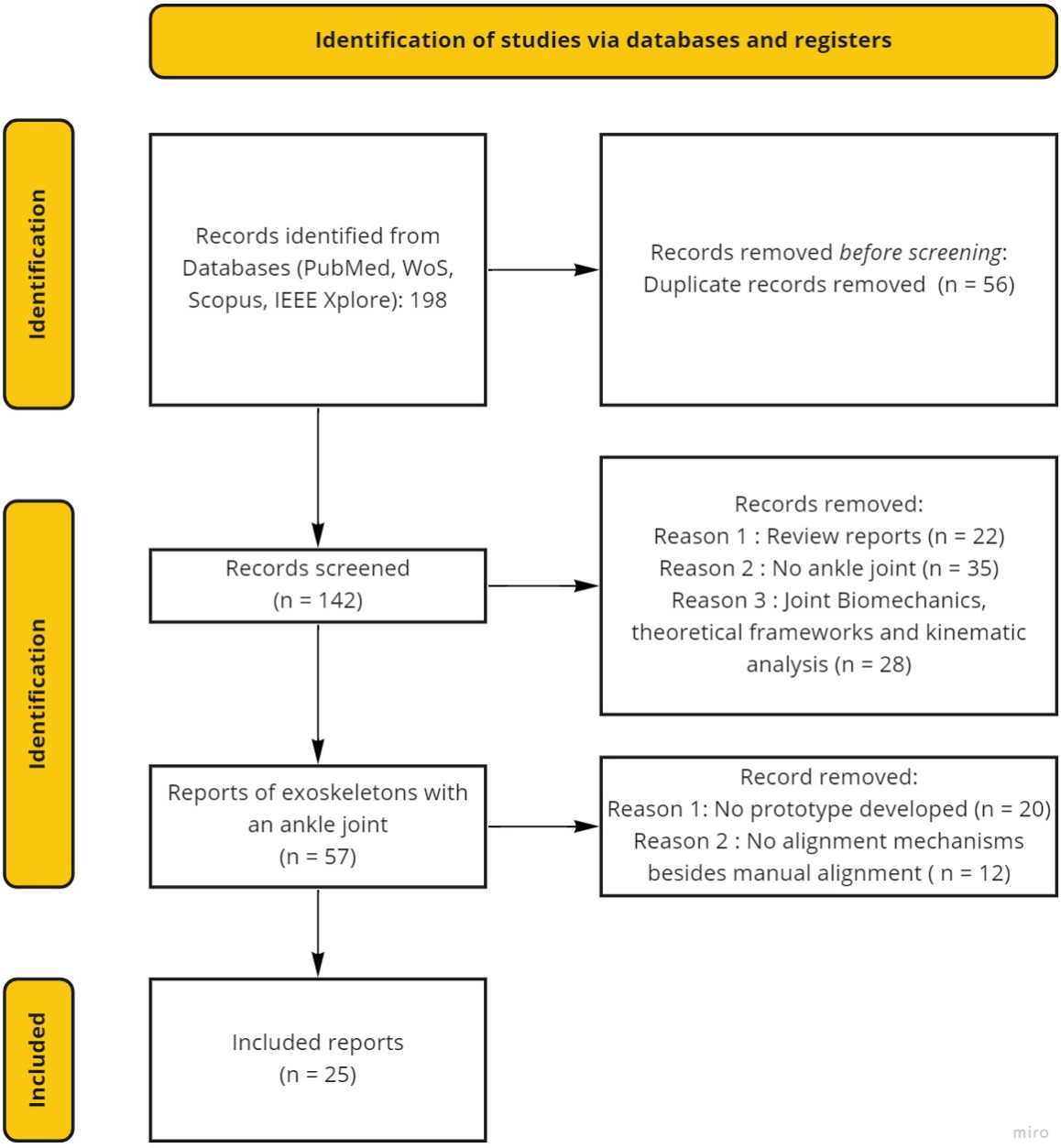

Figure 2.14: Diagram of the literature selection process following PRISMA guidelines.

Table 2.2: Summary of the state of the art of alignment solutions found in the literature. Degrees of freedom are abbreviated: F/E - Flexion/Extension; Ab/Ad - Abduction/Adduction; D/P - Dorsiflexion/Plantarflexion; Iv/Ev - Inversion/Eversion. Distal mass represents the reported mass of the device at the ankle joint. An NA in this column represents studies that did not report mass at the ankle.

Device Name	Actuated Joint	Actuation type	Solution Type	Alignment Solution	Distal Mass (kg)
Quasi-passive exoskeleton [71]	Knee (F/E)	Variable damper	Compliance	Carbon fiber plate attached to a shoe for Iv/Ev	1.46
AFO with MACCEPA [20]	Ankle (D/P)	MACCEPA	Compliance	Toe and heel carbon fiber plates	1.7
Lighweight AFO [72]	Ankle (D/P)	Eletrical	Compliance	Carbon fiber compliant braces	0.5
Ultra-lighweight AFO [73]	Ankle (P/D)	Electrical and tendon-driven	Compliance	Carbon fiber compliant footplates and shank cuffs	0.83
MIT Exoskeleton [74]	Ankle (D/P, Iv/Ev)	Eletrical	Kinematic redundancy	Passive ankle (IR/ER) joints	$<$3.6
FB-AXO [75]	Hip (F/E) and Knee (F/E)	Eletrical	Kinematic redundancy	Passive hip (IR/ER, Ab/Ad) and ankle (D/P and Iv/Ev) joints	NA
Reconfigurable ankle orthosis [76]	Ankle (D/P)	Eletrical	Kinematic redundancy	Passive ankle (Iv/Ev) with 3UPS reconfigurable to 3RPS-R	5.35
2 DOF AFO with shank brace [15]	Ankle (D/P)	Eletrical	Kinematic redundancy	Passive ankle (Iv/Ev) joint with torsion spring and damper	2.5
BLEEX Exo [77–80]	Hip (F/E, Ad/Ab) Knee (F/E) Ankle (P/D)	Hydraulic	Kinematic redundancy and compliance	Passive ankle (IR/ER, Ab/Ad), flexible toe (P/D) joints	NA
AFO with 4-bar mechanism [81]	Ankle (P/D)	Electrical and tendon-driven	Kinematic redundancy and compliance	Passive ankle (Iv/Ev) joint and a 4-bar polycentric joint	NA
HUMA [82]	Hip (F/E) and Knee (F/E)	Eletrical	Kinematic redundancy and compliance	Passive ankle (P/D, Iv/Ev) and compliant spring steel at foot sole	NA
S-Assist [83]	Hip (F/E) and Knee (F/E)	Eletrical	Kinematic redundancy and compliance	Passive ankle (Iv/Ev, IR/ER) joints and compliant frame	NA
CJAE - 3 DOF [84]	Ankle (D/P, Iv/Ev)	Eletrical	Kinematic redundancy and compliance	3 DOF ankle and custom-fitted compatible axis	2.6
Soft exosuit [85, 86]	Ankle (P/D)	Eletrical and tendon-driven	Soft	Soft exosuit	0.9
Bio-inspired exosuit [87]	Ankle (D/P, Iv/Ev)	Pneumatic	Soft	Soft exosuit	NA
Soft Ankle Orthosis [18]	Ankle (P/D)	Eletrical and tendon-driven	Soft	Soft frame	1.54
Strap-based soft AFO [88]	Ankle (P/D)	Eletrical and tendon-driven	Soft	Strap-based	1.2
WAXO [89]	Ankle (P/D)	Eletrical and strut-based	Soft	Soft-frame	0.35
MIT Soft Exo [90, 91]	Ankle (D/P)	Eletrical and strut-based	Soft	Soft-frame	2.3

This review found four devices that implemented only compliant solutions, either at joint or brace levels.

The design of a quasi-passive exoskeleton is detailed in [71]. In this exoskeleton, misalignment compensation is accomplished by attaching a carbon fiber plate to a shoe, which increases compliance for inversion/eversion. The overall distal mass, including actuation, is 1.46 kg.

The work presented in [20] is based on an active AFOs, with a dorsiflexion/plantarflexion DOF powered by a Mechanically Adjustable Compliance and Controllable Equilibrium Position Actuator (MACCEPA). The alignment solution is based on two carbon fiber plates at the level of the toe and heel (principle of frame compliance). The compliance of this material allows for small movements in the sagittal and frontal planes. The overall mass of the device is 1.7 kg, including 1.1 for the actuation.

The AFO designed by [72] is a lightweight alternative. The only active DOF is the dorsiflexion/plantarflexion of the ankle. The misalignment compensation is achieved through the use of a compliant brace at the level of the shank and a compliant lower foot plate, both made of carbon fiber. The device weighs 1 kg, with 0.5 kg at the waist and 0.5 kg at the ankle.

The design from [73] also focuses on a lightweight device where misalignment compensation is realized at the level of the cuffs and foot soles. These fixations are composed of compliant carbon fibers that increase comfort at the fixations and help reduce the effects of misalignment, realizing an alignment solution through brace compliance. The full design weighs 2.51 kg, distributed as 1.68 kg at the waist for actuation and 0.83 kg at the ankle.

Four more devices were found to implement only kinematic redundancy solutions, mainly related to the release of the inversion/eversion DOF.

The Anklebot design of the Massachusetts Institute of Technology (Massachusetts Institute of Technology (MIT)) has the main purpose of training stroke patients [74]. The main differentiating factor of this device is its 3-DOF approach which allows for full rotation of the ankle joint. Two of these DOFs are actuated (dorsiflexion/plantarflexion and inversion-eversion). Internal/external rotations are allowed since there is no structure at the level of the ankle/foot other than a pair of shoes. The rest of the device is fixed to the user through a knee brace, a shoulder strap, and a strap over the shoe. This device is not considered a soft exoskeleton, since the connection is made through braces. The overall device weights less than 3.6 kg, with the actuation weighting 2 kg.

The work from [75] presents the design of a full-body exoskeleton called ”FB-AXO”. This exoskeleton has two modules for the lower and upper limbs and its main application is for daily use. The misalignment compensation at the ankle level is realized through two passive revolute joints that allow for the two DOFs described before, corresponding to a solution of kinematic redundancy. The overall lower body modulus weighs 13 kg. The weight of the ankle modulus is not stated.

The device in [76] is a reconfigurable ankle rehabilitating robot for training balance/proprioception and

ROM/strengthening exercises. The design implements two in-series revolute joints that allow for plantarflexion/dorsiflexion and supination/pronation (a complex movement that has both inversion/eversion and abduction/adduction). Furthermore, this device implements two kinematic redundancy solutions, a 3UPS mechanism (universal-prismatic-spherical) and a 3RPS-R (revolute-prismatic-spherical) mechanism, with the former improving alignment for ROM/strengthening exercises and the latter for balance/proprioception training. The actuation modulus weights 3.75 kg, while the total AFO weights 5.35 kg.

The design from [15] is another two-DOF AFO. In this case, both dorsiflexion/plantarflexion as well as inversion/eversion are freed. The effectiveness of the solution is increased through the introduction of a structure that locates the axis of rotation of the DOFs of the device, allowing for better alignment. The frame of the device weights 1.25 kg, while the actuation weights another 1.25 kg.

The remaining five rigid devices implemented both kinematic redundancy and compliance solutions.

The BLEEX exoskeleton, designed to augment human gait in overground walking, has a complex kinematic chain, with 8 DOFs per lower limb, including four powered DOFs. Thus, it is an important case of the implementation of several DOFs in a single structure to increase mobility and comfort. All passive DOFs were implemented as revolute joints (kinematic redundancy principle) with the exception of the toe DOF, which is released by adding a compliant material at the footplate (solution trough frame compliance) [77–80]. The mass of the ankle modulus is not mentioned.

The design in [81] is of an AFOs that addresses the issue of kinematic mismatch by including a 4-bar linkage mechanism at the level of the ankle joint. The 4-bar linkage is implemented in the AFOs's joint, in order to mimic the natural movement of the ICR during dorsiflexion and plantarflexion and reduce misalignment. This prototype was designed on top of a previous iteration where a 2 DOF structure was realized by including both talocrural and subtalar joints in the AFOs, with their centers rotating not in the sagittal plane but around the planes of the biological joints [92]. This improves alignment through better kinematic compatibility with the human joint. The overall device weighs 1.44 kg, 0.88 kg without the actuation.

The Human Universal Mobility Assistance (HUMA) lower limb exoskeleton described in [82] includes 12 DOFs to assist with human locomotion. The misalignment compensation at ankle level is realized in a spring steel plate for foot sole compliance and two springs, one for inversion/eversion and one for dorsiflexion/plantarflexion, fulfilling an alignment solution through compliance. The weight of the ankle modulus of the device is not mentioned.

The S-assist is a lower limb exoskeleton with 7 DOFs per leg. All three DOFs at the ankle (plantar flexion/dorsiflexion, inversion/eversion, and internal/external rotation) are freed and passive [83]. As such, this kinematic structure is an example of misalignment compensation through kinematic redundancy. Furthermore, this design presents a compliance mechanism consisting of a buckle-free support frame

that reduces undesired interactions. The weight of the ankle modulus of the device is not mentioned.
Finally, the C-JAE is a 3-DOF robotic exoskeleton with compatible joint axis [84]. In this device, the dorsi/plantarflexion axis was mapped to the talocrural joint according to anatomical data from the literature. Furthermore, the oblique axis was then custom-fitted to a 50th-percentile male subject. Accordingly, the inversion/eversion DOF was also mapped to the subtalar axis and also custom fitted to a 50th-percentile male subject. The internal/external rotation was implemented through a curve guide and the corresponding rail was fitted on the cuff mount. The overall weight of the device is 2.6 kg, 1.245 kg without the actuation.
Further devices are within the category of soft exoskeletons. Soft exoskeletons and exosuits solve the misalignment issue by using soft structures that envelop the actuated joint [18, 85–91]. These devices are part of the results of this narrative review to bring new contributions for addressing misalignment problems using lightweight, non-anthropomorphic solutions. An overview of these 19 devices can be found in figure 2.15.

2.2.4 Discussion

Of the 13 rigid devices, all included some type of vertical manual alignment, such that they are usable for users with a range of different heights. No device supported horizontal adjustment of the joint's location. Approximately 69% included kinematic redundancy solutions, either by releasing biological DOFs or introducing non-biological DOFs. 61% of the devices implemented compliant solutions. Of these devices, all but one included carbon fiber plates in their structure, which is an indicator for the use of this material, since it both ensures some motion in the desired axis and provides the necessary rigidity and strength for assistive applications. However, this material can increase the cost of the whole product when compared with more conventional lightweight materials like aluminum. Nevertheless, it is an adequate solution both at the fixation level and to allow for some movement at the joint level.
All rigid solutions allowed for at least some movement of the inversion/eversion DOF of the ankle. Compliant solutions fulfilled the release of this DOF through the introduction of a compliant material at the joint level and, as such, have an inversion/eversion DOF with reduced ROM. Kinematic redundancy solutions implemented specific joints to free this DOF and as such allow for better kinematic compatibility and a ROM closer to biological during gait, with the disadvantage of increased weight, complexity, and worse torque transmission. Nevertheless, this shows that the release of this DOF is fundamental in addressing one of the causes of misalignment, the kinematic mismatch. Whether this is implemented through compliant kinematic strategies depends on the device's characteristics and application. In devices intended for gait rehabilitation where full support is required and less importance is given to torque transference, a small ROM of the inversion/eversion DOF can be beneficial. However, this solution is not possible when the design intends to be as comfortable as possible. For this, an inversion/eversion

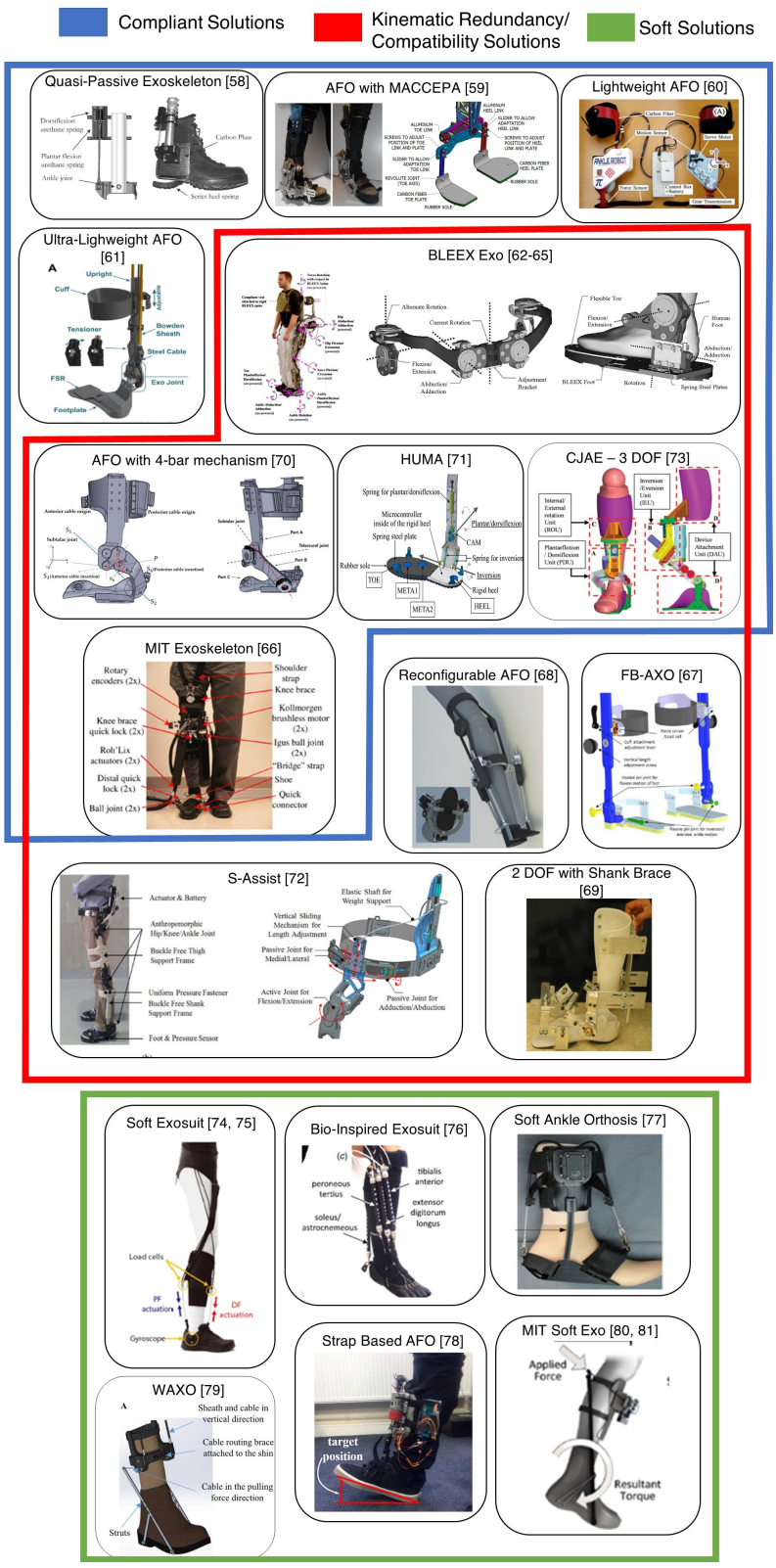

Figure 2.15: Ankle alignment solutions found in the literature.

that is closer to the full biological ROM is necessary, which can only be achieved through kinematic solutions. Furthermore, kinematic redundancy solutions lead to devices with higher mass, which can compromise user acceptance by affecting comfort and usability, as well as torque transmission due to the increased inertia. The average mass of devices that only implemented kinematic solutions is 3.82 kg, while devices that only implemented compliant solutions had an average mass of 1.12 kg. Nevertheless, the increased weight can be acceptable if the application warrants the introduction of kinematic solutions. Kinematic redundancy solutions can also be implemented by adding non-biological DOFs. These solutions not only increase the ROM but can also compensate for fixation displacements. The only device that introduced non-biological DOFs [76] showed promise due to its versatility in tackling two different rehabilitation scenarios. However, the solutions greatly added complexity and mass to the structure, which resulted in this device being the heaviest among the studied AFOs.

Of the 19 devices considered in this section, 6 (approximately 32%) were based on a soft design. This shows that soft orthosis and exosuits are becoming increasingly prominent avenues for exoskeleton research, considering this research is still in its infancy. The oldest study of a soft design is from 2013, while the oldest study of an anthropomorphic design is almost a decade older. These devices still have some disadvantages to be addressed, however. First, all devices except one relied on remote actuation, which greatly reduces transmission efficiency due to cable friction and mechanical inconsistencies related to cable length and stiffness [73]. Furthermore, despite being based on materials like textiles, these devices still carried a considerable mass. This mass is generally due to the actuation and is located proximally. In comparison, two lightweight designs of rigid AFOs achieved distal masses of 0.5 kg and 0.83 kg, which is remarkably lower, although located at the ankle. Considering the issues soft solutions have concerning power transmission, which results in a reduced metabolic benefit to the user, a relatively high distal weight will further heighten this design flaw.

2.3 Conclusions

Understanding the causes and effects of misalignment and its connection with spurious forces and torques at the HRI is necessary if one wants to develop effective alignment solutions. Soft-tissue and musculoskeletal adverse effects represent most of the exoskeleton-related complications [25]. These arise from interactions at the HRI, with one of the causes of increased interactions being human-robot joint misalignment. This is a phenomenon present in anthropomorphic devices that has four main causes. Studies have shown that this misalignment leads to increased forces and torques at the HRI [27–32], ultimately posing as a safety hazard for the user [24]. As such, a proper assessment of misalignment and related effects should be done.

This can be done through four different types of measures. Direct misalignment assessment can be

done through IR marked-based motion capture. It is seldom used in literature, with a possible reason being that the introduction of an exoskeleton and/or a treadmill generally obscures the necessary markers to assess both human and robotic joint positions. Interaction as the HRI can be assessed directly through the use of sensors or indirectly through IR marked-based motion capture. Direct assessment can further be divided by the interactions measured. Pressure interactions are generally assessed using FSRs, either singularly at discrete points at the interface or organized in a matrix. Both techniques allow for real-time average and peak pressure measurements and their measures can be comparable to safety values from the literature. Shear interactions at the fixation can be assessed either directly through the use of 3 or 6-axis load cells or indirectly through motion capture data, where the distance between two markers (one in the user's limb and one in the device's fixation) is used to assess fixation displacement relative to the user's soft tissue. The use of load cells integrated into the device's structure has been successful in capturing the transference of forces and torques to the user. Fixation displacement trough motion capture is effective for displacements of a couple of millimeters [60–62]. Regarding musculoskeletal interaction assessment, this technique is not common and, due to safety reasons, can only be done in surrogate devices like a dummy limb [24, 48]. Overall, both direct and indirect assessment of misalignment effects is possible. However, most of the literature points to the fact that pressure forces are more commonly assessed directly through FSRs sensors, while sheer forces can be captured indirectly through motion capture. Both these methods will be used in the experimental work in Chapter 3, as well as a direct assessment of misalignment magnitude

It was found that alignment solutions of lower limb exoskeletons and AFOs can be divided into three groups, manual alignment, compliance, and kinematic redundancy [27]. A literature search found that manual alignment is the most widely implemented solution, with all the devices researched having this solution implemented. Compliant solutions are generally based on the introduction of carbon plates at the interfaces (to increase comfort) or at the joint level (to release the inversion/eversion DOF of the ankle). These solutions are generally lightweight but lack effectiveness in compensating for misalignment. Kinematic redundancy solutions, which introduce additional DOFs through revolute or prismatic joints, are very effective at compensating for misalignment but are very complex to design and implement in a way that does not compromise the device's metabolic benefit since they generally increase the mass of the device and can affect torque transmission. Overall, manual alignment and compliant solutions benefit from being simple, small, and light, and have been widely implemented. Kinematic redundancy solutions are very effective at compensating for misalignment but are very complex to design and implement in a way that does not compromise the device's metabolic benefit. However, these solutions have been increasingly adopted in novel exoskeletons, and breakthroughs are expected regarding their shortcomings. Every method has its weaknesses and, as such, a proper evaluation of the prototype's kinematic structure and HRI is fundamental to guide the design and implementation of alignment solutions.

3

Misalignment and Interaction Assessment

To properly develop an alignment solution we need, first, to effectively assess the magnitude of misalignment and its effects in our prototypes. In this work, this assessment was made through three different sources of data: motion capture data (assesses misalignment and displacement); pressure at the HRI measured by FSRs (assesses interactions); comfort and satisfaction questionnaire (assesses user perception of the prototypes). Regarding the interactions measured, no direct assessment was made of sheer forces, and motion capture data was used as a surrogate for qualifying these interactions. An experimental protocol was developed in collaboration with LABIOMEP and BIRDLab, to assess which of three AFOs with different HRI designs had lower alignment and interactions and higher user perception. Finally, the results allowed the proper dimensioning of the alignment solutions in Chapter 4 using the support of experimental data.
As such, this Chapter describes the different initial designs, the systems, the results, and the main takeaways gathered from this experiment.

3.1 Introduction on the Ankle Foot Orthosis

The SmartOs project includes three AFOs (two team-developed models by BIRDLab and the ankle module of the H2 active exoskeleton), which differ in the fixation mechanism to the shank and foot segments. This study's working hypothesis is that the three different prototypes have significant differences regarding misalignment and its effects, due to their different designs regarding the HRI. These designs are as follows.
The two prototypes developed at BIRDLab were denominated SMARTOs Frontal (SOF) and SMARTOs

Lateral (SOL), according to the locations of their shin-guard (figure 3.1 a and b), for the purposes of this study [5]. The two main characteristics are the use of shin guards, one covering the frontal part of the shin (SOF) and one covering the lateral part (SOL), and the introduction of a commercially available running shoe at the foot level, in order to improve comfort and ergonomics. The frame of these devices is an aluminum structure (AL5754) coated in neoprene that can be manually aligned to fit users with heights between 1.70 and 1.90 m and a maximum body weight of 100 kg. The actuator and electronics have been theorized but not yet implemented in these prototypes. These models have a structure at the level of the ankle joint that mimics both the volume and mass of these electronics, guaranteeing that the structure's inertia is approximately the same as if the whole apparatus was present.

H2 (Technaid S.L., Spain) is a robotic exoskeleton developed to assist impaired human walking by means of six actuated joints, namely both hip, knee, and ankle joints [93]. The exoskeleton is fully modular, allowing the user to wear any of the joints or any combination of joints. The ankle modulus used for this work was developed to treat drop foot problems. The device was designed for adults between 1.50 and 1.95 m in height and a maximum body weight of 100 kg. Fixation to the user is ensured at three locations: two adjustable straps at the shank's height and a specific platform, size 42, that connects to the foot. The fixations at the shank level are made through adjustable Velcro straps with foam pads to minimize pressure. The mechanical structure is made of stainless steel and type 7005 aluminum. The assistance of the AFO of H2 can be controlled by different control strategies, including the zero impedance controller. This control algorithm allows that the device timely follows the user's motion intention, which is detected by strain gauges sensors embedded in the shank structure, acting with a passive behavior. Gait speed can be adapted by the operator, but the device also adapts the programmed speed to fit the user's gait. Both devices can be seen in figure 3.1.

(a) **(b)** **(c)**

Figure 3.1

3.2 Materials and Methods

3.2.1 Participants

Misalignment and interactions were assessed on 10 young male healthy subjects (180.3 $\pm$ 4.0 cm, 81.1 $\pm$ 10.1 kg, and 25.8 $\pm$ 4.4 years old). All participants were healthy without reporting any known locomotion or balance impairment, and they had not suffered any musculoskeletal injury in the previous six months. Participants were chosen with similar shank lengths (35.1 $\pm$ 3.18 cm) and perimeters (38.5 $\pm$ 2.59 cm) to ensure that the devices were fixed in approximately similar anatomical regions. All participants were informed of the study's objectives and methodology and were provided with an informed consent form, which they read and signed. The study was approved by the University of Minho Research in Life and Health Sciences Ethics Committee, with the protocol number CEICVS 006/2020.

3.2.2 Instrumentation and Data Collection

A motion capture system with 12 cameras (Oqus, Qualisys – Motion-Capture System, Göteborg, Sweden) capturing at 100 Hz was used to measure human lower-limb kinematics during the trials, as well as orthosis kinematics (e.g. robotic joint position in space). For this experiment, the marker set in figure 3.2 was used to capture the human gait kinematics, while the marker sets in figures 3.3, 3.4 and 3.5 were used to capture the kinematics of the AFOs. Overall, 30 markers were used on the human body and 9 markers were used for each of the prototypes. The latter set was chosen so two (SOF and SOL) or three (H2) rigid bodies could be modeled for further analysis. All markers were placed by the same operator using the anatomical standards described in [94]. For the ground-level walking trials, Ground Reaction Forces (GRF), Center of Pressure (CoP), and Force Platform Moments (FPMs) data were provided at 1000 Hz, by using six force platforms embedded in the floor: two force platforms FP4060 (Bertec, Ohio, United States of America), two force platforms FP6090 (Bertec, Ohio, United States of America), and two force platform 9281 EA – FP4060 (Kistler, Winterthur, Switzerland).

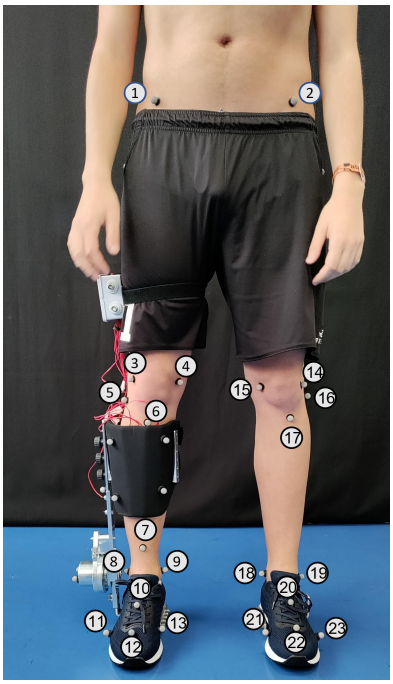

(a) Front view

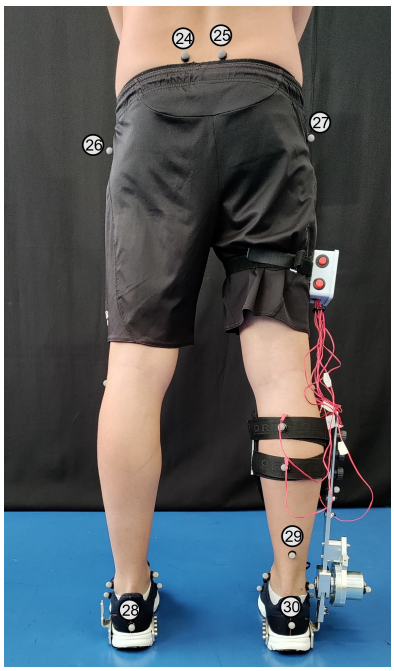

(b) Back view

Figure 3.2: Marker set for the human body modeling.

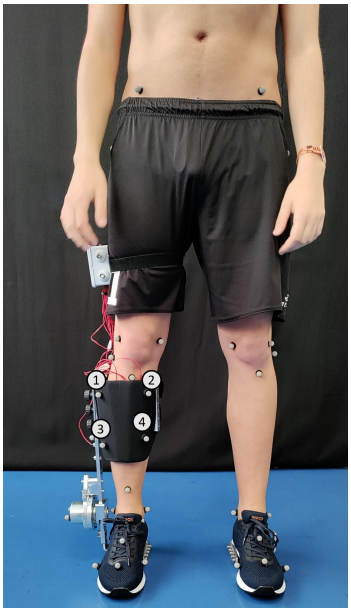

(a) Front view

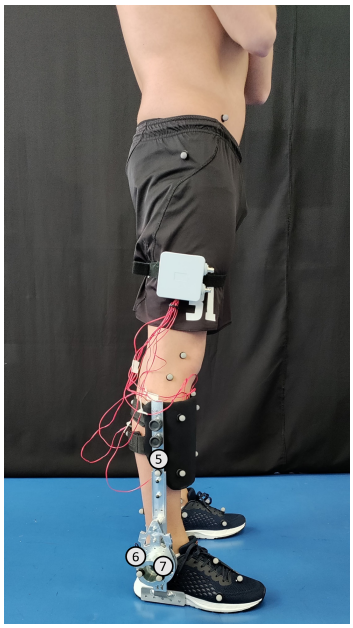

(b) Lateral view

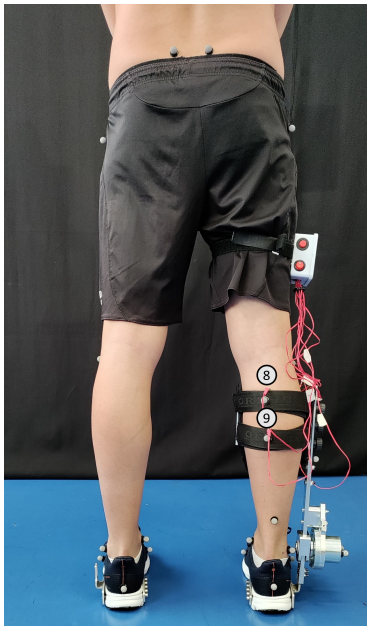

(c) Back view

Figure 3.3: Marker set for the SOF device modeling.

(a) Front view **(b)** Lateral view

Figure 3.4: Marker set for the SOL device modeling.

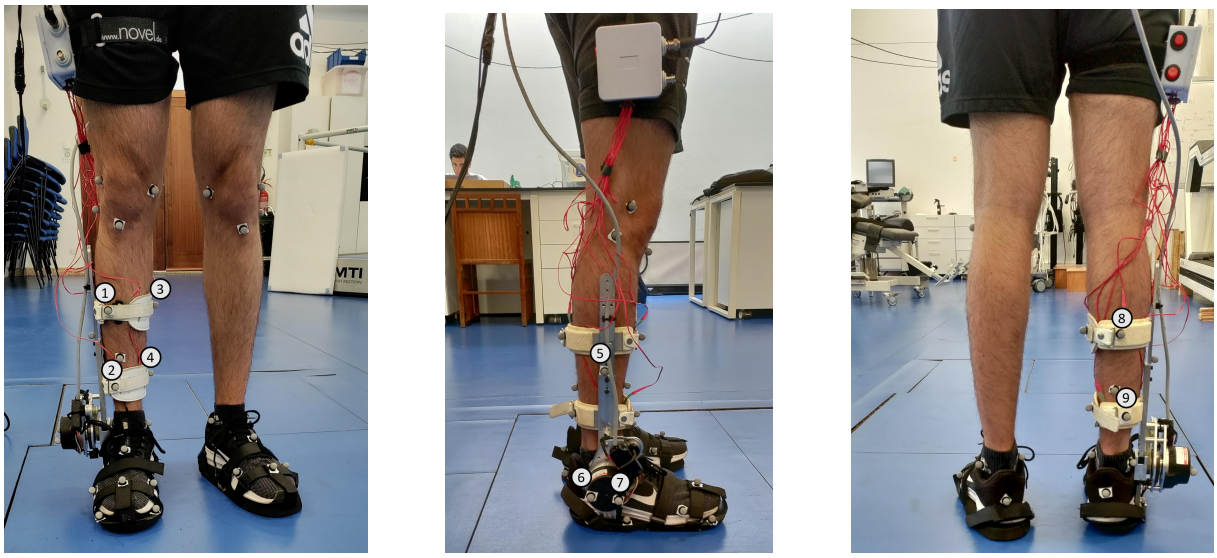

(a) Front view **(b)** Lateral view **(c)** Back view

Figure 3.5: Marker set for the H2 device modeling.

Pressures at the interfaces between the user and the device were measured by a system of 8 circular FSRs. These devices rely on a material that changes its resistance when force is applied, outputting a voltage. This voltage was received and processed by an Arduino Nano microcontroller board operating at 100 Hz. Each FSR was calibrated independently prior to the protocol using the method described in [95] for pressure steps of 0, 20, 25, 35, 50, 75, 100, and 150 KPa. Results were fitted to an exponential

model, as presented in equation 3.1 through the curve fitting tool of MATLAB R2020b®(The MathWorks, Natick, MA, USA).

$$y = a.\exp(b.x) + c.\exp d.x \tag{3.1}$$

In this model, x represents the digital signal captured by the device and y is the resulting pressure in KPa. The results of this calibration can be seen in appendix A. Each sensor was labeled from 1 to 8 and fixed to the AFOs through double-sided tape as illustrated in figure 3.6. The FSRs were placed in anatomical areas where high-pressure values should be avoided due to the increased risk of discomfort and lesion [9, 96, 97]. The placement was done by the same operator throughout the protocol to reduce the occurrence of occasional and systematic errors, prior to the donning of the device by the user. Once the user donned the device, the sensors were repositioned according to the user's anatomy. Since recorded pressures and pain thresholds vary greatly with the type and stiffness of tissue they are applied to [8, 22, 96], an effort was done to place the sensors in the same anatomical area for each subject. This is especially important for FSRs 3 and 6 of SOF, 6 and 8 of SOL, and 3 and 8 of H2, where the intent was to place them at the bony prominence of the femur and not on the adjacent softer tissue.

(a) SOF sensor placement **(b)** SOL sensor placement **(c)** H2 sensor placement

Figure 3.6: FSR placement of each device.

The comfort and satisfaction questionnaire included 13 questions, scored through a 4-point Liker-scale (Strongly Disagree, Disagree, Agree, and Strongly Agree). Literature research was done on available questionnaires for assessing user satisfaction about AFOs. Since no questionnaire that targeted AFOs directly was found, a choice was made to use questions from the two available questionnaires indicated in [98] as "Generic Questionnaires", defined as the ones for use across all types of orthotic devices and clinical conditions. As such, the questionnaire is based on the adapted Client Satisfaction with Device - Orthotics and Prosthetic Users Survey (CSD-OPUS) [99], with one question from the Quebec User Evaluation of Satisfaction with Assistive Technology 2.0 (QUEST 2.0) questionnaire [100]. The original CSD-OPUS and QUEST 2.0 questionnaires can be found in Appendix B.

The OPUS is a self-report questionnaire with five different moduli, ranging from the assessment of upper and lower limb functional status to satisfaction with devices and services. Scored on a 4-point Likert

scale, this questionnaire has been validated by Rasch analysis [101, 102]. The consumer satisfaction modulus has an original and revised version that reduced the number of questions from 11 to 8 in order to improve unidimensionality (figure B.1), with satisfactory evidence of validity [98]. The QUEST 2.0 has 12 items that analyze user satisfaction with assistive technology devices, split into questions related to satisfaction with the device (eight questions, figure B.2) and with the service (four questions). The score is based on a 5-point Likert scale, ranging from 1 (not satisfied at all) to 5 (very satisfied) [98]. The questionnaires carry some overlap (e.g. question 5 of both questionnaires or CSD-OPUS's question 2 and QUEST 2.0's question 7). Nevertheless, CSD-OPUS was chosen to be the main basis for this experiment's questionnaire mainly due to question 1, which directly assesses the presence of abrasion and irritation on the user's skin. This is commonly the result of friction interactions at the level of the HRI, which are one of the main effects of misalignment [24,25,31,33] and one of the focus of this assessment. Thus, the questionnaire issued in this study used the original questions number 1, 4, 5, 6, 7, 10, 11, and 12 from the modified CSD-OPUS. Questions 2, 3, 8, and 9 were adapted from the original questions from CSD-OPUS to allow a better assessment of the differences between the prototypes and between the moduli of the same prototype. Question 13 was taken directly from the QUEST 2.0 questionnaire since there was a need to directly assess the user's opinion of the dimensions of the device like size, height, length, or width. The final questionnaire is in figure 3.7

	Strongly Agree	Agree	Disagree	Strongly Disagree	Not Applicable
1. My skin is free of abrasions and irritation	☐	☐	☐	☐	☐
2. The foot module of my device is comfortable	☐	☐	☐	☐	☐
3. The shank module of my device is comfortable throughout the day	☐	☐	☐	☐	☐
4. Overall, my device is comfortable throughout the day	☐	☐	☐	☐	☐
5. My device looks good	☐	☐	☐	☐	☐
6. My device is pain free to wear	☐	☐	☐	☐	☐
7. My device is durable	☐	☐	☐	☐	☐
8. The foot module of my device fits well	☐	☐	☐	☐	☐
9. The shank module of my device fits well	☐	☐	☐	☐	☐
10. Overall, my device fits well	☐	☐	☐	☐	☐
11. It is easy to put on my device	☐	☐	☐	☐	☐
12. The weight of my device is manageable	☐	☐	☐	☐	☐
13. My device has the proper dimensions (size, height, length, width)	☐	☐	☐	☐	☐

Figure 3.7: Questionnaire given to the participants, based on [98–100].

3.2.3 Experimental Protocol

Participants donned one of the three devices (chosen at random) in their right leg, with help from an operator. The operator was the same for all participants. The same operator recorded the subject's height, weight, shank length, and shank perimeter. It is important to note that the assistance of the ankle module of H2 was controlled by zero-impedance control to approximate the behavior of all AFOs in a passive mode. However, there are differences among the three prototypes since the SOF and SOL prototypes do not have any electronics, being comprised only of the structure.

Tests were made in two different experimental conditions, level-ground, and treadmill walking. The order of these conditions was randomized. For the level-ground trials, the participants were first asked to perform three trials of walking for 10 meters at a self-selected speed. Then, the participants were asked to repeat these trials at 1.6 km/h, the maximum speed for the ankle module of H2, with the help of a metronome (cadence 70 steps/min). For the treadmill trials, each participant performed first a familiarization trial (not more than 1 min) at 1.6 km/h to familiarize themselves with both the walking speed and the treadmill. Afterward, each participant performed a walking trial for 6 minutes and 30 seconds without interruptions, with data being collected for 30 seconds at 0, 3, and 6 minutes. A visual description of the protocol can be found in figure 3.8.

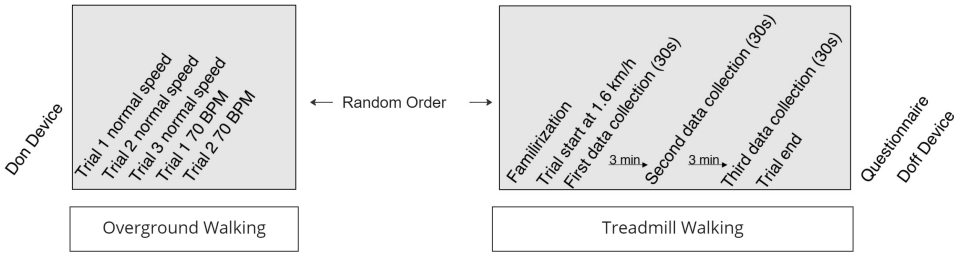

Figure 3.8: Protocol schematic. Each sequence represented is repeated for each orthosis in random order.

After a full protocol with the same prototype the user donned off (with help from the same operator) and answered a questionnaire on their experience with the device. This protocol was repeated for each device.

3.2.4 Data Analysis

All processing steps and statistical tests described in this section were performed in MATLAB 2018Rb®(The MathWorks, Natick, MA, USA) unless specified otherwise. Only the data captured in the ground-level walking trials were analyzed in the scope of this dissertation. For the preprocessing of motion capture data, first, the retro-reflective markers were identified by a dedicated operator through the identification method of the Qualisys Track Manager software (Automatic Identification of Markers), and the marker

trajectory was fitted to a polynomial interpolation function. Further processing of the data was done in Visual 3D® (C-Motion, Boyds, Maryland, USA). All markers' trajectory was filtered through a 6th order low pass Butterworth filter with a cutoff frequency of 6 Hz. Human joint centers were defined as the midpoint between the lateral and medial markers and segments were defined proximally by the relevant joint and distally by the lateral and medial markers except for the foot, which is defined by the marker in both instances. Human segment masses were determined as proportions of body mass through anthropometric equations native to the software. Native functions of Visual 3D®® (C-Motion, Boyds, Maryland, USA) were used to compute human 3D joint angles and torques and automatically detect gait events from force platform data. A threshold of 20 N was used to remove noise from the signals captured by the force platforms. Final models for all three devices and the human body can be seen in figure 3.9. The segments identified in green were similar for the three devices and modeled using markers 5, 6, and 7 of each set, while the shin-guards of SOF and SOL were modeled using markers 1, 2, 3, and 4 and the two straps of H2 were modeled using markers 1, 3, 8 (top strap) and 2, 4 and 9 (bottom strap). All data processing described in this subsection was directly done by a dedicated operator of LABIOMEP and not by the author of this dissertation.

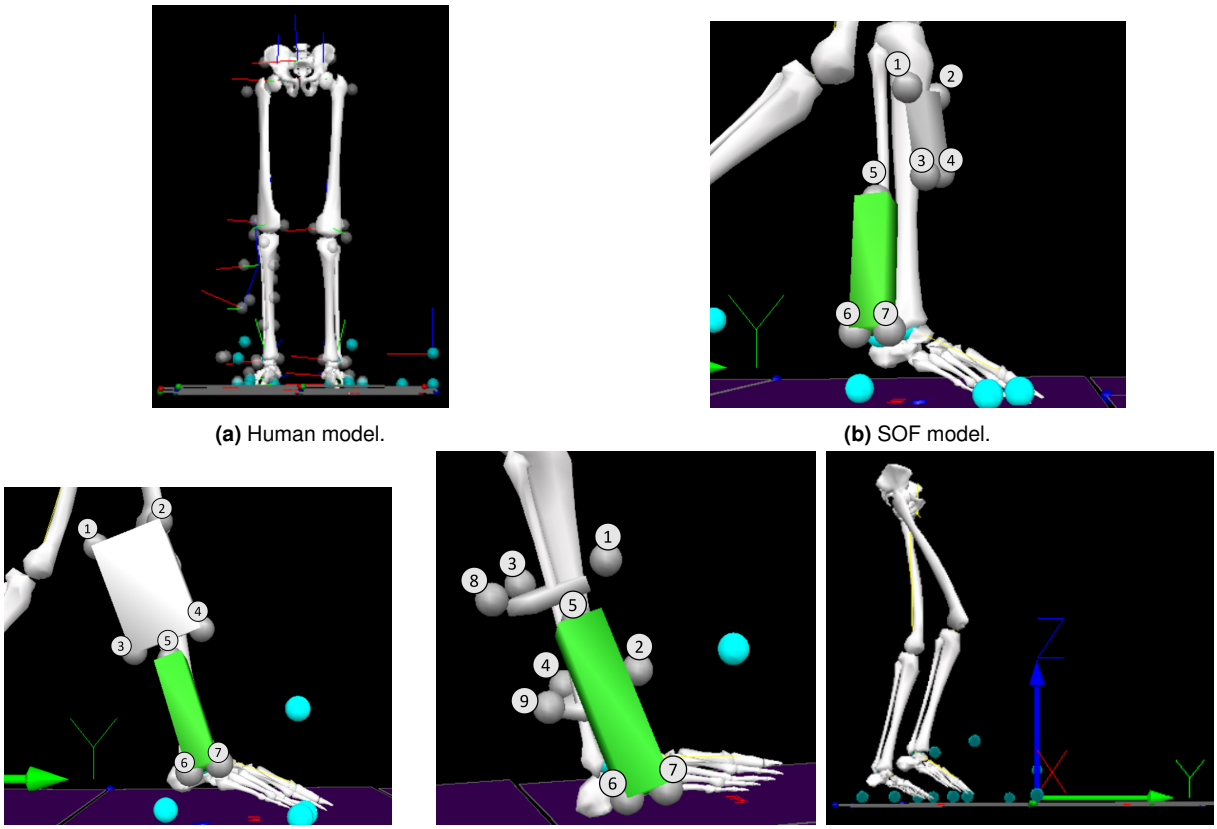

(a) Human model. **(b)** SOF model. **(c)** SOL model. **(d)** H2 model. **(e)** Model Axis.

Figure 3.9: Visual 3D® (C-Motion, Boyds, Maryland, USA) models.

Four different measures were computed from kinematic data using Visual 3D's® (C-Motion, Boyds, Maryland, USA) capabilities. The first two measures were used to assess misalignment, while the last two aimed to indirectly assess interactions at the HRI by measuring fixation displacement. The latter method, as described before, has been validated by [62]. All Visual 3D® (C-Motion, Boyds, Maryland, USA) data was split by gait cycle, normalized to 101 points, averaged, and exported to an ASCII file. This was done separately for each set of conditions (subject, speed, and device) A complete description of available functions and commands for the software's pipeline can be found at [103]. Signals were averaged across all 10 subjects and plotted for the three different devices to help assess the main differences. The four computed measures are:

1. Misalignment distance (My, Mz) - defined as the difference between the human joint's position and the robotic joint's in the sagittal plane.

2. Misalignment angle (Mα, Mβ and Mγ, corresponding to rotations x-x, y-y, and z-z) - defined as the angle between the human shank and "support" segment (segments in green in figure 3.9), calculated using the native Visual 3D® (C-Motion, Boyds, Maryland, USA) function $JOINTANGLE$. This function requires 7 main inputs (see figure 3.10, image a): Segment (Support); Reference Segment (Right Shank); Normalization (Off); Cardan Sequence (X-Y-Z) and negate each of the axis (false for each).

3. Strap displacement (Dx, Dy, and Dz) - defined as the strap's relative movement to the user's shank in the local reference frame (right shank), calculated using the Visual 3D® (C-Motion, Boyds, Maryland, USA) function $TARGETPATH$and removing the initial distance from every data point (since the objective was to assess the evolution throughout gait). This function requires 3 main inputs (see figure 3.10, b): Target (Visual 3D® (C-Motion, Boyds, Maryland, USA)'s name for marker position, markers labeled with an 8 in figures 3.3, 3.4 and 3.5); Reference Segment (Right Shank); Resolutions Coordinate System (Right Shank).

4. Shin-guard/Strap angular displacement (Dα, Dβ, and Dγ) - defined as the angle between either the shin-guard (SOF and SOL) or the top strap (H2) segment and the user's right shank, calculated using the Visual 3D® (C-Motion, Boyds, Maryland, USA) function $JOINTANGLE$. The same inputs were used as in point 2, with the only difference being the chosen segments.

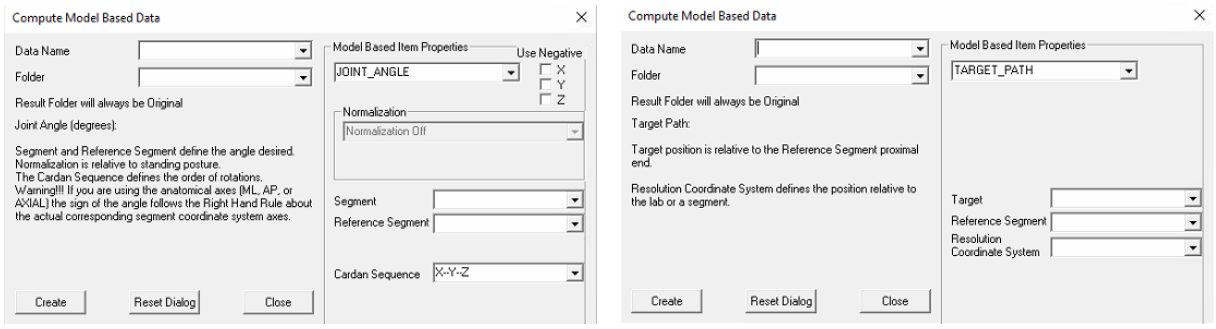

(a) JOINT ANGLE function UI. **(b)** TARGET PATH function UI

Figure 3.10: Visual 3D® (C-Motion, Boyds, Maryland, USA) UI for functional programming.

Angular misalignment and displacement measures were offset from their initial. For rotational misalignment, this is important since the reproducibility of marker position across subjects cannot be guaranteed. As such, this systematic error in marker placement will lead to initial angles that vary widely between subjects and that do not correspond with reality.

For the preprocessing of pressure data, first, the frames of each right heel strike (RHS) were exported from Visual 3D® (C-Motion, Boyds, Maryland, USA) to an ASCII and imported to MATLAB R2020b®(The MathWorks, Natick, MA, USA). This data was then downsampled to the same frequency as the pressure data (80 Hz, on average) allowing to segment each FSR signal into gait cycles according to the corresponding RHS. The maximum/peak pressure value of each gait cycle was extracted. Statistical tests were applied to assess normality, through a one-sample Kolmogorov-Smirnov test, and statistically significant differences regarding the peak pressure values, as described in table 3.1 (all for a 5% confidence interval). For all tests, the null hypothesis was that the compared conditions had no differences. In order to make a direct comparison between orthoses, it was necessary to group sensors placed at approximately the same anatomical location for the three AFOs.

Table 3.1: Statistical tests for FSR data analysis.

Result	Fixed Conditions	Compared Conditions	Measure	Test
Trial Variability	FSR, Speed, Orthosis	Trial1 vs Trial2 vs Trial3	Peak Pressure	Friedman
Speed Variability	FSR, Orthosis	Normal Speed vs 70 BPM	Peak Pressure	Wilcoxon signed-rank

Four different groups of 3 FSRs each (one FSR per device) were created, according to table 3.2. Boxplots comparing the maximum values within each group are presented to better assess differences between orthoses.

Table 3.2: FSR grouping per anatomical cluster. The number corresponds to the identification of FSR indicated in Figure 3.6

FSR Group	SOF	SOL	H2
Anterior Proximal	3	6	3
Anterior Distal	6	7	8
Posterior Proximal	7	5	1
Posterior Distal	8	8	6

A comparison with pressure safety values from the literature was done. While ISO/TS 15066 [104] adopted limit values for pressure, these are only applicable in accidental contacts and not for the type of continuous contacts that exist at the HRI, with [24] stating that pressures as low as half of the ones stated in this standard, applied for several minutes, can become painful. Literature showed that Pain Tolerance Threshold (PTT) (pressure at which pain becomes unbearable) and Pain Detection Threshold (PDT) or PPT (pressure magnitudes at which pain occurs) can be assessed through single point algometry [105] and Cuff Pressure Algometry (CPA) [106, 107]. The work in [105] divided the lower limb into three different homogeneous groups of sensitivity to pressure by assessing single point PPT at nine different locations in the leg (figure 3.11).

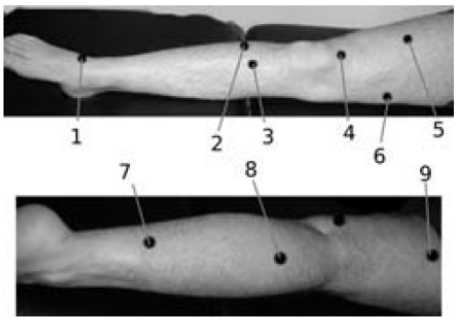

(a) Point locations.

Anatomical point	PPT (kPa)	Homogeneous group
P1	281.7	1
P2	545.5	3
P3	588.1	3
P4	628.1	3
P5	482.7	2
P6	281.9	1
P7	557.7	3
P8	416.6	2
P9	470.5	2

(b) PPT and group distribution.

Figure 3.11: Point PPT assessment. Taken from [105].

Following these results, one was allocated to each of the groups defined in 3.2. Since single-point algometry results in higher PPT [9, 24] and CPA more closely resembles the contact with cuffs or straps like in these devices, a comparison was also made with values from two systematic reviews [106, 107]. It is important to note, however, that [59] identifies a general lack of consensus regarding safety values, mainly due to the high variability of anatomical landmarks used in different research and the applications they are directed to. As such, consideration can be made that the studies used in this comparison

both shy away from the high anatomical variability problem, by measuring circumferential pressure, and replicate the intended use of these devices.

Questionnaire answers were translated to a numeric score by assigning values 1 (Strongly Disagree), 2 (Disagree), 3 (Agree), and 4 (Strongly Agree) to each answer. The sum of scores of the 8 questions (maximum score of 32) that were adapted from CSD-OPUS were translated to a Rasch measure using the table from [99]. These Rasch measures were analyzed through statistical tests and question scores were analyzed through direct comparison from average and per-answer scores. The normality of the Rasch measures was first assessed through a one-sample Kolmogorov-Smirnov test. Then, a Friedman test was used to test the null hypothesis that there was no difference between the three sets of Rasch measures, with each set corresponding to the answers for one of the AFOs. The significance level chosen was 5%. The Rasch measures provided were for a 9-question version of CSD-OPUS, with the additional item being - "Clothes are free of wear and tear". As such, a decision was made to award a full score (4 - Strongly Agree) to this question, since neither the operators nor the participants report any wear or tear of the participant's clothes related to the use of the device. Following the Friedman test, post-hoc tests were done using Tukey's honestly significant difference test (Tukey's HSD). To better assess which questions scored higher between devices, each question's score was averaged for all the participants. Then, SOF's individual question scores were subtracted from those of the other device and plotted in a bar chart.

3.3 Results

3.3.1 Misalignment and Displacement Measures

Figures 3.12, 3.13, 3.14 and 3.15 present the results of misalignment distance, misalignment angle, strap displacement and shin-guard/strap angular displacement, respectively, averaged for 10 subjects and plotted for each orthosis. The initial misalignments captured were -1.11 cm, -0.90 cm, and -0.48 cm horizontally and -1.75 cm, -1.82 cm, and -2.76 cm vertically, for SOF, SOL, and H2, respectively. Regarding these measures, there are differences between devices in misalignment distance (Mz). H2 is the AFO that presents the highest misalignment, at the beginning and trough out the gait cycle. Figure 3.12 also shows that the misalignment distance is not constant across gait. As well for the misalignment angle (Mα and Mβ), figure 3.13 shows that the H2 device has the highest misalignment angle. There are not any apparent differences between SOF and SOL. For the displacement values (figures 3.14 and 3.15), H2 has higher displacement paths (Dx, Dy, and Dz) and angles (Dα, Dβ, and Dγ) overall, with no differences between the two models developed by BIRDLab. These two measures indirectly represent interactions between the fixations and the user's soft tissues.

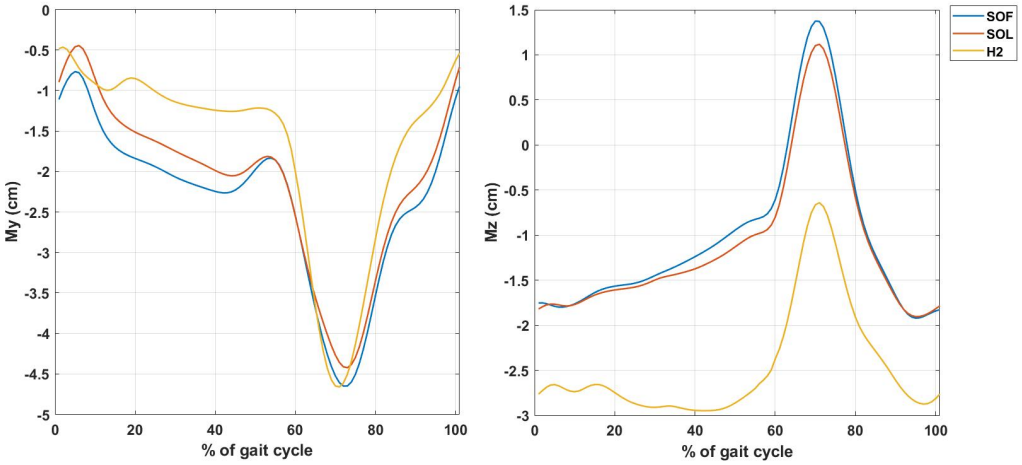

Figure 3.12: Vertical (Mz) and horizontal (My) misalignment plots averaged for all subjects.

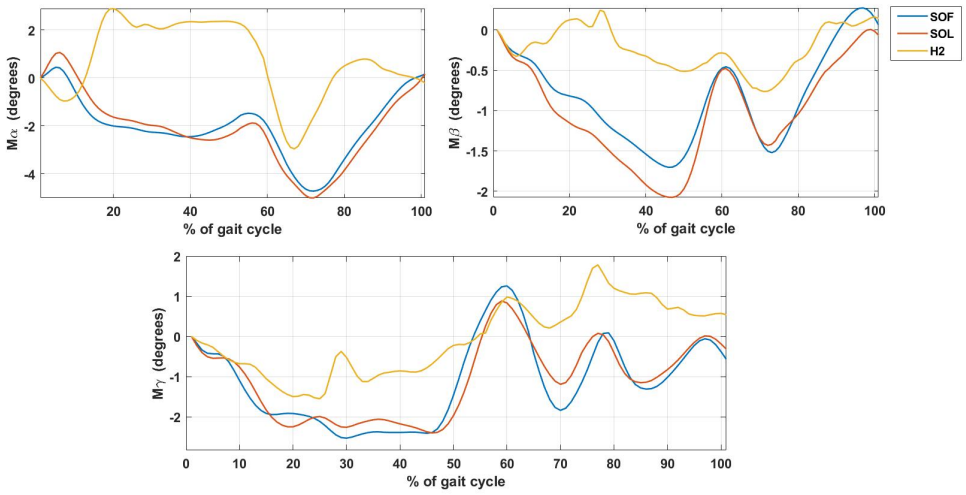

Figure 3.13: Misalignment angle (Mα, Mβ, Mγ) plots averaged for all subjects.

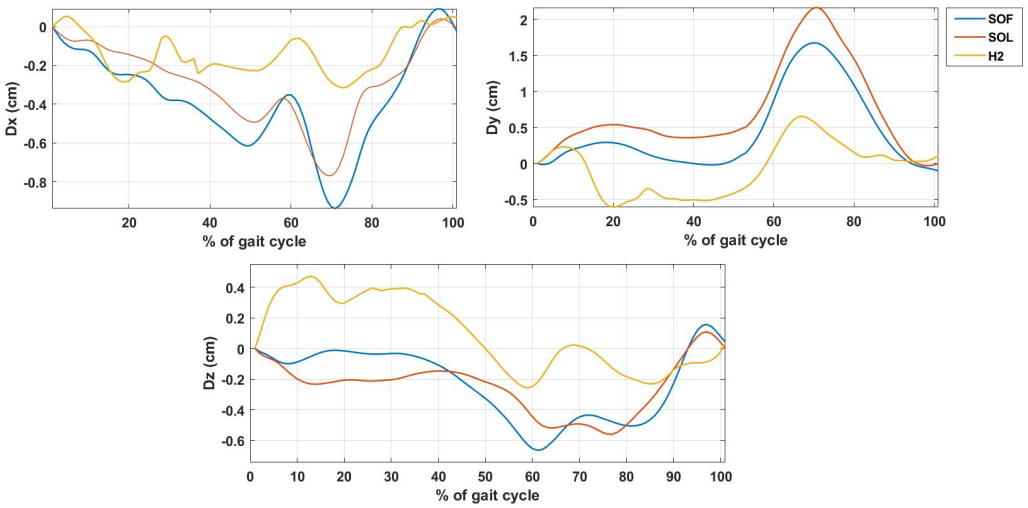

Figure 3.14: X, Y, and Z displacement plots averaged for all subjects.

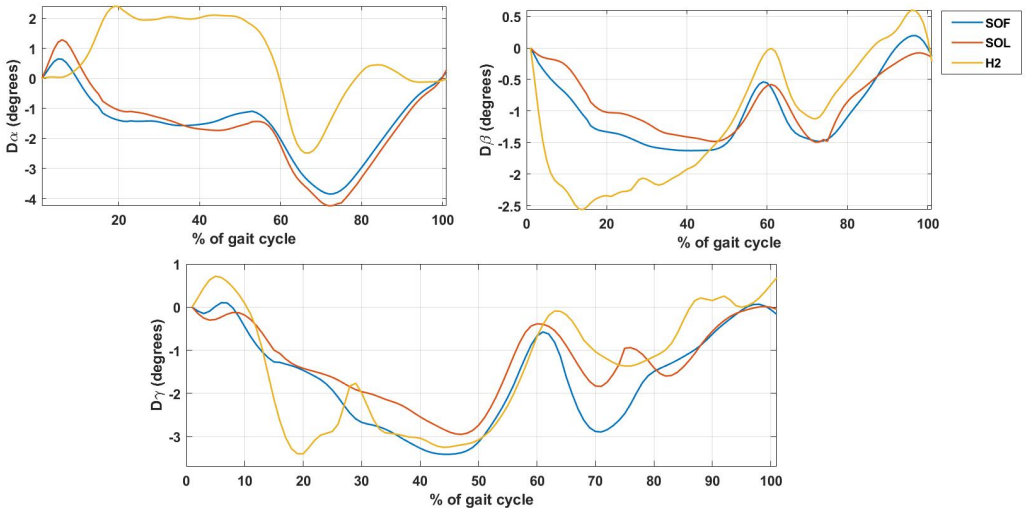

Figure 3.15: Angular displacement (Dα, Dβ, Dγ) plots averaged for all subjects.

3.3.2 Pressure on Human-AFO Interface

This sub-Chapter presents the results regarding the pressure measures on the Human-AFO interface to assess the Human-AFO interactions. Table 3.3 shows that, overall, there are no statistically significant differences in the peak pressure values between the three trials, suggesting that the average of the three trials can be correctly used. In the vast majority of situations, the differences between trials are not statistically significant, meaning a signal that is the average of the three trials can be safely used.

Table 3.3: p-values obtained from Friedman tests to test the null hypothesis that there are no statistically significant differences in the maximum pressure values between the three trials for three AFOs. In red are presented conditions where the null hypothesis was not verified.

	H2	SOF	SOL
FSR1	0.199	0.772	0.549
FSR2	0.025	0.076	0.670
FSR3	0.459	0.459	0.819
FSR4	0.154	0.093	0.407
FSR5	0.199	0.332	0.741
FSR6	0.497	0.412	0.023
FSR7	0.539	0.497	0.045
FSR8	0.656	0.670	0.459

(a) Self-selected speed.

	H2	SOF	SOL
FSR1	0.479	0.063	0.973
FSR2	0.729	0.891	0.975
FSR3	0.349	0.072	0.756
FSR4	0.338	0.193	0.581
FSR5	0.368	0.549	0.097
FSR6	0.283	0.729	0.004
FSR7	0.972	0.717	0.614
FSR8	0.356	0.584	0.282

(b) Speed of 70 steps/min.

By testing speed variability, a conclusion can be drawn regarding the relation between speed and pressure interactions and if this should be taken into consideration in the following tests. The results of Wilcoxon signed-rank tests can be found in table 3.4. As can be seen in table 3.4, there is not a statistically significant difference between both speeds, meaning that the user's speed does not significantly alter pressure interactions at the HRI. As such, for the following tests, only results for the self-selected speed were considered. Corresponding boxplots were made for each of the FSR groups (figure 3.16). By analyzing the boxplots it is verified that the SOF device had lower pressure for all of the four groups, while SOL and H2 have somewhat similar results for the posterior groups. The biggest differences are for sensors of the anterior groups, mainly due to the fitness of the frontal shin-guard compared with the other two fixation mechanisms. This is in opposition to both posterior groups, where sensors were placed at the same type of fixations.

Table 3.4: p-values obtained from Wilcoxon signed ranked tests to test the null hypothesis that there are no statistically significant differences in the maximum pressure values between the two different speeds for three AFOs. In red are presented conditions where the null hypothesis was not verified.

	H2	SOF	SOL
FSR1	1.000	1.000	1.000
FSR2	1.000	0.375	1.000
FSR3	1.000	0.508	1.000
FSR4	0.727	1.000	1.000
FSR5	0.453	0.727	0.508
FSR6	0.727	0.039	0.039
FSR7	1.000	1.000	1.000
FSR8	0.727	0.508	1.000

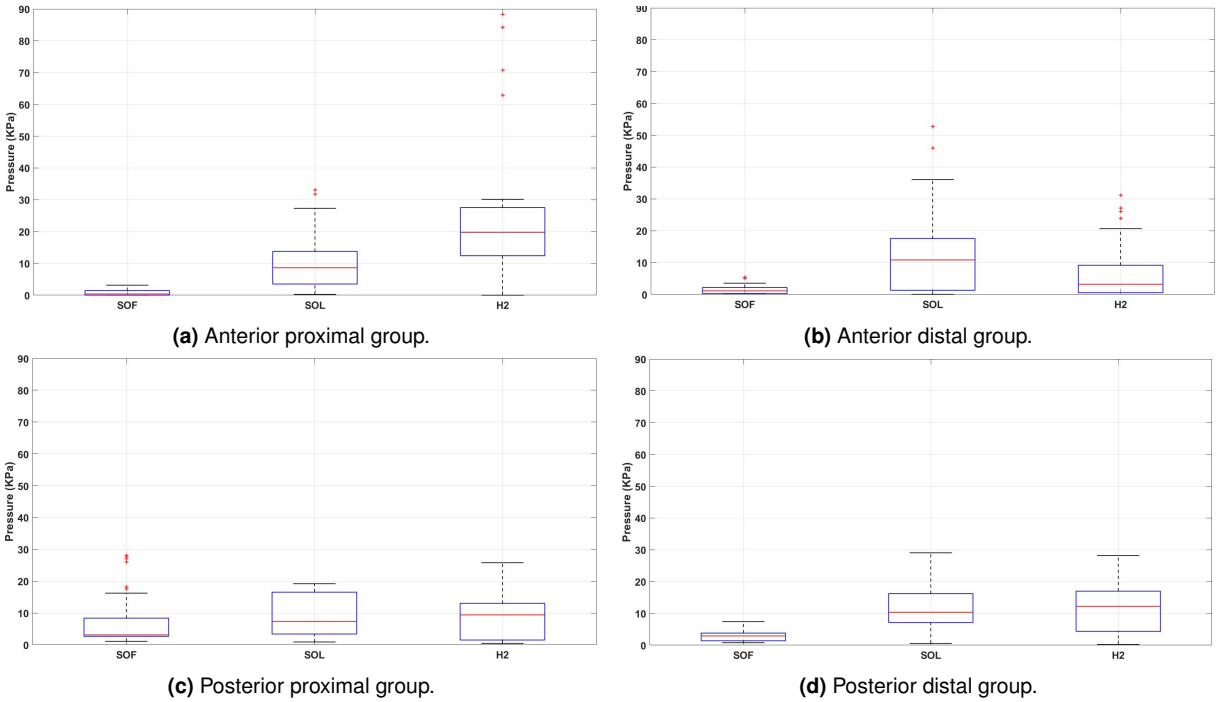

(a) Anterior proximal group.

(b) Anterior distal group.

(c) Posterior proximal group.

(d) Posterior distal group.

Figure 3.16: Boxplots of peak pressure values.

3.3.3 Questionnaire on User's Satisfaction

Each participant assessed comfort for each orthosis after roughly the same amount of time wearing the three devices. Two different scores were calculated by adding up the scores of each individual question, one for the complete questionnaire and one for the CSD-OPUS questions. Results are illustrated in

figure 3.17.

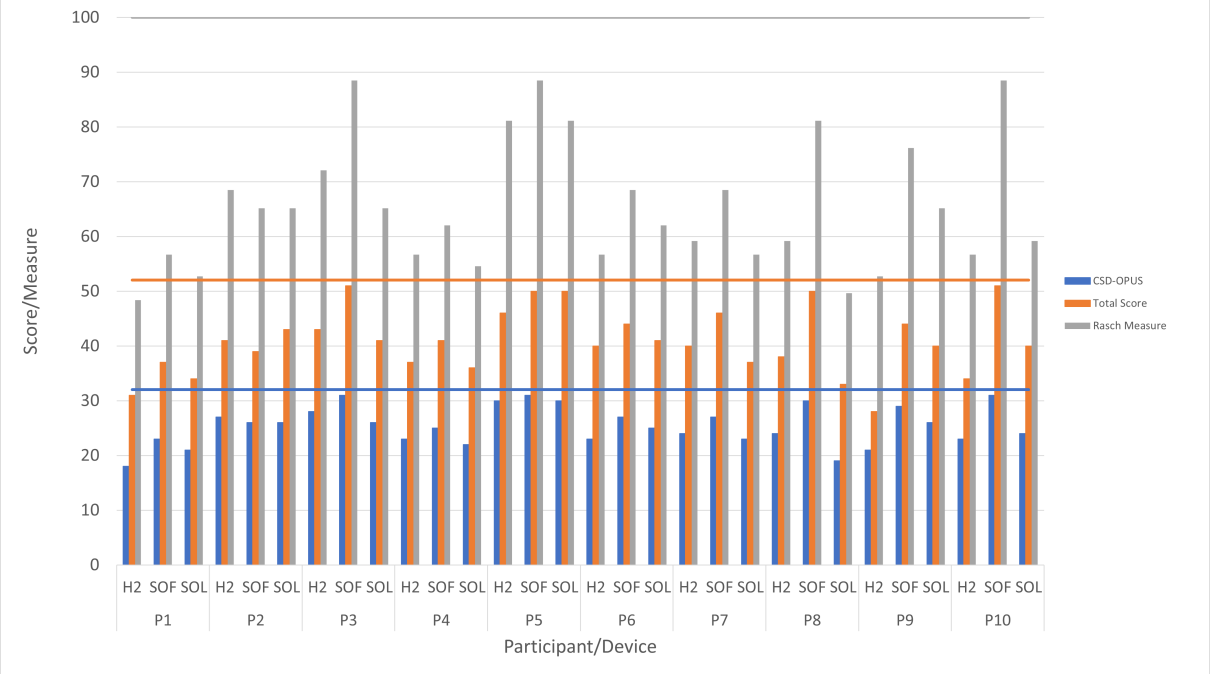

Figure 3.17: Questionnaire scores and measures by participant and device. Blue bars correspond to the score of the questions from CSD-OPUS, orange bars to the total score of the questionnaire, and grey bars to corresponding Rash Measures. Maximum values are 32, 52, and 100, respectively, represented by horizontal bars of the same color.

The Friedman test is done from the Rasch measures resulting in a p-value of 0.0031 ($p < 0.05$), indicating that there are statistically significant differences in the user's perception regarding the three AFOs. The results of the post-hoc Tukey test are presented in table 3.5. These results report a higher user satisfaction for the SOF device than other AFOs (p-values of 0.016 and 0.006 > 0.05), with no clear difference between H2 and SOL (p-value of 0.937). To better assess in which questions SOF had higher scores than the other devices, each question's score was averaged for all the participants.

Table 3.5: p-Value scores of the pairwise tests of Rasch Measures.

Device A	Device B	p-Value
H2	SOF	0.016
H2	SOL	0.937
SOF	SOL	0.006

Results of the direct comparison between SOF and SOL/H2 are illustrated in figure 3.18.

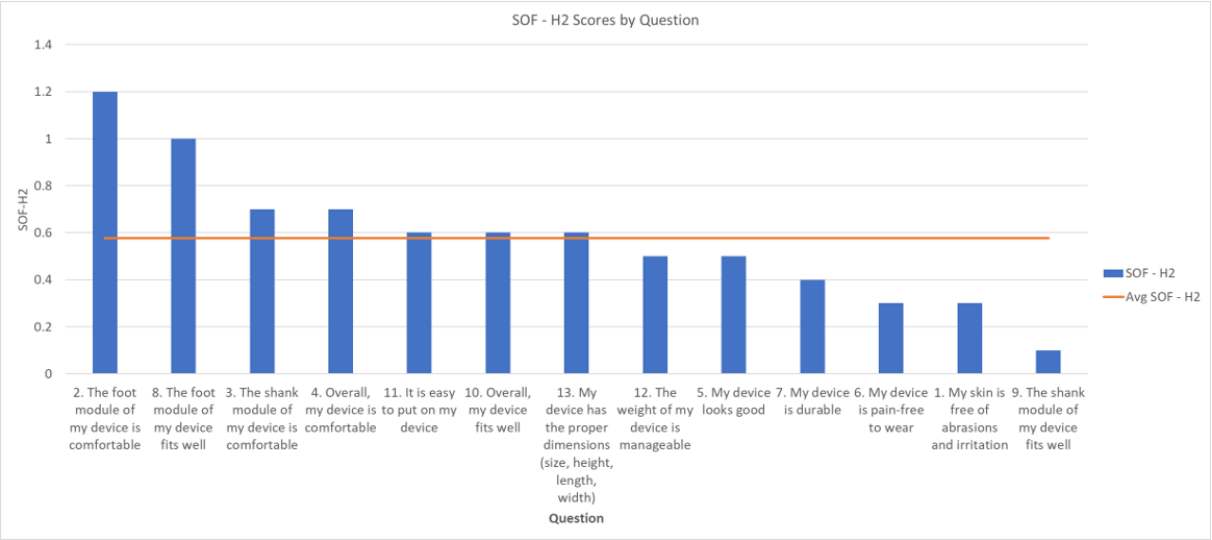

(a) SOF vs H2 comparison.

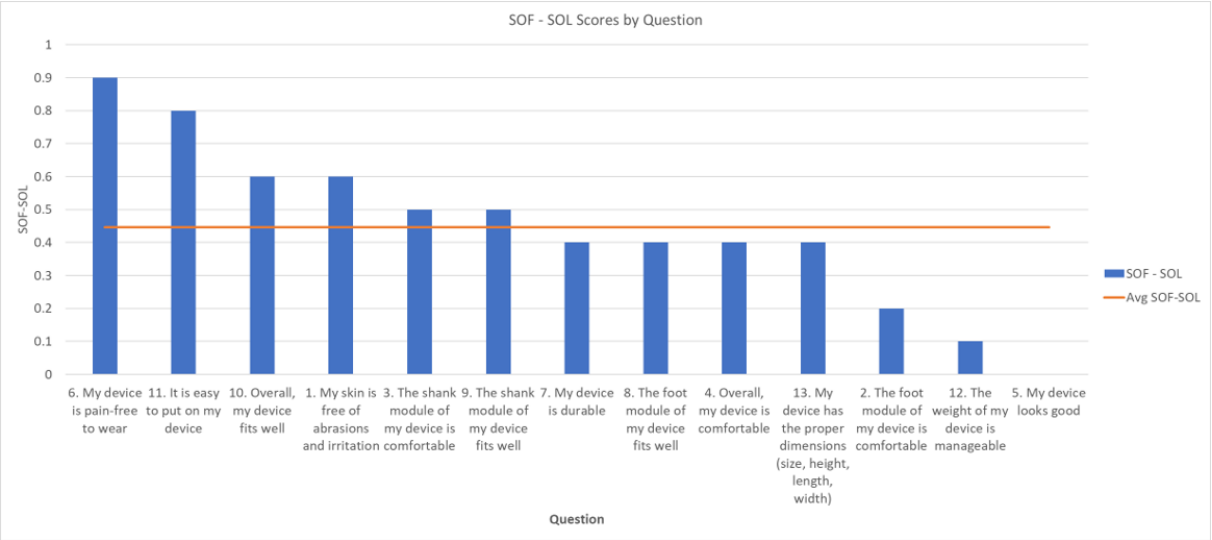

(b) SOF vs SOL comparison

Figure 3.18: Questionnaire individual question comparison.

The main differences are clear for each prototype. SOF has largely higher scores than H2 mainly in relation to the foot module (questions 2 and 8), shank module (question 3), and overall comfort and fitness (question 4), with scores more than 1 point apart in the Likert scale. These questions also had higher scores than the average difference between questions.

On the other hand, SOF has largely higher scores than SOL with regards to pain during the device's use (question 6), ability to don the device (question 11), the fitness of the device (question 10), and presence of abrasions and irritation (question 1). The scores were overall closer between SOF and H2 than between SOF and SOL, with the average difference between SOF and H2 equal to 0.58 and between SOF and SOL equal to 0.45.

3.4 Discussion

Literature shows that human-robot joint misalignment leads to spurious forces and torques at HRI [27–31]. These can be pressure interactions (forces normal to the tissue surface) above safe levels or sheer/friction interactions (forces tangent to the tissue surface) [24]. As such, this protocol aims to directly assess misalignment through motion capture data ([33,48,60,108,109]) and directly or indirectly assess these interactions. To achieve this goal, pressure sensors were placed at the HRI that allow direct quantification of this type of interaction [49–54], while motion capture data allows the capture of relative movement between the device's fixations (e.g. cuffs, straps) and the human limb, giving an indirect assessment of sheer interactions. Higher recorded misalignments are expected to lead to higher recorded interactions. Finally, user-perceived comfort and satisfaction were also assessed through a modified version of two available questionnaires, the CSD-OPUS ([99]) and the QUEST 2.0 [100].

Misalignment and Displacement Measures

Motion data analysis allows making direct conclusions regarding misalignment and relative displacement between the fixations and the human limb. Misalignment measures (figure 3.12) show differences in the Z axis, with both SOF and SOL devices having a smaller initial misalignment in comparison with H2, with no apparent differences for the Y axis. Initial misalignments are around 1 and 1.5 cm for My and Mz, respectively, which is within the values found in literature [33, 48]. Furthermore, misalignment during gait is not constant. This agrees with what is stated in the literature [9, 27]. In fact, this variation during gait is likely due to either slippage of the connections and/or migration of the ICR of the biological which, due to the kinematic mismatch between both joints, is not followed by the AFO [81]. For the Z axis, misalignment diminishes in the H2 device during the swing phase of the gait. However, it is important to note that, during this gait phase, theoretical power transmission for the robotic joint to the user or vice-versa is not significant. In fact, it is to be expected that the largest torques are present during stance and, as such, misalignment during this phase will lead to higher spurious forces and torques at the HRI than during the swing phase. As such, SOF and SOL show lower misalignment in the stance phase, indicating lower misalignment-related interactions at the HRI. Overall, there is a need for manual alignment in all three devices. Furthermore, solutions that address the kinematic mismatch between the two joints are clearly necessary, since high misalignment variation can be identified across gait.

Displacement along the Z axis is the value that can more closely be correlated with sheer or friction interactions (as described in [22]) and, as such, is the most important to consider. The results show higher displacements along the Z axis for H2 during the initial stance phases and for SOF and SOL around the beginning of the swing phase. Nevertheless, the displacements are very small in magnitude, and differences between maximum displacements between H2, SOF, and SOL are within 2 mm, which cannot be

separated from some systematic or occasional error that could have occurred, as shown in [60]. As such, in this analysis, all three devices have approximately the same behavior. The displacements recorded are within the range present in other studies [60, 61]. Nevertheless, vertical displacement should be taken into account when introducing alignment solutions. Regarding displacement rotations, differences were only observed around the sagittal plane (Dα measure in figure 3.15 a). This is to be expected since it is the motion plane where actuation happens in the case of H2, which can result in an increase in relative movement. Nevertheless, all three curves for the three measures have approximately the same behavior and values, and as such, an exact conclusion cannot be made regarding which device has the lowest displacement rotations.

Pressure on Human-AFO Interface

Pressure data analysis shows fewer pressure interactions for the frontal design (SOF), then the lateral design (SOL), and then the H2 design. Safety assessment, however, is also fundamental, to ascertain if the pressures recorded are below recognized safety values [9, 24]. A full comparison with safety thresholds for pressure can be found in table 3.6.

Table 3.6: Captured and literature values for PDT, PTT and single-point PPT. Literature values from [105–107].

Pressure Values (kPa)	SOF	SOL	H2	PDT		PTT		PPT
				Healthy	Chronic Pain	Healthy	Chronic Pain	
Group Anterior Proximal	0.88± 1.01	10.84± 8.8	24.66± 20.72	16-34	10-18	42-91	<25	545.5 (P2)
Group Anterior Distal	1.43± 1.26	12.55± 12.88	6.91± 8.32					588.1 (P3)
Group Posterior Proximal	7.52± 8.46	8.98± 6.23	9.42± 7.44					416.6 (P8)
Group Posterior Distal	2.89± 1.73	12.02± 7.7	11.68± 7.63					416.6 (P8)

As shown, recorded values are largely below Pressure Pain Threshold (PPT) values from single-point algometry. These results can be a good initial benchmark to assess safety and pain onset but do not directly correlate to exoskeleton fixations [24]. Following the analysis with circumferential algometry, analysis for both healthy and subjects with chronic pain problems is important, since this last category can be also part of the target of these types of rehabilitation devices. The SOF device showed results where the average value plus one standard deviation for all four shin-guard locations is below the pain detection threshold for healthy subjects. The same occurs for patients that suffer from chronic pain except for the posterior proximal group. For the SOL AFO, only the posterior proximal group has an average plus standard deviation below pain detection thresholds for healthy individuals, with results from the anterior distal group being close to the upper bound of PTT for chronic pain patients. This can largely be attributed to the type and material of fixation, an important factor in pressure distribution [24, 25]. Finally, the value for the anterior proximal group of the H2 device surpasses safety levels even in healthy subjects, which is a major counter indication for its use. Furthermore, the posterior groups show values close to detection thresholds, another contraindication. The main difference between SOF and SOL can be attributed to the different materials of the straps since these devices report similar misalignments. However, pressures recorded for the H2 device are higher than both SOF and SOL, which can be explained in part by the misalignment reported previously. In fact, while the polymer of the straps in the SOL device is in direct contact with the user's skin, the H2 straps have foam pads to increase comfort [93], which does not translate to lower pressures. This can indicate that these pressures are due to spurious forces in relation to misalignment. Overall, recorded values for the SOF device are largely within safety levels from literature, which is a good indication of its adoption.

Questionnaire on User's Satisfaction

Questionnaire results show higher comfort scores for the SOF device. Furthermore, the comparison with H2 shows valid shank and foot design choices. Both the introduction of a shin guard against the straps and a commercially available running shoe against the H2's shoe sole seems to reduce the user's discomfort. Furthermore, the main differences between SOF and SOL lie in the fixations at the level of the shin guard. While the frontal model relies on Velcro fixations, the lateral model relies on straps made of a stiffer polymer and a tighter fit, resulting ultimately in pain, discomfort, abrasions, and irritations, in accordance with the higher pressure values recorded. Furthermore, by having the shin guard located laterally, the anterior straps are in contact with the bony prominences of the tibia, which have lower thresholds for pain. This is in contrast to the SOF design, where the location of the shin guard ensures a better distribution of pressures, reducing pain and discomfort. These results are especially important because they indicate not general discomfort but concrete pain and lesions. Two studies [66, 110] have used the NASA TLX questionnaire [111], which assesses task load, and a simple 0-100 analog scale

for comfort. However, when these studies found significant comfort scores between test conditions, no significant difference was found in NASA TLX scores. On the other hand, the questionnaire used in this work found significant differences between the three devices regarding user satisfaction and allowed to assess which device's characteristics most contributed to these devices. This has not been observed in the literature.

As such, the SOF device has been shown to score higher regarding the user's comfort perception, while also showing higher scores for the occurrence of pain and pressure-related lesions. Within the scope of research done, this is the first work that proposes a correlation between the results of these questionnaires and misalignment.

3.5 Conclusions

An experimental protocol was developed to determine which of the three devices (a commercially available exoskeleton H2 and two prototypes developed in-house, characterized by the use of a frontal or lateral shin-guard) leads to reduced misalignment, interactions at the interface, and user-perceived comfort. The performed tests validate the working hypothesis that the devices had significant differences in most of the data analyzed. Results are consistent with the literature, showing that the SmartOs Frontal design has a design with less misalignment and interactions and increased user-perceived comfort. Motion capture data showed that the H2 AFO has larger misalignments, results concurrent with the questionnaire, and pressure data, which are important contraindications for its prolonged use. In the case of the two SmartOs devices. their main structure is similar, with the only difference being the shin guard, which leads to small differences in motion capture data. No differences were found regarding displacement measures for all three AFOs, which can indicate no difference regarding shear interactions on all three AFOs.

Regarding user perception, the SOF device showed higher scores than its lateral counterpart by leading to less pain, abrasion, and irritation while showing higher scores for H2 due to the SOF's shin and foot moduli and overall comfortability. Furthermore, pressure data measured with eight FSR at relevant pressure points showed that the SOF AFO leads to fewer pressures at the HRI than the SOL and H2 AFOs and that the interactions recorded in the case of this device were pain-free for the user, something that directly correlates with the results from the questionnaire. Overall, the SOF design is better suited to be considered for future use in the SmartOs project. Thus, Chapter 4 will propose alignment solutions for the SOF design. The misalignment and displacement results from this protocol will guide this design.

4

Alignment Solutions

Within this chapter, five different alignment solutions are presented. These solutions were developed according to the paradigm for alignment solutions presented in Chapter 2 for AFOs, as well as the needs identified in Chapter 3.

4.1 Introduction

The work presented in Chapter 2 provided a comprehensive view of the types of alignment solutions to be implemented and the most commonly implemented solutions in AFOs and lower limb exoskeletons with an ankle joint. On the other hand, Chapter 3 thoroughly compared three devices with different fixation philosophies, both regarding their human-robot joint misalignment, interface interactions, and user-perceived comfort. This work allowed an informed choice to be made regarding the fixation mechanism where alignment solutions should be implemented, the SOF (initial design in figure 4.1).

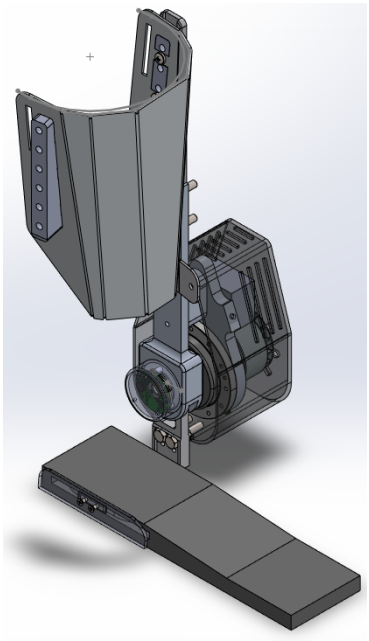

Figure 4.1: Initial CAD design of the SOF AFO.

The SOF's design can be separated into three moduli: foot, shank structure, and shin guard. The foot modulus is constituted by an ergonomic sports shoe, a footplate, and a medial plate. Within the CAD design, this shoe is replaced by a representative component (figure 4.2). The footplate is inserted into the shoe, machined beforehand, and screwed to the medial plate using two M3 screws. H2 users had reported discomfort related to this device's shoe foot structure solution (a footplate where the user attached its shoe through Velcro straps), which prompted this design choice [35].

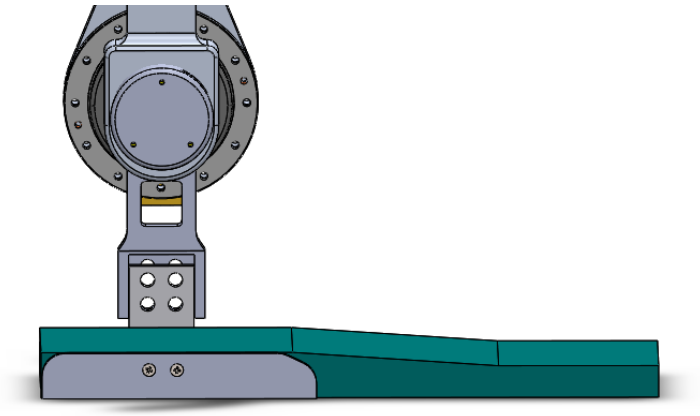

Figure 4.2: SOF foot initial design. Image from [35]

The shank structure of SOF (figure 4.3) realizes two fixations, distally and proximally. The distal fixation connects the footplate to the motor connector plate, where the actuation module is implemented (figure 4.3 a). This fixation is realized through four screw holes at the footplate and two continuous

openings at the motor connector plate. This allows for a regulation of 5 mm in height. Proximally, the motor connector plate is fixed to the shank upright through two M6 and two M5 screws, and to the shin guard through three M6 screws (figure 4.3 b and c, respectively). The first fixation does not allow any change in height, while the fixation to the shin guard can be changed to a maximum of 4.5 cm. During the studies described in this work, both connections were kept at the lowest possible configuration.

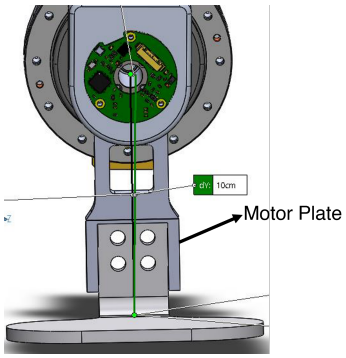

(a) Shank distal fixation.

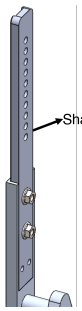

(b) Motor plate and shank upright fixation.

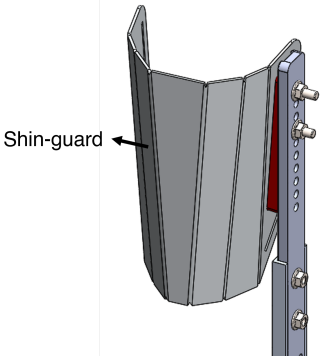

(c) SOF shank initial design. Image from [35]

Figure 4.3: Shank structure design

The shin guard was designed to increase the contact area between the user's shank and the AFO in order to better distribute stress, thus increasing comfort (figure 4.4). This shin guard was developed to cover approximately $\frac{2}{3}$ of the patient's leg and to be placed 10 cm below the user's knee joint. This was realized in [35] by designing the shin guard around the model of a shank of a person with a height of 1.50 meters.

Figure 4.4: SOF shin guard initial design. Image from [35]

By considering the results in Chapter 3 and the initial design described before, effective solutions can be designed. Results from Chapter 3 showed an average initial misalignment of -1.9 cm vertically and -1 cm horizontally. As such, solutions should allow the vertical and horizontal coordinates of the robotic joint

to be increased. Furthermore, an average maximum vertical displacement of -0.7 cm points to the need to develop a compensation mechanism. The standard deviations of these three measures will be used to dimension two manual alignment solutions and one kinematic redundancy solution. Furthermore, one more manual alignment solution and one kinematic redundancy solution will also be designed and validated in this Chapter.

4.2 Methods

4.2.1 Mechanical Design of Alignment Solutions

By considering the misalignment requirements and the alignment solutions reviewed in Chapter 2, this work idealized and designed 5 alignment solutions: 3 manual alignment solutions and 2 solutions based on kinematic redundancy. All solutions and simulations were designed in SolidWorks 2021® (Dassault Systèmes, Vélizy-Villacoublay, France). Table 4.1 presents these solutions and the related measure according to Chapter 3. Technical drawings of all alignment solutions can be found in Appendix C.

Table 4.1: Alignment solutions to be implemented into the SOF design.

Solution	Measure	Type of Solution	Solution
1	Initial Vertical Misalignment	Manual Alignment	Adjust joint's vertical position
2	Initial Horizontal Misalignment	Manual Alignment	Adjust joint's horizontal position
3	Poor shin guard fitness	Manual Alignment	Adjust shin guard position
4	Misalignment across gait	Kinematic redundancy	Release Iv/Ev through a revolute joint
5	Linear cuff displacement	Kinematic redundancy	Introduce a prismatic joint

Data from Chapter 3 was used to guide the dimensioning of solutions **"Adjust joint's vertical position"**, **"Adjust joint's horizontal position"** and **"Introduce a prismatic joint"**. To do this, three measures were calculated: initial vertical misalignment; initial horizontal misalignment; and maximum vertical displacement. These measures correlate with solutions **"Adjust joint's vertical position"**, **"Adjust joint's horizontal position"**, and **"Introduce a prismatic joint"**, respectively. The range of these measures is presented in table 4.2. The corresponding plots (figure 4.5) show the average of these measures for all 10 participants and, shaded, the standard deviation.

Table 4.2: Range of measures for solution dimensioning

Measure	Range (cm)	Solution
Initial vertical misalignment (cm)	-2.89 to -0.62	M1
Initial horizontal misalignment (cm)	-1.9 to -0.31	M2
Maximum vertical displacement (cm)	-0.97 to 0.33	S1

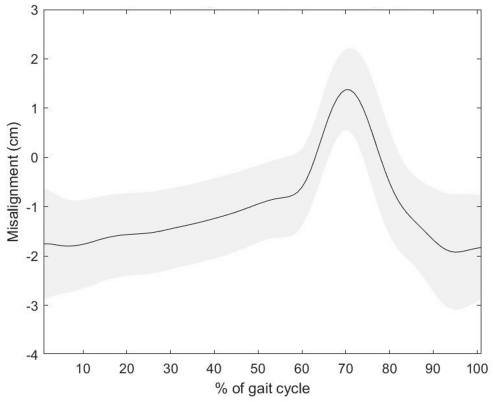

(a) Vertical (Z) misalignment.

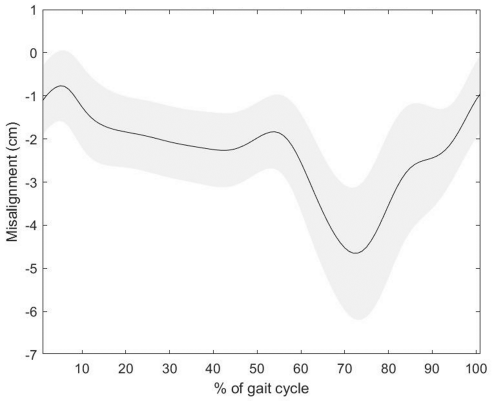

(b) Horizontal (Y) misalignment.

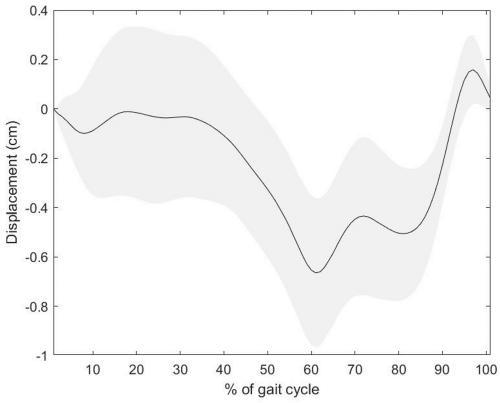

(c) Vertical (Z) displacement.

Figure 4.5: Average and standard deviations for vertical and horizontal misalignment and vertical displacement.

Manual alignment solutions were chosen since they are present in all devices explored in Chapter 2. Furthermore, they are easy to implement, carry low complexity, and have low mass and volume [27]. While they increase user complexity by increasing Don and Doff times, this was taken into account when developing the solutions, and, as such, they were developed in a way that required only an initial fit for the user.

Alignment solution 1 (**"Adjust joint's vertical position"**) was developed considering the measure "Vertical initial misalignment" (table 4.2). This measure indicates an initial misalignment that ranges from

-2.89 cm to -0.62 cm. As such, there is a need to increase the Z coordinate of the robotic joint. The main purpose of this solution is to allow for this vertical adjustment. This solution was realized by adding six sets of screw holes at the connection between the footplate and the motor connector plate. These screw holes are 0.5 cm apart and allow for vertical regulation of the motor connector plate. If needed, additional screws can be inserted to increase mechanical stability. The height of the motor connector plate was kept the same, while the cut that supports the screws was increased by 1 cm. As such, the height of the motor connector plate can now vary from the initial position to 2.5 cm above the initial position. The initial design did not allow for height adjustment of the robotic joint. Figure 4.6 shows the initial design (a) and the lowest (b) and highest (c) vertical heights of the new design.

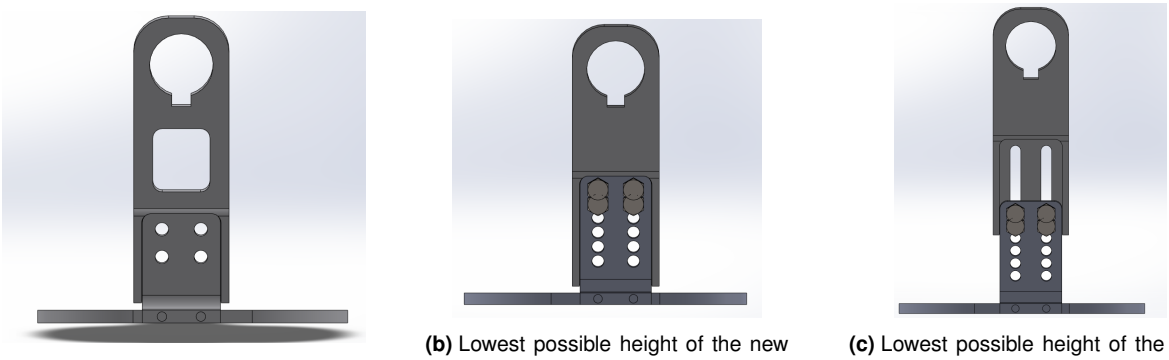

(a) Initial design.

(b) Lowest possible height of the new design.

(c) Lowest possible height of the new design.

Figure 4.6: Vertical alignment solution design. In (b) the robotic joint is in the same position as in the initial design. In (c) the robotic joint had its vertical position increased by 2.5 cm.

Alignment solution 2 (**"Adjust joint's horizontal position"**) was developed considering the measure "Horizontal initial misalignment". This measure indicates an initial misalignment that ranges from -1.9 cm to -0.31 cm. As such, the horizontal position of the joint should be adaptable, which is the purpose of this solution. In the initial design, the footplate is connected to the shoe through an outsole plate. The current design does not allow for horizontal adjustment of this outsole plate. Furthermore, while the used CAD model of the outsole plate only includes two M3 screw holes, the prototype used in Chapter 3 realizes this connection through five screws. This was replicated in the final design by replacing the two initial holes with the five of the final prototype. While the centers of the initial holes were 1.22 cm apart, those of the final design were 0.5 cm apart. Finally, four more screw holes were within the same distance, and the length of the outsole plate was increased by 2 cm. This realized the alignment solution by allowing the user to adjust the horizontal position of the robotic joint to a maximum of 2 cm in steps of 0.5 cm. The initial and final designs are illustrated in figure 4.7

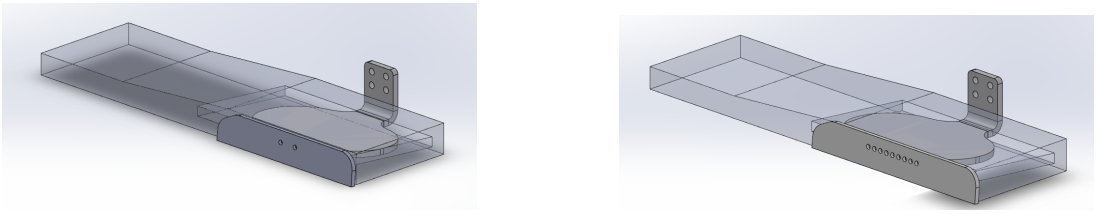

(a) Initial design.

(b) Design of the horizontal alignment solution.

Figure 4.7: Horizontal alignment solution design. In (b), the horizontal position of the robotic joint was increased by 2.0 cm.

The alignment solution **"Adjust shin guard position"** allows for better alignment of the shin guard. Since the fixation realized by the shin guard is rather rigid, its contact with low-compliant tissues will lead to increased interactions, and, as such, a fitting of the shin guard in softer tissue is necessary to increase comfort. From the protocol in Chapter 3, it was found that the subject with the lowest shank length had the shin guard in contact with his knee joint. This subject had a height of 1.70, which is within the range of heights allowed by the initial design [35]. The initial design allowed only lowering the height of the shin guard by 0.9 cm by providing an additional screw hole at the connection between the shin guard and the proximal upright. It was found to not be sufficient to prevent contact with less compliant tissue close to the knee joint. As such, the height of the shin guard should be adaptable, which is the main purpose of this solution. This was done by adding an additional hole at the connection between the shin guard and the proximal upright of the AFO and two additional screw holes at the connection between the proximal upright and the distal motor connector plate. Each of these alterations allowed the shin guard to be lowered an additional 0.9 cm. The final design allows lowering the shin guard by a total of 3.6 cm, whereas the initial design only allowed for 0.9 cm.The initial design as well as the final solution are illustrated in figure 4.8.

(a) Initial design.

(b) Design of the shin guard alignment solution.

Figure 4.8: Shin guard alignment solution. In (b), the shin guard has lowered a total of 1.8 cm through the two additional sets of holes at the connection between the two bars

The solution **"Release inversion/eversion through a revolute joint"** was developed to partly solve

the kinematic mismatch between the user and the AFO. As noted in Chapter 2, a common strategy to solve kinematic mismatch is by releasing the inversion/eversion DOF of the robotic joint. Furthermore, Chapter 3 showed that misalignment varied significantly across gait, which closely relates to kinematic mismatch. As such, this solution released the inversion/eversion DOF by introducing a revolute joint at the footplate level, designed by splitting the footplate structure in two. The axis of this joint was kept perpendicular to the plane of actuation to avoid the transmission of actuation torque to this DOF. A more complex design with mechanical end stops should still be implemented in order to increase the safety and applicability of the solution. The initial design of the footplate, as well as the design of this solution, are illustrated in figure 4.9.

(a) Initial design. **(b)** New design after the revolute joint was implemented.

Figure 4.9: Design of the solution **"Release inversion/eversion through a revolute joint"**.

Finally, the solution **"Introduce a prismatic joint"** was designed considering the measure "Maximum vertical displacement" (table 4.2). This measure indicates a cuff displacement between -0.97 and 0.33 cm. As such, this displacement should be eliminated since it correlates with shear forces at the HRI. The low vertical compliance of the initial design does not allow for compensation for this displacement. A prismatic DOF was introduced in the shank structure of the AFO, of which the main purpose is to compensate for the measured displacement. This solution consists of a rail mechanism between the shin guard and the proximal upright. Although this solution is not directly present in the literature, none of the studies reviewed in Chapter 2 did a direct assessment of fixation displacement. The proximal upright of the shank structure was cut following the guide's geometry and functions as the rail, while an additional part was introduced between this bar and the shin guard fixation that functions as the guide. This guide is fixed to the structure through screws, following the same mechanisms as the initial design. The prismatic joint has a vertical ROM of 1 cm, following the requirements in table 4.2. The guide is made of aluminum (AL6082). Figure 4.10 illustrates the initial design and the solution implemented.

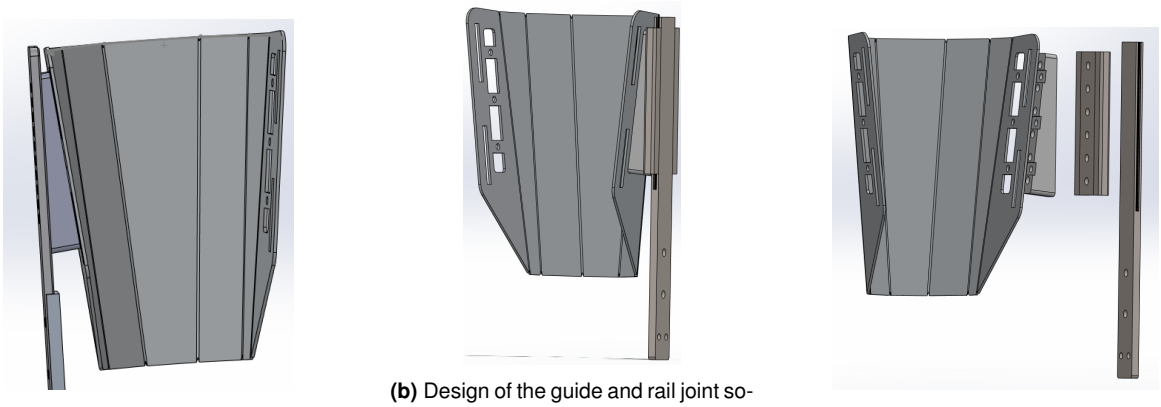

(a) Initial design.

(b) Design of the guide and rail joint solution.

(c) Exploded view of the new design.

Figure 4.10: Design of the solution **"Introduce a prismatic joint"**.

4.2.2 Validation of Alignment Solutions

To validate the solution **"Adjust joint's vertical position"**, it is necessary to guarantee the mechanical integrity of the structure. As such, mechanical simulations were made using the simulation tool from SolidWorks 2021® (Dassault Systèmes, Vélizy-Villacoublay, France). This simulation was based on previous work done in this prototype by [35]. In this simulation, the structural integrity of the connection between the footplate and the motor connector plate is tested by applying a torque of 65 N.m. where the actuation module would be. Due to the inability of the software to define bolt connectors in a situation of a continuous bolt hole, representative components were used to mimic this connection. Furthermore, the sole of the footplate was fixed, rigid connections were defined between the footplate and the motor fixation (in order to simulate the fixation) and contact sets were defined between the non-touching faces of the footplate and the bolt's representative components. The quality of the mesh was defined to be 3 mm with curvature-based elements, which increases the quality of the mesh in higher curvature areas. The material used for both structures was the aluminum alloy Al6082-T651, which is the material of the initial prototype, while the bolt's representative components were made of class 8.8 steel bolts.

Regarding the alignment solution **"Adjust joint's horizontal position"**, validation was done through a mechanical simulation. The work in [35], which describes the development of the initial prototype, does not include any validation for the fixation between the footplate and the outsole plate. The same torque of 65 N.m. was applied to the motor connector plate. Interactions of the bonded type were defined between the motor connector plate and the footplate. This ensures that these components are treated as being "welded" together. This was done because this fixation was not under study. A contact set (*No Penetration* and *Surface to Surface Contact*) was defined between the face of the footplate that connects with the outsole plate and three M3 screw connectors of galvanized steel were defined in this connection. The basis of the footplate was fixed. The footplate and motor connector plate had the same

material as in the test described before, while the material of the outsole plate was set to Al6082-T651. Furthermore, real-life tests were done on the prototype. Part of these tests was done through the experimental protocol in Chapter 3, where it was proven that prolonged use of the AFO did not compromise its structural integrity. Furthermore, the same prototype was tested with an initial version of the actuation module, wherein the actuator applied a torque similar to the real use case. Test results showed that the structural integrity of the fixation between the footplate and the outsole plate was not compromised. Since the new design does not change the structure significantly, a choice was made to not perform additional validation tests.

The mechanical stability of the new shank structure implemented in the solution **"Adjust shin guard position"** was tested using the same simulation tool from SolidWorks 2021®(Dassault Systèmes, Vélizy-Villacoublay, France). The work in [35] further described a similar test for the initial design of this structure. In this test, a torque of 65 N.m was applied where the actuation module would be. Furthermore, bolt connectors were defined between the shin guard insert and the proximal upright and between the proximal upright and distal motor connector plate. Contact sets were defined (*No Penetration* and *Surface to Surface Contact*) between the coincident faces of the shin guard insert and the proximal upright and between the proximal upright and the distal motor connector plate, ensuring that they are in contact. A similar material (Al6082-T651) and class 8.8 steel bolts were used. Fixed geometry was applied to the shin guard insert.

The solution **"Release inversion/eversion through a revolute joint"** was validated through a motion test. To do this, a model of the human foot and leg was imported into the CAD software and fixed to the sole. This human model had the following dimensions: shank length of 40.5 cm; shank radius of 5.59 cm; foot length of 25.7 cm; foot width of 8 cm. The angle between the leg and the foot was increased and decreased by 25° (above biological levels [45]) and an interference test was done between the foot and leg models and the orthosis structure. This is illustrated in figure 4.11. This test assesses the ROM of the implemented revolute joint by recording the angles where there is a collision between the leg or foot and the AFO. The study was done at 60 frames per second for 15 seconds. Within the first five seconds, the joint performed an eversion motion, followed by an inversion motion during the next five seconds towards the initial position and an eversion motion for the last five seconds.

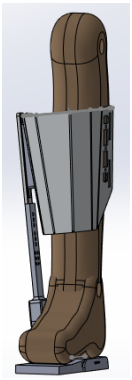

(a) Initial position of the study.

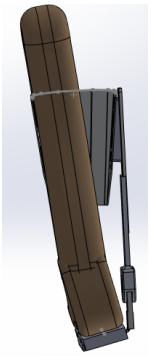

(b) First interference during inversion.

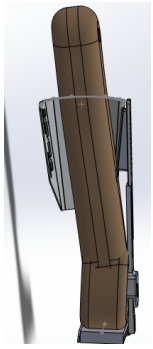

(c) First interference during eversion.

Figure 4.11: Motion study for the revolute joint solution.

The solution **"Introduce a prismatic joint"** was also validated through a motion study. Within this, the same model of a human leg and foot was imported into the CAD software. This model was fixed to the posterior face of the shin guard and the guide position was set at 0.5 cm below the top of the rail. The model was set to rotate 12 ° in each direction in the frontal plane (figure 4.12), thus provoking a linear movement of the guide. An interference check between the guide and the top and bottom parts of the rail was done. This allowed assessing the compensation ability of the rail.

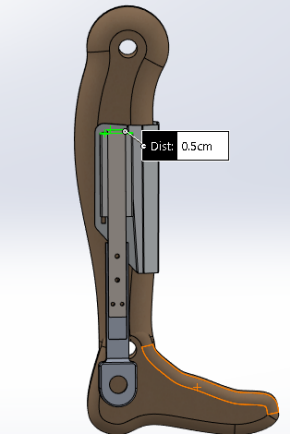

(a) Initial position of the study.

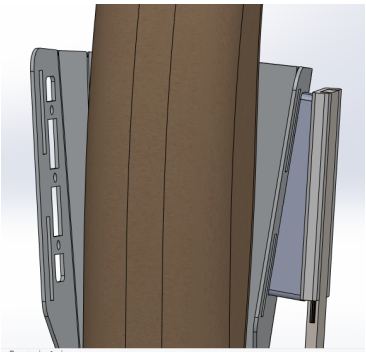

(b) First interference during inversion.

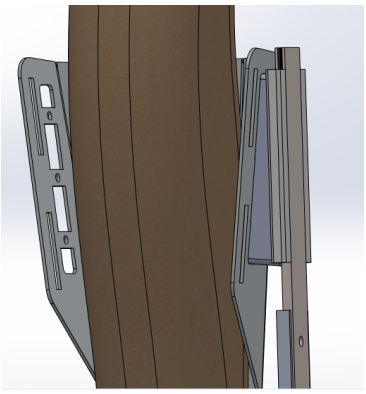

(c) First interference during eversion.

Figure 4.12: Motion study for the revolute joint solution.

Finally, the final prototype with all five solutions implemented was validated through a mechanical simulation study. In this test, a torque of 65 N.M was applied at the actuation level. Fixed geometry fixations were defined at the bottom of the footplate and at the shin guard insert. Contact sets (*No Penetration* and *Surface to Surface Contact*) were defined between the following components: the outsole plate and the footplate; the upper component of the revolute joint and the motor connector plate; the motor connector plate and the shank upright and the guide of the prismatic joint and the shin guard

insert. Bonded interactions were defined between the following components: the lower and upper parts of the revolute joint; both motor connector bars and the rail and guide of the prismatic joint.

4.3 Results

In order to guarantee that the structures subject to mechanical tests kept their structural integrity under the applied stresses, a Factor of Safety (FoS) of 1.5 was selected as the threshold to validate each solution. This FoS is defined as the quotient between the material's yield strength and the calculated Von Mises stress. The results for the validation of the vertical alignment solution are illustrated in figure 4.13. As per the same figure, the lowest FoS equals 1.682, above the set threshold.

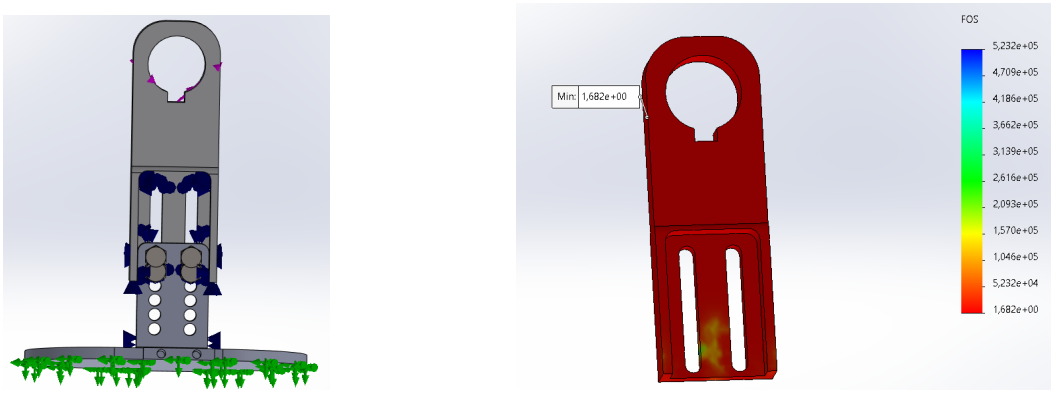

(a) Simulation conditions. **(b)** Simulation results.

Figure 4.13: Simulation conditions and results for the vertical alignment solution.

Results for the horizontal alignment solution are illustrated in figure 4.14. As per the same figure, the lowest FoS at the connection for the footplate equals 1.81, while the lowest FoS for the outsole plate equals 1.27. The FoS at the connection for the footplate is above the set threshold, while the one for the outsole plate is not. This is due to stress concentrations at the screw holes and will be further explored in the discussion section of this chapter.

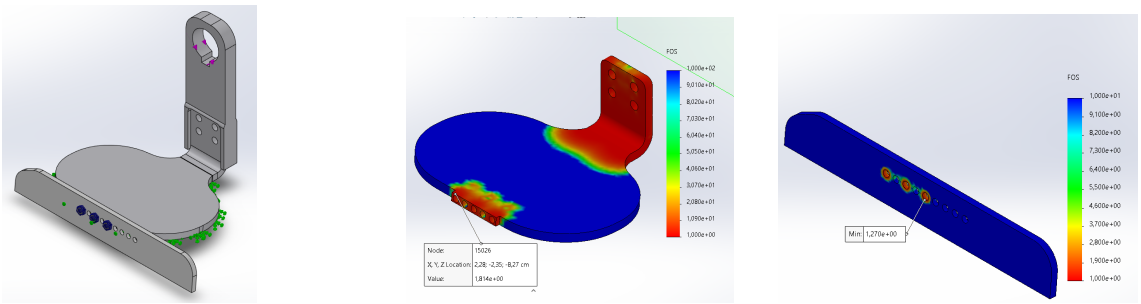

(a) Simulation conditions. **(b)** Simulation results for the footplate. **(c)** Simulation results for the outsole plate.

Figure 4.14: Simulation conditions and results for the horizontal alignment solution.

Similarly, simulation results for the shin guard alignment solution are found in figure 4.15. In this case, the lowest simulated value for the FoS is equal to 1.705, which is higher than the defined threshold.

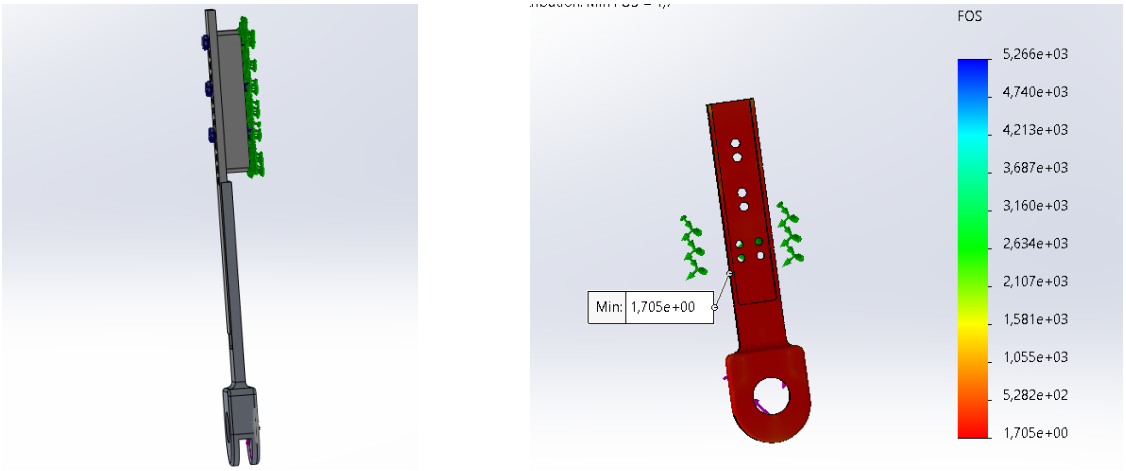

(a) Simulation conditions. **(b)** Simulation results.

Figure 4.15: Simulation conditions and results for the shin guard alignment solution.

The results of the motion study for the revolute joint solution can be found in figure 4.16, which details a plot of the angle variation across the motion study.

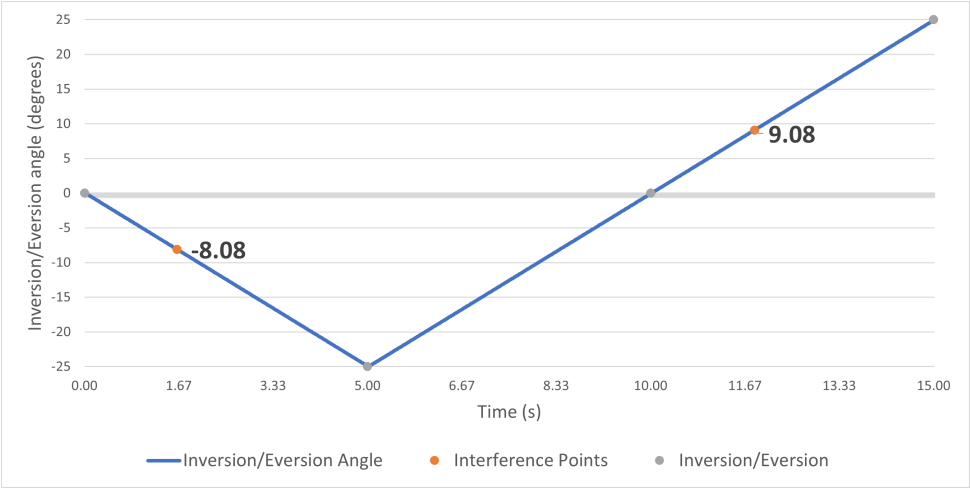

Figure 4.16: Angle variation across the motion study for the inversion/eversion release solution.

The results of the study found initial interference at around 8° for eversion and 9° for inversion. While biological ROMs for these DOFs are higher than these values [44], a study has found that during human gait the ROMs of eversion and inversion are around 5° [112]. Thus, the ROM of this solution was deemed sufficient for the application.

Finally, the results of the motion study for the prismatic joint solution can be found in figure 4.17, wherein is presented the angle rotation in the frontal plane.

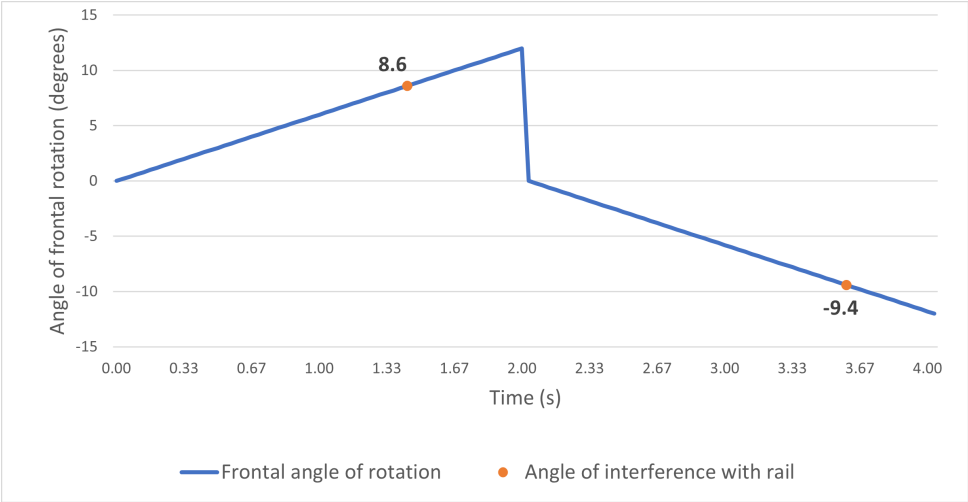

Figure 4.17: Angle variation across the motion study for the prismatic joint solution.

This study shows initial interference at around 8° for the positive rotation and 9° for the negative rotation. These results were found to be appropriate, since the prismatic joint managed to compensate for the full one cm set as a requirement, converting a rotation movement of the model into a linear movement of the guide. The final design of the AFO with the five implemented solutions is in figure 4.18.

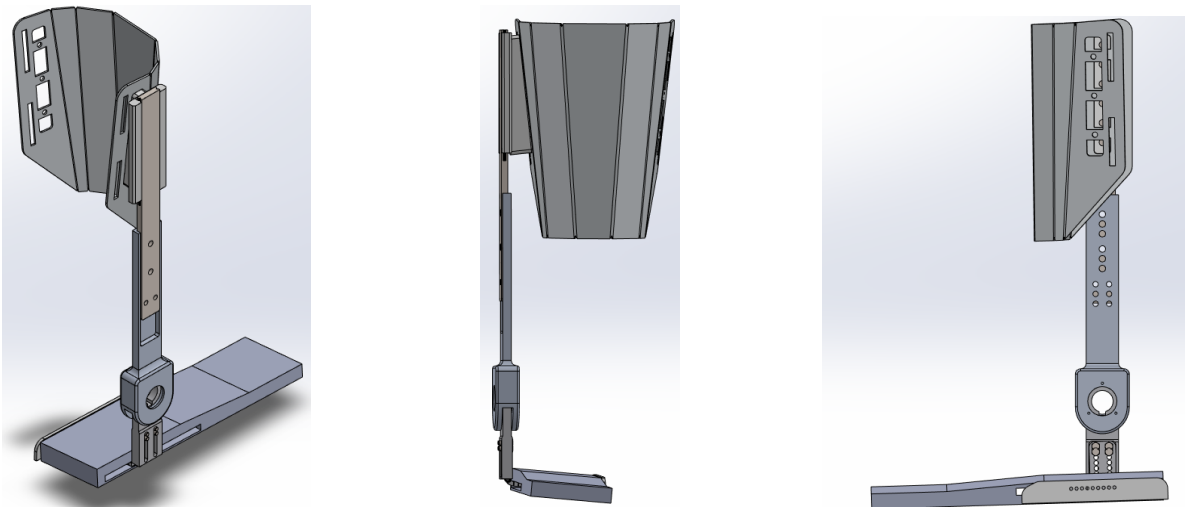

(a) Isometric view. **(b)** Frontal view. **(c)** Lateral view.

Figure 4.18: Final design of the AFO with the five solutions implemented.

The simulation conditions and results of the final prototype can be found in figure 4.19.

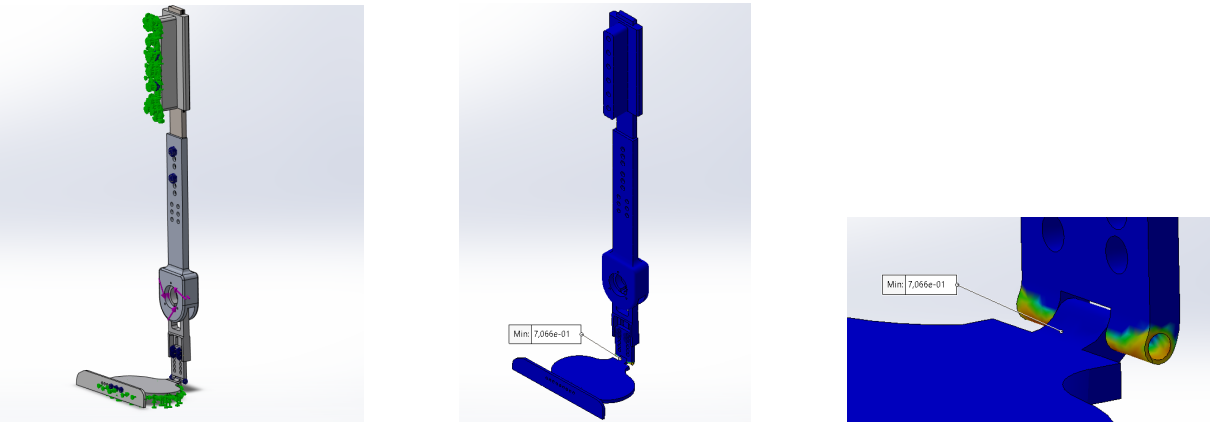

(a) Simulation conditions. **(b)** Simulation results. **(c)** Close up of the revolute joint.

Figure 4.19: Simulation conditions and results for the final design. Parts in blue recorded an FoS higher than 1.5.

The lowest FoS for this simulation was 0.7, which is below the threshold defined.

4.4 Discussion

The design for the alignment solution **"Adjust joint's vertical position"** has been proven to allow an initial vertical alignment within the requirements defined in table 4.2. Furthermore, mechanical stress tests have shown that structural integrity is kept under the expected stresses of normal use. This solution is, as such, fully developed for manufacturing and implementation into the current design. Within literature. manual alignment solutions allow only for vertical alignment so that the device is usable by subjects of different heights. The literature's manual alignment solutions are not implemented directly to align the robotic and user's joints. As such, the range of these solutions is not stated. Furthermore, within the scope of the research done, this work is the first to utilize experimental data to dimension a vertical manual alignment solution. The two studies referenced for direct assessment of misalignment through motion capture used this technique to validate previously designed alignment solutions [33, 48]. The alignment solution **"Adjust joint's horizontal position"** fully realizes the requirements defined in table 4.2. Although the FoS of the outsole plate was below the defined threshold, a choice was made that the design had sufficient mechanical stability. In fact, while the original prototype had not been validated in [35], real-life tests were done after production. Part of these tests was done through the experimental protocol in Chapter 3, where it was proven that prolonged use of the AFO did not compromise its structural integrity. Furthermore, the same prototype was tested with an initial version of the actuation module, wherein the actuator applied a torque similar to the real use case. Test results showed that the structural integrity of the fixation between the footplate and the outsole plate was not compromised. Since the new design does not change the structure significantly, a choice was made

to accept the current design as safe. As such, this solution is fully realized and ready to be produced and implemented. From the literature, no horizontal alignment solution was found. Since no study used direct misalignment assessment to dimension manual alignment solutions, a hypothesis for the lack of horizontal alignment solutions is that, visually, horizontal misalignment is not evident. As such, it is possible that the authors of these studies did not find a need for this kind of solution. Nevertheless, this work shows that such a solution is needed and should be implemented.

The alignment solution **"Adjust shin guard position"** fully realizes the objective of the user being allowed to lower the vertical position of the shin guard. Furthermore, the stress studies proved that the implemented solution did not compromise the structural integrity of the design. As such, this solution is fully realized and ready for production. The original design from [35] only allowed the shin guard's position to be increased by 4.5 cm. This work proves that an adaptation that lowers the shin guard's position is necessary to better realize the structure's design to a wider range of users.

The kinematic redundancy solution that releases inversion/eversion rotations was implemented according to the high variability of misalignment during gait and due to its frequent use in the literature. Motion studies showed a ROM of 8° for eversion and 9° for inversion, before the user's limb reaches the shin guard, which is adequate for anatomic gait. However, the ROM of the implemented joint is 360°, since no mechanical end stops were implemented. The full anatomical ROM of the inversion/eversion DOF of the ankle joint is between 25° and 30° for eversion and around 52° for inversion [45]. As such, solutions from the literature have implemented mechanical end-stops for these joints to avoid safety hazards [75] [76]. Study [27] states that designed solutions should not have a larger workspace than the user's joint. As such, these safety features should be implemented into the current design before production.

The solution **"Introduce a prismatic joint"** fully realizes the requirements stated in 4.2. Furthermore, this solution increases the overall mass of the AFO by approximately 74 grams, representing an 8% increase from the original mass of 917 grams (excluding the actuation modulus). No similar solution was found in the literature for AFOs. This is mainly due to the need to first assess the displacement to properly dimension the solution, which was not done. Nevertheless, study [33] describes the validation of a similar solution for a knee exoskeleton. The study reported that its alignment solution weighed 190 grams. Although the solution included, besides a prismatic joint, two revolute joints, these were directly implemented on existing braces. As such, it is expected that the prismatic joint is the main contributor to this added mass. The solution in [33] represents a mass that doubles that of the solution here described. Nevertheless, its validation showed improved comfort and performance [110]. As such, the weight of the implemented solution may not be problematic for real-life validation. Nevertheless, a mechanism that prevents the guide from escaping the rail through its top opening should still be implemented before production.

Finally, the validation results for the final design show a FoS above the required threshold for all compo-

nents except the revolute joint. However, as described before, this solution is not fully realized, since the current design still needs the implementation of mechanical end stops. As such, a follow-up study of the mechanical stability of the final design with a new iteration of the revolute joint solution is still required. In fact, this next iteration should also increase the mechanical durability of this connection.

4.5 Conclusion

From the work done in Chapter 2 and Chapter 3, five solutions were idealized. These solutions followed what was found to be the overall trend from the literature regarding alignment solutions and the results from the experimental protocol. As such, three manual alignment solutions, one solution that freed the inversion/eversion DOF and one solution that introduced a prismatic joint, were successfully designed, implemented, and validated (where applicable) following the dimensions assessed in Chapter 3 and the guidelines for mechanical simulations of the previous prototype from [35]. All three manual alignment solutions are ready for production and implementation, while the two kinematic redundancy solutions still need further adjustments. The final design with all five alignment solutions implemented was validated, with the results indicating the need to increase the mechanical durability of the revolute joint solution.

5

Conclusions

Within this Chapter, the main conclusions are drawn of the work done in this dissertation and provide an overview of possible future work.

5.1 Concluding Remarks

This dissertation had three distinct parts, each corresponding to Chapter 2 through Chapter 4. The work in each Chapter was done towards the main goal, to develop solutions that would solve the misalignment problem in an AFO prototype of SmartOs project.

In Chapter 2, first, a comprehensive review of misalignment causes and effects on the basis of literature was given. It was found that human-robot joint misalignment is inevitable and that it arises from the impossibility of, initially, properly aligning the two joints and from the inherent kinematic mismatch of the two structures. Furthermore, the literature shows that this phenomenon leads to spurious forces and torques at the level of the interface between the human and the exoskeleton. These interactions are one of the main reasons behind user abandonment of these devices since they greatly compromise the user's comfort during use and can even pose a safety risk to the user. Secondly, a comprehensive review of misalignment and interaction assessment strategies was done. Five different measures were found to assess misalignment: direct misalignment assessment through motion capture; fixation displacement through motion capture; pressure assessment through FSR sensors; shear stresses assessment through load cells; musculoskeletal interaction assessment through a dummy limb. Finally, the state-of-the-art on alignment solutions in AFO and exoskeletons was presented. It was found that all devices implemented manual alignment solutions. Furthermore, a majority introduced an additional inversion/eversion DOF to partly solve the kinematic mismatch between the human-robot systems. This implementation was done either through the introduction of compliant materials at the joint level or through revolute joints. Finally, soft exoskeletons are still in an early phase of research but are increas-

ingly looking for a viable alternative to anthropomorphic exoskeletons to solve misalignment issues.
In Chapter 3, human-AFO misalignment and interactions were assessed in an experimental environment for the three different prototypes. The protocol followed the recommendations on misalignment assessment from the literature, by using motion capture data to assess misalignment and displacement, FSRs to collect pressure and interactions in HRI, and a comfort and satisfaction questionnaire to assess user's perception of the prototypes. It was found that the SmartOs Frontal (SOF) design performed better in most measures, namely misalignment, pressure interactions, and fixation displacements. Furthermore, it was the AFO with the higher satisfaction level rated by the participants. As such, this device was chosen to develop the alignment solutions. Experimental results also contributed in identifying the magnitude values and, as such, guided the design of solutions done in Chapter 4.
Finally, in Chapter 4, five different alignment solutions were designed using the orientations from the previous chapters and, when applicable, properly validated. These comprised three manual alignment solutions that allowed the user to adjust both joint and shin-guards position, a solution based on a revolute joint that released the inversion/eversion DOF of the joint, and a prismatic joint that compensated from the maximum vertical displacement captured in Chapter 3. All solutions, when applicable, passed their validation tests. The three manual alignment solutions are ready for production and implementation, while the remaining solutions need further work to make them more robust for real-life use.

5.2 Answers to Research Questions

The research initiatives conducted in this dissertation allow for answering the following RQs.

- RQ1: How is the human-robot joint misalignment assessed?
    - This RQ was answered in Chapter 2. Literature research found that human-robot joint misalignment can be assessed through five different measures: direct misalignment assessment through motion capture; fixation displacement through motion capture; pressure assessment in the HRI through FSR sensors; shear stresses assessment through load cells; and musculoskeletal interaction assessment through a dummy limb.
- RQ2: Which are the main solutions designed to reduce misalignment in lower limb orthoses?
    - This RQ was answered in Chapter 2. Literature research found that there are four main types of solutions to reduce misalignment in lower limb devices: manual alignment; kinematic redundancy; compliance and soft structures. A narrative review of 19 AFOs and lower limb exoskeletons which implemented alignment solutions found that all implemented some type of alignment solution. Furthermore, four devices implemented only compliance solutions, four

implemented only kinematic redundancy solutions, five implemented both compliance and kinematic redundancy solutions, and six implemented structures made of soft materials.

- RQ3: Which AFO's fixation mechanism, within the three available, leads to the smallest misalignment and interactions and high user satisfaction?
  - The protocol from Chapter 3 gave an overview of the misalignment of three different fixation philosophies and allowed to conclude that the SOF design led to reduced misalignment and interactions and higher user-perceived comfort. This was done through an assessment of the human-robot joint misalignment, fixation displacement, pressure data, and a user-perceived comfort and pain questionnaire. This device introduces connections with the user in two-point, foot, and shank. The foot connection is realized through an ergonomic sports shoe fixed to the AFO's shank structure, while the shank fixation is achieved through a frontal shin guard.
- RQ4: Which are the needed alignment solutions in the AFO that answers RQ3?
  - The work in Chapter 3 allowed the assessment of three measures for which alignment solutions needed to be implemented, namely the vertical and horizontal initial misalignment and the maximum vertical fixation displacement. The same work gave further insight into other alignment solutions that could be implemented, while the work in Chapter 2 gave an overview of the most effective solutions to implement. The work in Chapter 4 answered this RQ by realizing the design of five alignment solutions, three based on manual alignment and two based on kinematic redundancy: "Adjust joint's vertical position"; "Adjust joint's horizontal position"; "Adjust shin guard position"; "Release inversion/eversion through a revolute joint"; and "Introduce a prismatic joint".

5.3 Future Work

First, an analysis of all three devices after the in-house models have their actuation modules implemented should be done, since it is not clear if the results would be significantly different. Furthermore, a direct assessment of shear stresses through one of the methods described in Chapter 2 should be done, since it will allow a better assessment of the interactions. Finally, the gait kinematics captured from the protocol and the treadmill data have yet to be analyzed. Since each device is expected to have a significant effect on normal gait kinematics, this analysis should be done. Nevertheless, remarkably different conclusions are not expected to be reached, since misalignment is closely related to human-robot kinematics. Regarding the implementation of alignment solutions, the three manual alignment solutions are ready for production and implementation, while the remaining two need further work to increase their safety and usability. Finally, validation of each solution in a real-life setting should be done.

References

[1] A. Esquenazi and M. Talaty, "Robotics for lower limb rehabilitation," *Physical Medicine and Rehabilitation Clinics of North America*, vol. 30, pp. 385–397, 5 2019.

[2] M. Volpini, V. Bartenbach, M. Pinotti, and R. Riener, "Clinical evaluation of a low-cost robot for use in physiotherapy and gait training," *J Rehabil Assist Technol Eng*, vol. 4, p. 2055668316688410, Jan. 2017.

[3] G. Morone, S. Paolucci, A. Cherubini, D. De Angelis, V. Venturiero, P. Coiro, and M. Iosa, "Robot-assisted gait training for stroke patients: current state of the art and perspectives of robotics," *Neuropsychiatr Dis Treat*, vol. 13, pp. 1303–1311, May 2017.

[4] "Labiomep - porto biomechanics laboratory," https://labiomep.up.pt/.

[5] "Birdlab - smartos project," http://birdlab.dei.uminho.pt/smartos//.

[6] N. Smidt, H. C. de Vet, L. M. Bouter, and J. Dekker, "Effectiveness of exercise therapy: A best-evidence summary of systematic reviews," *Australian Journal of Physiotherapy*, vol. 51, no. 2, pp. 71–85, 2005. [Online]. Available: https://www.sciencedirect.com/science/article/pii/S0004951405700362

[7] A. Ashburn, C. Partridge, and L. D. Souza, "Review article : Physiotherapy in the rehabilitation of stroke: a review," *Clinical Rehabilitation*, vol. 7, no. 4, pp. 337–345, 1993. [Online]. Available: https://doi.org/10.1177/026921559300700410

[8] A. Trulsson Schouenborg, M. Rivano Fischer, E. Bondesson, and A. Jöud, "Physiotherapist-led rehabilitation for patients with chronic musculoskeletal pain: interventions and promising long-term outcomes," *BMC Musculoskelet Disord*, vol. 22, no. 1, p. 910, Oct. 2021.

[9] E. Rocon, A. F. Ruiz, R. Raya, A. Schiele, J. L. Pons, J. M. Belda-Lois, R. Poveda, M. J. Vivas, and J. C. Moreno, *Human–Robot Physical Interaction*. John Wiley & Sons, Ltd, 2008, ch. 5, pp. 127–163. [Online]. Available: https://onlinelibrary.wiley.com/doi/abs/10.1002/9780470987667.ch5

[10] N. Postol, S. Lamond, M. Galloway, K. Palazzi, A. Bivard, N. J. Spratt, and J. Marquez, "The metabolic cost of exercising with a robotic exoskeleton: A comparison of healthy and neurologically impaired people," *IEEE Trans Neural Syst Rehabil Eng*, vol. 28, no. 12, pp. 3031–3039, Jan. 2021.

[11] C. Beyaert, R. Vasa, and G. E. Frykberg, "Gait post-stroke: Pathophysiology and rehabilitation strategies," *Neurophysiologie Clinique*, vol. 45, pp. 335–355, 2015.

[12] C. J. Winstein, J. Stein, R. Arena, B. Bates, L. R. Cherney, S. C. Cramer, F. Deruyter, J. J. Eng, B. Fisher, R. L. Harvey *et al.*, "Guidelines for adult stroke rehabilitation and recovery: a guideline for healthcare professionals from the american heart association/american stroke association," *Stroke*, vol. 47, no. 6, pp. e98–e169, 2016.

[13] M. Yamamoto, K. Shimatani, M. Hasegawa, and Y. Kurita, "Effect of an ankle–foot orthosis on gait kinematics and kinetics: case study of post-stroke gait using a musculoskeletal model and an orthosis model," *ROBOMECH Journal*, vol. 6, 07 2019.

[14] "American stroke association - foot drop," https://www.stroke.org/en/about-stroke/effects-of-stroke/physical-effects-of-stroke/physical-impact/foot-drop.

[15] A. Agrawal, S. K. Banala, S. K. Agrawal, and S. A. Binder-Macleod, "Design of a two degree-of-freedom ankle-foot orthosis for robotic rehabilitation," *Proceedings of the 2005 IEEE 9th International Conference on Rehabilitation Robotics*, vol. 2005, pp. 41–44, 2005.

[16] B. Chen, B. Zi, Y. Zeng, L. Qin, and W. H. Liao, "Ankle-foot orthoses for rehabilitation and reducing metabolic cost of walking: Possibilities and challenges," *Mechatronics*, vol. 53, pp. 241–250, 8 2018.

[17] M. Moltedo, T. Baček, T. Verstraten, C. Rodriguez-Guerrero, B. Vanderborght, and D. Lefeber, "Powered ankle-foot orthoses: The effects of the assistance on healthy and impaired users while walking," *Journal of NeuroEngineering and Rehabilitation*, vol. 15, 10 2018.

[18] J. Kwon, J. H. Park, S. Ku, Y. H. Jeong, N. J. Paik, and Y. L. Park, "A soft wearable robotic ankle-foot-orthosis for post-stroke patients," *IEEE Robotics and Automation Letters*, vol. 4, pp. 2547–2552, 7 2019.

[19] K. A. Shorter, G. F. Kogler, E. Loth, W. K. Durfee, and E. T. Hsiao-Wecksler, "A portable powered ankle-foot orthosis for rehabilitation," *Journal of Rehabilitation Research and Development*, vol. 48, pp. 459–472, 2011.

[20] M. Moltedo, T. Bacek, K. Junius, B. Vanderborght, and D. Lefeber, "Mechanical design of a lightweight compliant and adaptable active ankle foot orthosis," *Proceedings of the IEEE RAS and*

EMBS International Conference on Biomedical Robotics and Biomechatronics, vol. 2016-July, pp. 1224–1229, 7 2016.

[21] S. Duerinck, E. Swinnen, P. Beyl, F. Hagman, I. Jonkers, P. Vaes, and P. Roy, "The added value of an actuated ankle-foot orthosis to restore normal gait function in patients with spinal cord injury: A systematic review," *Journal of rehabilitation medicine : official journal of the UEMS European Board of Physical and Rehabilitation Medicine*, vol. 44, pp. 299–309, 03 2012.

[22] N. Jarrassé and G. Morel, "Connecting a human limb to an exoskeleton," *IEEE Transactions on Robotics*, vol. 28, pp. 697–709, 2012.

[23] B. Phillips and H. Zhao, "Predictors of assistive technology abandonment," *Assistive technology : the official journal of RESNA*, vol. 5, pp. 36–45, 02 1993.

[24] J. Bessler, G. B. Prange-Lasonder, L. Schaake, J. F. Saenz, C. Bidard, I. Fassi, M. Valori, A. B. Lassen, and J. H. Buurke, "Safety assessment of rehabilitation robots: A review identifying safety skills and current knowledge gaps," *Frontiers in Robotics and AI*, vol. 8, 3 2021.

[25] J. Bessler, G. B. Prange-Lasonder, R. V. Schulte, L. Schaake, E. C. Prinsen, and J. H. Buurke, "Occurrence and type of adverse events during the use of stationary gait robots—a systematic literature review," *Frontiers in Robotics and AI*, vol. 7, 11 2020.

[26] J. Wang, X. Li, T. H. Huang, S. Yu, Y. Li, T. Chen, A. Carriero, M. Oh-Park, and H. Su, "Comfort-centered design of a lightweight and backdrivable knee exoskeleton," *IEEE Robotics and Automation Letters*, vol. 3, pp. 4265–4272, 10 2018.

[27] M. B. Naf, K. Junius, M. Rossini, C. Rodriguez-Guerrero, B. Vanderborght, and D. Lefeber, "Misalignment compensation for full human-exoskeleton kinematic compatibility: State of the art and evaluation," *Applied Mechanics Reviews*, vol. 70, 9 2018.

[28] M. Cempini, S. M. M. D. Rossi, T. Lenzi, N. Vitiello, and M. C. Carrozza, "Self-alignment mechanisms for assistive wearable robots: A kinetostatic compatibility method," *IEEE Transactions on Robotics*, vol. 29, pp. 236–250, 2013.

[29] D. H. Wang, J. Guo, K. M. Lee, C. J. Yang, and H. Yu, "An adaptive knee joint exoskeleton based on biological geometries," *Proceedings - IEEE International Conference on Robotics and Automation*, pp. 1386–1391, 2011.

[30] A. Schiele and F. C. V. D. Helm, "Kinematic design to improve ergonomics in human machine interaction," *IEEE Transactions on Neural Systems and Rehabilitation Engineering*, vol. 14, pp. 456–469, 12 2006.

[31] D. Zanotto, Y. Akiyama, P. Stegall, and S. K. Agrawal, “Knee joint misalignment in exoskeletons for the lower extremities: Effects on user’s gait,” *IEEE Transactions on Robotics*, vol. 31, pp. 978–987, 8 2015.

[32] A. Schiele and F. C. van der Helm, “Influence of attachment pressure and kinematic configuration on phri with wearable robots,” *Applied Bionics and Biomechanics*, vol. 6, pp. 157–173, 2009.

[33] S. V. Sarkisian, M. K. Ishmael, G. R. Hunt, and T. Lenzi, “Design, development, and validation of a self-aligning mechanism for high-torque powered knee exoskeletons,” *IEEE Transactions on Medical Robotics and Bionics*, vol. 2, pp. 248–259, 5 2020.

[34] “Technaid - h2 exoskeleton,” https://www.technaid.com/products/robotic-exoskeleton-exo-exoesqueleto/.

[35] C. E. Ribeiro, “Design of a wearable active ankle-foot orthosis for both sides,” Master’s thesis, Universidade do Minho, Guimarães, Portugal, Apr. 2021.

[36] J. S. C. Figueiredo, “Smart wearable orthosis to assist impaired human walking,” Ph.D. dissertation, Universidade do Minho, Guimarães, Portugal, Jul. 2019.

[37] N. Itoh, D. Imoto, S. Kubo, K. Takahashi, N. Hishikawa, Y. Mikami, and T. Kubo, “Gait training using a stationary, one-leg gait exercise assist robot for chronic stroke hemiplegia: a case report,” *J Phys Ther Sci*, vol. 30, no. 8, pp. 1046–1051, Jul. 2018.

[38] R. Berriozabalgoitia, B. Sanz, A. B. Fraile-Bermúdez, E. Otxoa, I. Yeregui, I. Bidaurrazaga-Letona, I. Duñabeitia, A. Antigüedad, M. Domercq, J. Irazusta, and A. Rodriguez-Larrad, “An overground robotic gait training program for people with multiple sclerosis: A protocol for a randomized clinical trial,” *Front Med (Lausanne)*, vol. 7, p. 238, Jun. 2020.

[39] Y. He, D. Eguren, T. P. Luu, and J. L. Contreras-Vidal, “Risk management and regulations for lower limb medical exoskeletons: a review,” *Med Devices (Auckl)*, vol. 10, pp. 89–107, May 2017.

[40] M. Cenciarini and A. M. Dollar, “Biomechanical considerations in the design of lower limb exoskeletons,” *IEEE International Conference on Rehabilitation Robotics*, 2011.

[41] B. Lee, S. C. Lee, and C. soo Han, “Design of fixations for an exoskeleton device with joint axis misalignments,” *International Journal of Precision Engineering and Manufacturing*, vol. 21, pp. 1291–1298, 7 2020.

[42] U. Della Croce, A. Leardini, L. Chiari, and A. Cappozzo, “Human movement analysis using stereophotogrammetry: Part 4: assessment of anatomical landmark misplacement and its effects

on joint kinematics," *Gait & Posture*, vol. 21, no. 2, pp. 226–237, 2005. [Online]. Available: https://www.sciencedirect.com/science/article/pii/S0966636204000785

[43] D. Zanotto, T. Lenzi, P. Stegall, and S. K. Agrawal, "Improving transparency of powered exoskeletons using force/torque sensors on the supporting cuffs," *IEEE International Conference on Rehabilitation Robotics*, 2013.

[44] J. Dul and G. Johnson, "A kinematic model of the human ankle," *Journal of Biomedical Engineering*, vol. 7, no. 2, pp. 137–143, 1985. [Online]. Available: https://www.sciencedirect.com/science/article/pii/0141542585900433

[45] J. Jiang, K. M. Lee, and J. Ji, "Review of anatomy-based ankle–foot robotics for mind, motor and motion recovery following stroke: design considerations and needs," *International Journal of Intelligent Robotics and Applications*, vol. 2, pp. 267–282, 9 2018.

[46] M. Gálvez and A. Aceves-Lopez, "A review on compliant joint mechanisms for lower limb exoskeletons," *Journal of Robotics*, vol. 2016, 08 2016.

[47] S. Fatone and A. H. Hansen, "A model to predict the effect of ankle joint misalignment on calf band movement in ankle-foot orthoses," *Prosthetics and Orthotics International*, vol. 31, pp. 76–87, 3 2007.

[48] J. Bessler-Etten, L. Schaake, G. B. Prange-Lasonder, and J. H. Buurke, "Assessing effects of exoskeleton misalignment on knee joint load during swing using an instrumented leg simulator," *Journal of NeuroEngineering and Rehabilitation*, vol. 19, p. 13, 12 2022. [Online]. Available: https://jneuroengrehab.biomedcentral.com/articles/10.1186/s12984-022-00990-z

[49] K. Ghonasgi, S. N. Yousaf, P. Esmatloo, and A. D. Deshpande, "A modular design for distributed measurement of human–robot interaction forces in wearable devices," *Sensors*, vol. 21, pp. 1–17, 2 2021.

[50] L. Levesque, S. Pardoel, Z. Lovrenovic, and M. Doumit, "Experimental comfort assessment of an active exoskeleton interface," in *2017 IEEE International Symposium on Robotics and Intelligent Sensors (IRIS)*, 2017, pp. 38–43.

[51] J. Tamez-Duque, R. Cobian-Ugalde, A. Kilicarslan, A. Venkatakrishnan, R. Soto, and J. L. Contreras-Vidal, "Real-time strap pressure sensor system for powered exoskeletons," *Sensors*, vol. 15, no. 2, pp. 4550–4563, 2015. [Online]. Available: https://www.mdpi.com/1424-8220/15/2/4550

[52] A. Rathore, M. Wilcox, D. Z. M. Ramirez, R. Loureiro, and T. Carlson, "Quantifying the human-robot interaction forces between a lower limb exoskeleton and healthy users," *Proceedings of the*

Annual International Conference of the IEEE Engineering in Medicine and Biology Society, EMBS, vol. 2016-October, pp. 586–589, 10 2016.

[53] Y. Wang, J. Qiu, H. Cheng, and X. Zheng, "Analysis of human–exoskeleton system interaction for ergonomic design," *Human Factors*, 2020.

[54] M. Wilcox, A. Rathore, D. Z. M. Ramirez, R. C. Loureiro, and T. Carlson, "Muscular activity and physical interaction forces during lower limb exoskeleton use," *Healthcare Technology Letters*, vol. 3, pp. 273–279, 2016.

[55] J. G. Dabling, A. Filatov, and J. W. Wheeler, "Static and cyclic performance evaluation of sensors for human interface pressure measurement," *Annu Int Conf IEEE Eng Med Biol Soc*, vol. 2012, pp. 162–165, 2012.

[56] J. Bessler, L. Schaake, R. Kelder, J. Buurke, and G. Prange, "Prototype measuring device for assessing interaction forces between human limbs and rehabilitation robots - a proof of concept study," *IEEE ... International Conference on Rehabilitation Robotics : [proceedings]*, vol. 2019, pp. 1109–1114, 06 2019.

[57] *On the Biomimetic Design of the Berkeley Lower Extremity Exoskeleton (BLEEX)*, 2005.

[58] Schiele, *An Explicit Model to Predict and Interpret Constraint Force Creation in pHRI with Exoskeletons*. IEEE Xplore, 2008.

[59] L. Armitage, S. Turner, and M. Sreenivasa, "Human-device interface pressure measurement in prosthetic, orthotic and exoskeleton applications: A systematic review," *Medical Engineering and Physics*, vol. 97, pp. 56–69, 11 2021.

[60] M. Cempini, A. Marzegan, M. Rabuffetti, M. Cortese, N. Vitiello, and M. Ferrarin, "Analysis of relative displacement between the hx wearable robotic exoskeleton and the user's hand jner journal of neuroengineering and rehabilitation analysis of relative displacement between the hx wearable robotic exoskeleton and the user's hand," *Journal of NeuroEngineering and Rehabilitation*, vol. 11, p. 147, 2014. [Online]. Available: http://www.jneuroengrehab.com/content/11/1/147http://www.jneuroengrehab.com/content/11/1/147

[61] Y. Akiyama, Y. Yamada, and S. Okamoto, "Interaction forces beneath cuffs of physical assistant robots and their motion-based estimation," *Advanced Robotics*, vol. 29, pp. 1315–1329, 10 2015.

[62] M. Ferrarin, J. Stallard, R. Palmieri, and A. Pedotti, "Estimation of deformation in a walking orthosis for paraplegic patients," *Clinical Biomechanics*, vol. 8, no. 5, pp. 255–261, 1993. [Online]. Available: https://www.sciencedirect.com/science/article/pii/026800339390035G

[63] G. Katsube, S. Qi, T. Itami, K. Yano, I. Mori, and K. Kameda, “Ankle foot orthosis that prevents slippage for tibial rotation in knee osteoarthritis patients,” in *2021 43rd Annual International Conference of the IEEE Engineering in Medicine & Biology Society (EMBC)*, 2021, pp. 4728–4731.

[64] B. Celebi, M. Yalcin, and V. Patoglu, “Assiston-knee: A self-aligning knee exoskeleton,” in *2013 IEEE/RSJ International Conference on Intelligent Robots and Systems*, 2013, pp. 996–1002.

[65] J. Schorsch, A. Keemink, A. Stienen, F. van der Helm, and D. Abbink, “A novel self-aligning mechanism to decouple force and torques for a planar exoskeleton joint,” *Mechanical Sciences*, vol. 5, pp. 29–35, 08 2014.

[66] A. Schiele, “Ergonomics of exoskeletons: Subjective performance metrics,” *2009 IEEE/RSJ International Conference on Intelligent Robots and Systems, IROS 2009*, pp. 480–485, 12 2009.

[67] A. Mahmoudi Khomami and F. Najafi, “A survey on soft lower limb cable-driven wearable robots without rigid links and joints,” *Robotics and Autonomous Systems*, vol. 144, p. 103846, 2021. [Online]. Available: https://www.sciencedirect.com/science/article/pii/S0921889021001317

[68] M. D. C. Sanchez-Villamañan, J. Gonzalez-Vargas, D. Torricelli, J. C. Moreno, and J. L. Pons, “Compliant lower limb exoskeletons: a comprehensive review on mechanical design principles,” *J Neuroeng Rehabil*, vol. 16, no. 1, p. 55, May 2019.

[69] A. T. Asbeck, R. J. Dyer, A. F. Larusson, and C. J. Walsh, “Biologically-inspired soft exosuit,” in *2013 IEEE 13th International Conference on Rehabilitation Robotics (ICORR)*, 2013, pp. 1–8.

[70] M. A. Koch, J. M. Font-Llagunes, and P. Fink, “Lower-limb exosuits for rehabilitation or assistance of human movement: A systematic review,” *Applied Sciences*, 2021. [Online]. Available: https://doi.org/10.3390/app

[71] C. J. Walsh, K. Endo, and H. Herr, “A quasi-passive leg exoskeleton forload-carrying augmentation,” *International Journal of Humanoid Robotics*, vol. 9, pp. 487–506, 2007.

[72] L. F. Yeung, C. Ockenfeld, M. K. Pang, H. W. Wai, O. Y. Soo, S. W. Li, and K. Y. Tong, “Design of an exoskeleton ankle robot for robot-assisted gait training of stroke patients,” *IEEE International Conference on Rehabilitation Robotics*, pp. 211–215, 8 2017.

[73] G. Orekhov, Y. Fang, C. F. Cuddeback, and Z. F. Lerner, “Usability and performance validation of an ultra-lightweight and versatile untethered robotic ankle exoskeleton,” *Journal of NeuroEngineering and Rehabilitation*, vol. 18, 12 2021.

[74] A. Roy, H. I. Krebs, D. J. Williams, C. T. Bever, L. W. Forrester, R. M. Macko, and N. Hogan, “Robot-aided neurorehabilitation: A novel robot for ankle rehabilitation,” *IEEE Transactions on Robotics*, vol. 25, pp. 569–582, 2009.

[75] S. Christensen, S. Rafique, and S. Bai, “Design of a powered full-body exoskeleton for physical assistance of elderly people,” *International Journal of Advanced Robotic Systems*, vol. 18, 2021.

[76] A. C. Satici, A. Erdogan, and V. Patoglu, “Design of a reconfigurable ankle rehabilitation robot and its use for the estimation of the ankle impedance,” *2009 IEEE International Conference on Rehabilitation Robotics, ICORR 2009*, pp. 257–264, 2009.

[77] H. Kazerooni, R. Steger, and L. Huang, “Hybrid control of the berkeley lower extremity exoskeleton (bleex),” *International Journal of Robotics Research*, vol. 25, pp. 561–573, 5 2006.

[78] *On the Biomimetic Design of the Berkeley Lower Extremity Exoskeleton (BLEEX)*, 2005.

[79] A. Zoss, H. Kazerooni, and A. Chu, “On the mechanical design of the berkeley lower extremity exoskeleton (bleex),” *2005 IEEE/RSJ International Conference on Intelligent Robots and Systems, IROS*, pp. 3465–3472, 2005.

[80] A. B. Zoss, H. Kazerooni, and A. Chu, “Biomechanical design of the berkeley lower extremity exoskeleton (bleex),” *IEEE/ASME Transactions on Mechatronics*, vol. 11, pp. 128–138, 4 2006.

[81] T. Lee, I. Kim, and Y. S. Baek, “Design of a 2dof ankle exoskeleton with a polycentric structure and a bi-directional tendon-driven actuator controlled using a pid neural network,” *Actuators*, vol. 10, pp. 1–17, 1 2021.

[82] D. J. Hyun, H. Park, T. Ha, S. Park, and K. Jung, “Biomechanical design of an agile, electricity-powered lower-limb exoskeleton for weight-bearing assistance,” *Robotics and Autonomous Systems*, vol. 95, pp. 181–195, 9 2017.

[83] Y. Lee, Y. J. Kim, J. Lee, M. Lee, B. Choi, J. Kim, Y. J. Park, and J. Choi, “Biomechanical design of a novel flexible exoskeleton for lower extremities,” *IEEE/ASME Transactions on Mechatronics*, vol. 22, pp. 2058–2069, 10 2017.

[84] A. H. Weerasingha, A. D. Pragnathilaka, W. P. Withanage, R. K. Ranaweera, and R. A. Gopura, “C-jae: 3 dof robotic ankle exoskeleton with compatible joint axes,” *MERCon 2018 - 4th International Multidisciplinary Moratuwa Engineering Research Conference*, pp. 270–275, 7 2018.

[85] *A soft robotic exosuit improves walking in patients after stroke*, 2017. [Online]. Available: http://stm.sciencemag.org/

[86] L. N. Awad, A. Esquenazi, G. E. Francisco, K. J. Nolan, and A. Jayaraman, “The rewalk restore™ soft robotic exosuit: A multi-site clinical trial of the safety, reliability, and feasibility of exosuit-augmented post-stroke gait rehabilitation,” *Journal of NeuroEngineering and Rehabilitation*, vol. 17, 6 2020.

[87] Y. L. Park, B. R. Chen, N. O. Pérez-Arancibia, D. Young, L. Stirling, R. J. Wood, E. C. Goldfield, and R. Nagpal, "Design and control of a bio-inspired soft wearable robotic device for ankle-foot rehabilitation," *Bioinspiration and Biomimetics*, vol. 9, 3 2014.

[88] *Towards an intelligent wearable ankle robot for assistance to foot drop*, 2019.

[89] Y. Bougrinat, S. Achiche, and M. Raison, "Design and development of a lightweight ankle exoskeleton for human walking augmentation," *Mechatronics*, vol. 64, 12 2019.

[90] L. M. Mooney, E. J. Rouse, and H. M. Herr, "Autonomous exoskeleton reduces metabolic cost of human walking," *Journal of NeuroEngineering and Rehabilitation*, vol. 11, no. 1, p. 151, Nov 2014. [Online]. Available: https://doi.org/10.1186/1743-0003-11-151

[91] L. M. Mooney and H. M. Herr, "Biomechanical walking mechanisms underlying the metabolic reduction caused by an autonomous exoskeleton," *Journal of NeuroEngineering and Rehabilitation*, vol. 13, 1 2016.

[92] H. S. Choi, C. H. Lee, and Y. S. Baek, "Design of a pneumatic actuated ankle-foot orthosis which has talocrural and subtalar joint," *2019 IEEE 16th International Conference on Rehabilitation Robotics (ICORR)*, 2019.

[93] M. Bortole, A. Venkatakrishnan, F. Zhu, J. C. Moreno, G. E. Francisco, J. L. Pons, and J. L. Contreras-Vidal, "The h2 robotic exoskeleton for gait rehabilitation after stroke: Early findings from a clinical study wearable robotics in clinical testing," *Journal of NeuroEngineering and Rehabilitation*, vol. 12, 6 2015.

[94] H. Tsushima, M. E. Morris, and J. Mcginley, "Test-retest reliability and inter-tester reliability of kinematic data from a three-dimensional gait analysis system," *J Jpn Phys Ther Assoc*, vol. 6, pp. 9–17, 2003.

[95] M. P. Castro, M. Meucci, D. P. Soares, P. Fonseca, M. Borgonovo-Santos, F. Sousa, L. Machado, and J. P. Vilas-Boas, "Accuracy and repeatability of the gait analysis by the walkinsense system," *BioMed Research International*, vol. 2014, 2014.

[96] D. L. Bader, P. R. Worsley, and A. Gefen, "Bioengineering considerations in the prevention of medical device-related pressure ulcers," *Clinical Biomechanics*, vol. 67, pp. 70–77, 7 2019.

[97] P. C. Silva, M. T. Silva, and J. M. Martins, "Evaluation of the contact forces developed in the lower limb/orthosis interface for comfort design," *Multibody System Dynamics*, vol. 24, pp. 367–388, 10 2010.

[98] E. Bettoni, G. Ferriero, H. Bakhsh, E. Bravini, G. Massazza, and F. Franchignoni, "A systematic review of questionnaires to assess patient satisfaction with limb orthoses," *Prosthetics and Orthotics International*, vol. 40, pp. 158–169, 4 2016.

[99] "Orthotics prosthetics users survey," https://www.sralab.org/rehabilitation-measures/orthotics-prosthetics-users-survey.

[100] "Quebec user evaluation of satisfaction with assistive technology." [Online]. Available: https://www.sralab.org/rehabilitation-measures/quebec-user-evaluation-satisfaction-assistive-technology

[101] E. Bravini, F. Franchignoni, G. Ferriero, A. Giordano, H. Bakhsh, F. Sartorio, and S. Vercelli, "Validation of the italian version of the client satisfaction with device module of the orthotics and prosthetics users' survey," *Disability and Health Journal*, vol. 7, pp. 442–447, 2014.

[102] L. Magnusson, G. Ahlström, N. Ramstrand, and E. I. Fransson, "Malawian prosthetic and orthotic users' mobility and satisfaction with their lower limb assistive device," *Journal of Rehabilitation Medicine*, vol. 45, pp. 385–391, 2013.

[103] "Visual 3d wiki - model based items," https://c-motion.com/v3dwiki/index.php?title=Model_Based_Items.

[104] ISO Central Secretary, "Robots and robotic devices — collaborative robots," International Organization for Standardization, Geneva, CH, Standard ISO/TS 15066:2016, 2016. [Online]. Available: https://www.iso.org/standard/62996.html

[105] R. P. J. M. Belda-Lois and M. J. Vivas, *Case Study: Analysis of Pressure Distribution and Tolerance Areas for Wearable Robots*. John Wiley & Sons, Ltd, 2008, ch. 5, pp. 127–163. [Online]. Available: https://onlinelibrary.wiley.com/doi/abs/10.1002/9780470987667.ch5

[106] T. Kermavnar, V. Power, A. de Eyto, and L. O'Sullivan, "Computerized cuff pressure algometry as guidance for circumferential tissue compression for wearable soft robotic applications: A systematic review," *Soft Robotics*, vol. 5, 10 2017.

[107] T. Kermavnar, V. Power, A. D. Eyto, and L. W. O'Sullivan, "Computerized cuff pressure algometry as guidance for circumferential tissue compression for wearable soft robotic applications: A systematic review," *Soft Robotics*, vol. 5, pp. 1–16, 2 2018.

[108] Y. Akiyama, S. Okamoto, Y. Yamada, and K. Ishiguro, "Measurement of contact behavior including slippage of cuff when using wearable physical assistant robot," *IEEE Transactions on Neural Systems and Rehabilitation Engineering*, vol. 24, pp. 784–793, 7 2016.

[109] N. D'Elia, F. Vanetti, M. Cempini, G. Pasquini, A. Parri, M. Rabuffetti, M. Ferrarin, R. M. Lova, and N. Vitiello, "Physical human-robot interaction of an active pelvis orthosis: Toward ergonomic assessment of wearable robots," *Journal of NeuroEngineering and Rehabilitation*, vol. 14, 4 2017.

[110] S. V. Sarkisian, M. K. Ishmael, and T. Lenzi, "Self-aligning mechanism improves comfort and performance with a powered knee exoskeleton," *IEEE Transactions on Neural Systems and Rehabilitation Engineering*, vol. 29, pp. 629–640, 2021.

[111] S. G. Hart and L. E. Staveland, "Development of nasa-tlx (task load index): Results of empirical and theoretical research," in *Human Mental Workload*, ser. Advances in Psychology, P. A. Hancock and N. Meshkati, Eds. North-Holland, 1988, vol. 52, pp. 139–183. [Online]. Available: https://www.sciencedirect.com/science/article/pii/S0166411508623869

[112] L. Moreira, J. Figueiredo, P. Fonseca, J. P. Vilas-Boas, and C. Santos, "Lower limb kinematic, kinetic, and emg data from young healthy humans during walking at controlled speeds," *Scientific Data*, vol. 8, p. 103, 04 2021.

A

Appendix A - FSR Calibration Results

Table A.1: Exponential regression results following calibration

Sensor	a	b	c	d	R2	R2 adjusted	RMSE
1	0.09091	6.00E-03	5.15E-16	0.04077	0.996	0.989	4.914
2	0.6481	0.00141	2.84E-15	0.03916	0.998	0.996	2.974
3	0.009555	0.009093	2.51E-17	0.0442	0.998	0.998	2.29
4	0.2552	0.0057	1.0821E-15	0.0411	0.994	0.988	5.062
5	0.2552	0.0057	0.005482	1.0821E-15	0.0411	0.9905	4.551
6	0.2129	0.00523	1.05E-15	0.04003	0.997	0.994	3.577
7	0.02374	0.008023	6.42E-17	0.04286	0.999	0.998	2.025
8	0.546	0.004385	2.00E-15	0.03932	0.996	0.992	4.313

B

Appendix B - Original Questionnaires

	Strongly Agree	Agree	Disagree	Strongly Disagree	Not Applicable
1. My skin is free of abrasions and irritation	☐	☐	☐	☐	☐
2. My device is comfortable throughout the day	☐	☐	☐	☐	☐
3. My device looks good	☐	☐	☐	☐	☐
4. My device is pain free to wear	☐	☐	☐	☐	☐
5. My device is durable	☐	☐	☐	☐	☐
6. My device fits well	☐	☐	☐	☐	☐
7. It is easy to put on my device	☐	☐	☐	☐	☐
8. The weight of my device is manageable	☐	☐	☐	☐	☐

Figure B.1: Modified Client Satisfaction with Device module of the Orthotics and Prosthetic Users Survey (CSD-OPUS). Taken from [98].

1	2	3	4	5
not satisfied at all	not very satisfied	more or less satisfied	quite satisfied	very satisfied

ASSISTIVE DEVICE

How satisfied are you with…

1. the **dimensions** (size, height, length, width) of your assistive device? *Comments:*	1	2	3	4	5
2. the **weight** of your assistive device? *Comments:*	1	2	3	4	5
3. the **ease in adjusting** (fixing, fastening) the parts of your assistive device? *Comments:*	1	2	3	4	5
4. how **safe and secure** your assistive device is? *Comments:*	1	2	3	4	5
5. the **durability** (endurance, resistance to wear) of your assistive device? *Comments:*	1	2	3	4	5
6. how **easy** it is to use your assistive device? *Comments:*	1	2	3	4	5
7. how **comfortable** your assistive device is? *Comments:*	1	2	3	4	5
8. how **effective** your assistive device is (the degree to which your device meets your needs)? *Comments:*	1	2	3	4	5

Figure B.2: 8-item subscale of the Quebec User Evaluation of Satisfaction with Assistive Technology 2.0 (QUEST 2.0). Taken from [98].

C

Appendix C- Technical Drawings

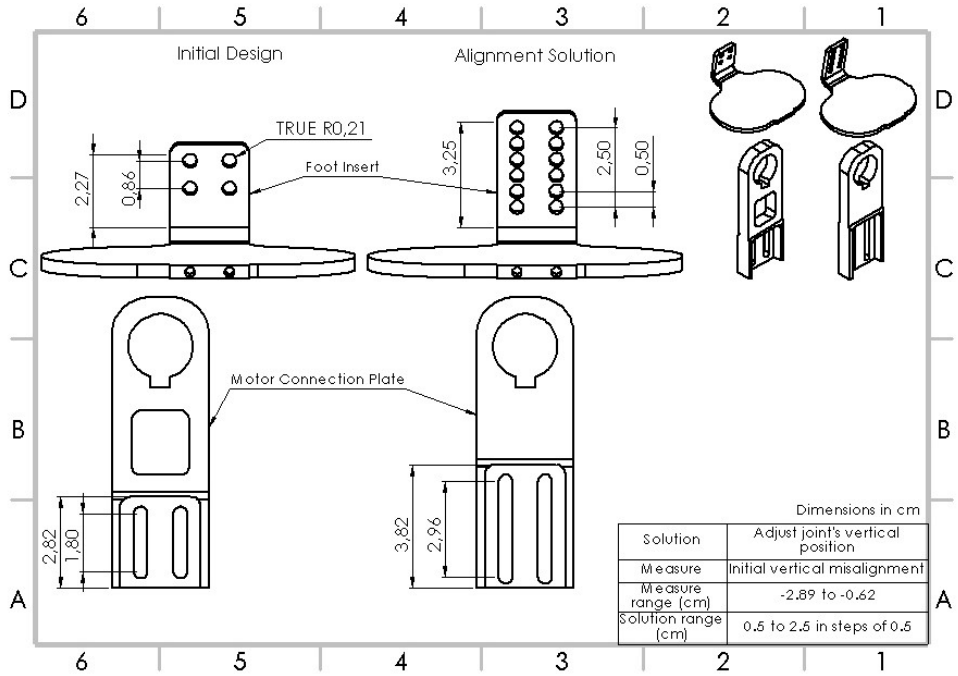

Figure C.1: Technical drawing of the initial and final designs for the vertical alignment solution.

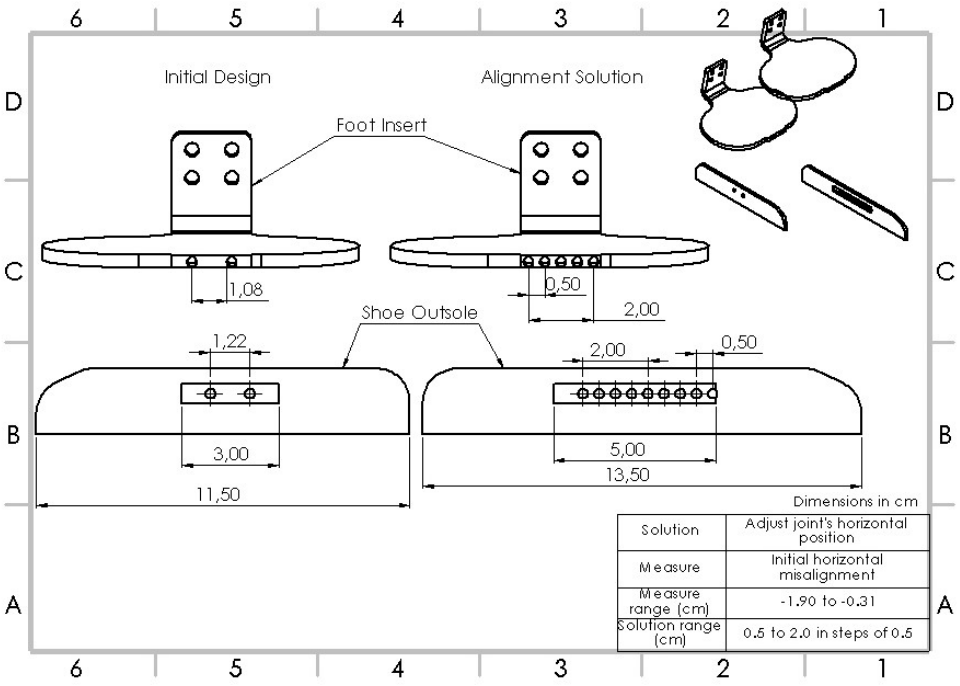

Figure C.2: Technical drawing of the initial and final designs for the horizontal alignment solution.

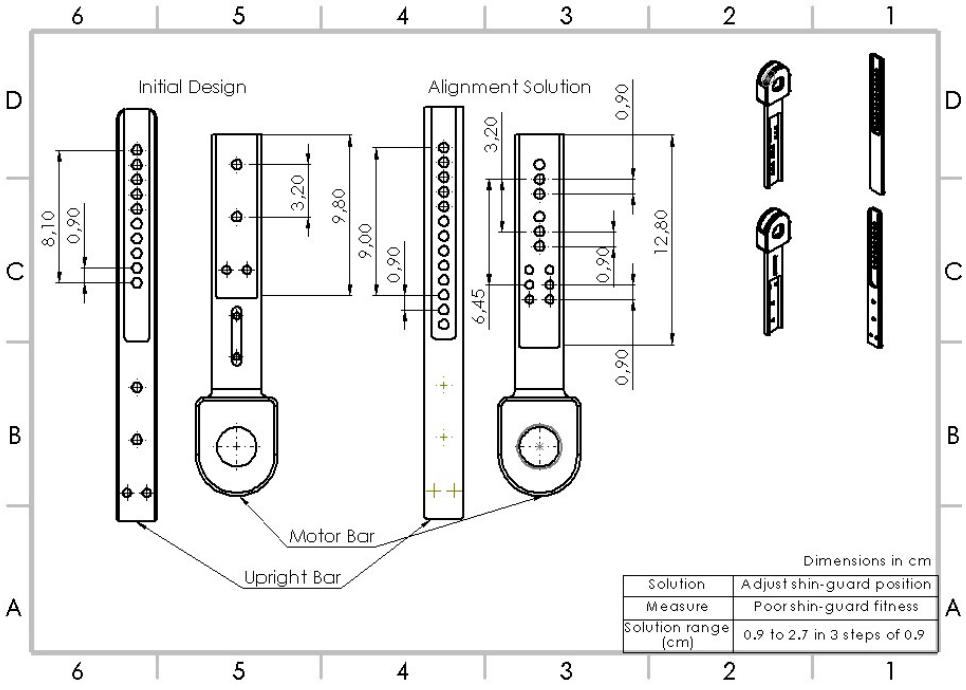

Figure C.3: Technical drawing of the initial and final designs for the shin guard alignment solution.

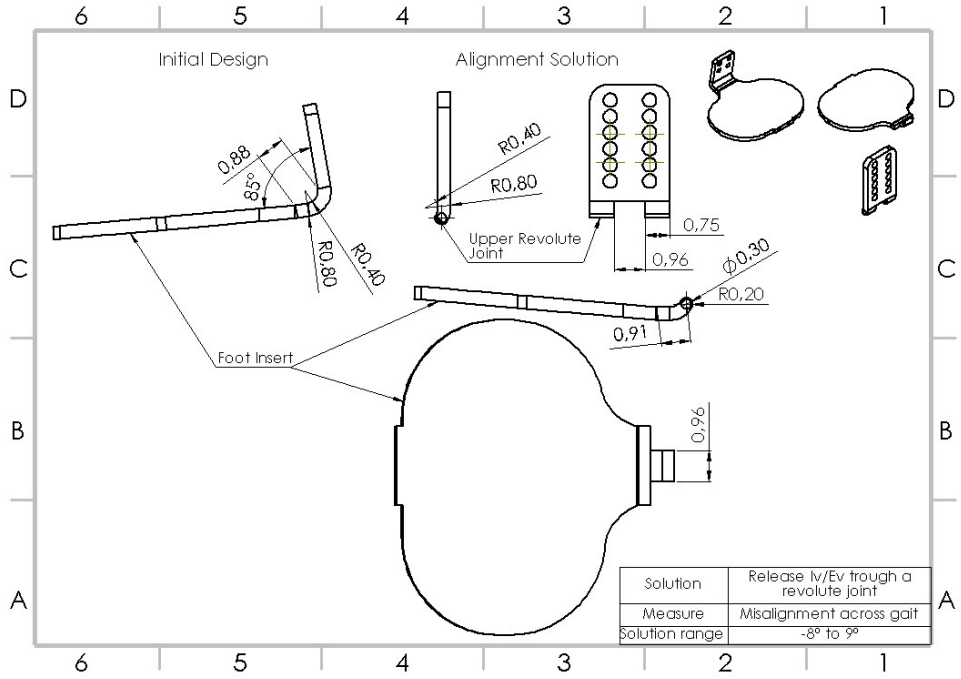

Figure C.4: Technical drawing of the initial and final designs for the solution to release the inversion/eversion DOF.

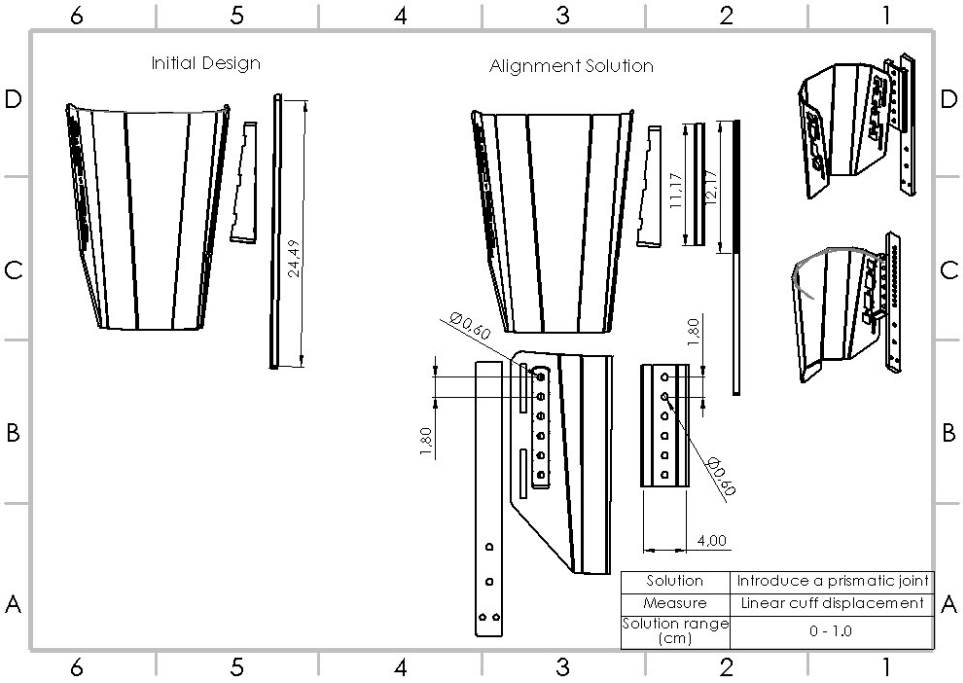

Figure C.5: Technical drawing of the initial and final designs for the solution **"Introduce a prismatic joint"**.